Thermodynamics of Strongly Interacting Fermi Gases

Martin W. Zwierlein

MIT-Harvard Center for Ultracold Atoms, Research Laboratory of Electronics, and Department of Physics, Massachusetts Institute of Technology, 77 Massachusetts Avenue, Cambridge, Massachusetts, 02139, USA

1. – Introduction

Strongly interacting gases of ultracold fermionic atoms provide an amazingly rich test-bed for many-body physics, and a platform for the search of novel states of matter. Ultracold atomic Fermi gases are a million times thinner than air (density $n \sim 10^{13}\,\mathrm{cm}^{-3}$) and up to 100 million times colder than interstellar space (temperature $T \sim 10$ nK). Typical Fermi energies are measured in μK: $E_F \sim k_B \times 1\,\mu\mathrm{K} \sim 10^{-10}\,\mathrm{eV}$. Interactions in these gases can be freely tuned to be as strong as quantum mechanics allows, by means of Feshbach resonances [1, 2, 3, 4]. Free tuning of the interaction strength has allowed the discovery of pair condensation and superfluidity in these Fermi gases in the crossover from Bose-Einstein condensation of tightly bound molecules to Bardeen-Cooper-Schrieffer (BCS) superfluidity of long-range Cooper pairs [5, 6, 7, 8, 9, 10, 11, 12, 13]. The remarkable properties of these gases have been uncovered in a sequence of experiments over the past years: Superfluidity and phase coherence in these gases was directly demonstrated via the observation of lattices of quantized vortices in rotating Fermi gases [14]. The critical velocity of the superfluid was found in [15] to be a good fraction of the Fermi velocity in the strongly interacting regime, demonstrating the robust nature of the superfluid. Upon cooling under slow rotation, a reduced moment of inertia was found below a critical temperature [16]. As a further hallmark of superfluidity, second sound, a relative motion of superfluid and normal parts of the gas, was directly observed in [17]. The characteristic drop of flow resistance expected for a superfluid was revealed in a transport experiment between two reservoirs [18]. Radio-frequency spectroscopy allowed the direct measurement of the single-particle excitation spectrum [19, 20, 21, 22, 23, 24]. Collective excitations revealed almost inviscous hydrodynamic flow even in the normal state above the superfluid critical temperature [12, 25, 26, 27, 28]. At the Feshbach resonance, the gas is said to be a "perfect fluid", as the mean-free-path for collisions is as short as at all possible: One interparticle spacing. This leads to quantum limited transport, for example a shear viscosity $\eta \simeq \hbar n$ [29] and a spin diffusion coefficient $D_s \simeq \hbar/m$ [30] that has a minimum value just given by constants of nature. The ratio of shear viscosity to entropy density comes close to a lower bound predicted for a wide class of theories [31], a property that strongly interacting Fermi gases at Nanokelvin temperatures share with the Quark-Gluon plasma created at several trillion Kelvin [32].

At the Feshbach resonance, where the interactions become limited by the unitarity of quantum mechanics, the gas enters a universal regime of scale-invariance. The only energy scales are the Fermi energy and the temperature. The thermodynamics of the gas become universal [33] and directly relate for example to the physics of dilute neutron matter in the crust of neutron stars. The equation of state of strongly interacting Fermi gases was measured with a precision that allows to distinguish between current theories of interacting Fermi gases [34, 35, 36, 37, 38, 39]. Such theories are often plagued by the fermion sign problem - the fact that fermions must be in a fully antisymmetric state - and their validity can now be tested in ultracold atom experiments, with direct impact into condensed matter, nuclear and particle physics.

Spin-imbalanced mixtures of strongly interacting fermions represent a novel system

without weakly interacting counterpart in condensed matter physics [40, 41, 42, 43, 44]. Indeed, to induce spin imbalance in conventional superconductors one would have to apply magnetic fields that are however expelled by the Meissner effect. In ultracold gases, chemical potential imbalance and orbital effects in the superfluid can be studied independently, the first via spin imbalance, the second via rotation. Spin imbalance has allowed the demonstration of the Clogston-Chandrasekhar (or Pauli) limit of superfluidity, where the mismatch in Fermi energies outweighs the gain in pairing energy. Beyond this limit lies an attractive Fermi liquid of quasi-particles, dressed spin impurities immersed in the majority Fermi sea - the Fermi polarons [45, 44, 46, 47].

2. – Universal Thermodynamics

Ultracold atomic Fermi gases provide us with a unique test-bed for many-body theories of strongly interacting fermionic matter. The key to their use as idealized model systems is the short range of interparticle interactions, which leads to universal behavior. The temperatures are so low that particles scatter purely in head-on collisions, i.e. in the s-wave channel - and only between opposite spins thanks to the Pauli principle. Indeed, the characteristic wavelength for the scattering waves, the de Broglie wavelength $\lambda = \sqrt{\frac{2\pi\hbar^2}{mk_BT}}$, is much larger than the range of the interatomic potential $R \sim 50 - 100\, a_0$, so that particle scattering does not reveal the intricacies of the interatomic potential. Interactions are then described by one parameter only, the scattering length a. Near Feshbach resonances, a becomes much larger than R. Furthermore, the diluteness of the gas ensures that also the interparticle spacing $n^{-1/3} \sim 10\,000\, a_0$ is much larger than R. Therefore, the system can be described by an idealized hamiltonian involving contact interactions only. This has the profound consequence that all thermodynamic variables of the gas can only depend on the three relevant length scales, the interparticle spacing $n^{-1/3}$, the de Broglie wavelength λ and the scattering length a. The equivalent energy scales are the Fermi energy $E_F = \frac{\hbar^2}{2m}(3\pi^2 n)^{2/3}$, k_BT and $\hbar^2/ma^2$, the latter describing, for positive a, the bound state energy of the two-body molecular state. For example, the pressure P of the homogeneous gas must be a function of n, T and a only: $P = P(n, T, a)$. We can proceed further via dimensional analysis. The density n sets a natural scale of pressure, namely the pressure of a non-interacting Fermi gas at zero temperature: $P_0 = \frac{2}{5} n E_F$. The density also provides a natural scale for temperature, the Fermi temperature $T_F = E_F/k_B$, as well as for length, namely the interparticle spacing or $1/k_F$. The ratio of P and P_0, a dimensionless number, must then be given by a dimensionless, universal function f_P that can only depend on the dimensionless ratios T/T_F and $1/k_Fa$, the latter comparing the interparticle spacing to the scattering length:

$$P = P_0\, f_P\left(\frac{T}{T_F}, \frac{1}{k_F a}\right) \tag{1}$$

The same considerations hold for all thermodynamic quantities. The energy of the gas E must be given by the energy of a non-interacting Fermi gas at zero temperature,

$E_0 = \frac{3}{5} N E_F$, times a universal dimensionless function:

$$E = E_0 \, f_E \left(\frac{T}{T_F}, \frac{1}{k_F a} \right) \tag{2}$$

In the same way the entropy must be given by Nk_B times a universal dimensionless function:

$$S = N k_B \, f_S \left(\frac{T}{T_F}, \frac{1}{k_F a} \right) \tag{3}$$

It is remarkable that with ultracold Fermi gases near Feshbach resonances, there exists a strongly interacting system in nature whose equation of state is universal, i.e. whose properties do not depend on a microscopic variable such as the interaction range, or whether we are dealing with a gas of ^{6}Li atoms or a gas of ^{40}K atoms. For the first time we are presented with a system whose thermodynamic properties should be exactly predictable by many-body theory - the hamiltonian is known. The problem of finding the equation of state is not only relevant to cold atomic gases. We are faced with the same situation in the case of dilute neutron matter, for example in the crust of neutron stars. The interaction between neutrons is described by a scattering length $a = -18.6\,\mathrm{fm}$ that is much larger than the interneutron distance $n^{-1/3} \sim 1\,\mathrm{fm}$, and we find ourselves in the same universal regime as one encounters with a dilute Fermi gas near a Feshbach resonance - despite a difference in particle densities of 25 orders of magnitude. Of course, neutron stars are far more complex objects - the interactions between neutrons acquire a finite range correction, protons are present, and the core might even be a quark superfluid [48]. But stripped of all complications, a theory of dilute neutron matter must at its core be able to describe a spin-1/2 Fermi gas with strong contact interactions, and it is at this level that a direct comparison to ultracold atomic gas experiments allows to validate current many-body theories.

Right at the Feshbach resonance, where the scattering length diverges and interactions are as strong as quantum mechanics allows (i.e. they are unitarity-limited), we encounter an even stronger degree of universality. In the absence of any interaction-dependent length scale the thermodynamics of this *unitary* gas can only depend on the interparticle distance $n^{-1/3}$ and the de Broglie wavelength λ. The dimensionless quantities P/P_0, E/E_0 or S/Nk_B will now only depend, in a universal way, on T/T_F or equivalently on $n\lambda^3$. Said otherwise, *any* dimensionless quantity involving thermodynamic quantities, must depend in a universal way on *any other* such dimensionless quantity. This has immediate consequences for the relation between thermodynamic variables. The entropy, for example, is now given by $S = Nk_B f_S(T/T_F)$, i.e. it is fully specified by T/T_F and the number of particles. The pressure is generally related to the energy of the system via

$$P = -\left. \frac{\partial E}{\partial V} \right|_{N,S} \tag{4}$$

where V is the volume of the system. Fixing particle number and entropy is equivalent to fixing T/T_F and thus to fixing E/E_0. Therefore

$$P = -\frac{E}{E_0}\left.\frac{\partial E_0}{\partial V}\right|_{N,S} = \frac{2}{3}\frac{E}{V} \tag{5}$$

We thus find the important relation $E = \frac{3}{2}PV$ for the unitary gas [33, 49, 50], valid at all temperatures, that is remarkably identical to that for a non-interacting gas.

Since we know that a strongly interacting Fermi gas forms a superfluid at low temperatures, the critical temperature T_c must be given by a universal number times the Fermi temperature T_F, and there must likewise be a universal number describing the critical entropy $S_c/Nk_B = f_S(T_c/T_F)$, and the critical energy $E_c/E_0 = f_E(T_c/T_F)$, etc.

At zero temperature, the thermodynamics of a unitary Fermi gas simplify even further. E/E_0 must tend to a universal constant ξ, i.e. the energy must be given by a universal dimensionless constant times the energy of a non-interacting Fermi gas at zero temperature:

$$E = \xi E_0 \tag{6}$$

As $P = \frac{2}{3}\frac{E}{V}$, P/P_0 must tend to the same universal constant ξ. The chemical potential $\mu = \left.\frac{\partial E}{\partial N}\right|_{S,V}$ likewise tends to the same constant ξ times the Fermi energy, $\mu = \xi E_F$. The constant $\beta = \xi - 1$ is called the Bertsch parameter, as G. Bertsch posed the challenge to find the ground-state energy of a Fermi gas with unitarity limited interactions [51].

The calculation of the Bertsch parameter has been the subject of many theoretical calculations over the past decade [52, 53]. With the advent of Feshbach-resonant Fermi gases, this number - and the entire thermodynamics of strongly interacting Fermi gases - became suddenly accessible to experimental measurement.

2˙1. *Thermodynamics of trapped gases.* – In actual experiments, the gas is trapped in a potential $U(\mathbf{r})$. This might lead one to the incorrect conclusion that cold atom experiments cannot obtain thermodynamic quantities relevant for the bulk system, i.e. the homogeneous system one would encounter in a (very large) box. Instead, as we will show here, the spatially varying trapping potential can be turned from a problem into the crucial feature that allows to obtain the entire thermodynamics of strongly interacting Fermi gases from - in principle - a single image of a trapped atom cloud. This only requires the local density approximation, in which local thermodynamic equilibrium is assumed to hold in an infinitesimal volume ΔV around every point $\mathbf{r}$ in the trapped gas. Each of these local volumes, at (locally constant) potential $U(\mathbf{r})$, can exchange particles with the surrounding ones, prompting us to pass to the grand-canonical description of fixed local chemical potential $\mu(\mathbf{r}) = \mu_0 - U(\mathbf{r})$, where μ_0 is the global chemical potential. The local density $n(\mathbf{r})$ is then given by the *bulk* equation of state for the homogeneous case $n(\mu, a, T)$ via the local chemical potential $\mu(\mathbf{r})$, the scattering length a and the

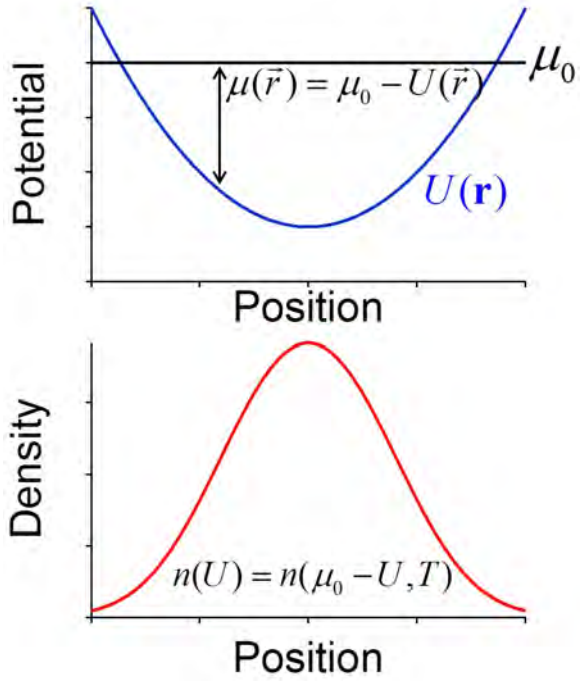

Fig. 1. – Local density approximation. The local chemical potential $\mu(\mathbf{r}) = \mu_0 - U(\mathbf{r})$, together with the temperature T, determines the local density $n(\mathbf{r}) = n(\mu_0 - U(\mathbf{r}), T)$ via the equation of state. In turn, the equation of state follows from the knowledge of $n(U)$.

temperature T, which is constant throughout the trapped gas in equilibrium:

$$n(\mathbf{r}) = n(\mu_0 - U(\mathbf{r}), a, T) \tag{7}$$

We see that thanks to the variation of the trapping potential, the density profile samples an extended region of the equation of state. We will show below for the unitary gas how to obtain from such density profiles and the knowledge of $U(\mathbf{r})$ alone the equation of state of the system. The local density approximation will be valid for short-range interactions and as long as we can neglect the discrete nature of the single-particle energy levels in the trap, i.e. as long as the range of occupied energy levels is much larger than one. For example at unitarity, the local density approximation will hold even at zero temperature as long as the Fermi energy is much larger than the spacing between energy levels in the trap.

2˙1.1. Zero temperature equation of state. As a simple application of the local density approximation, we can find the density profile of a unitary Fermi gas in the trap. We know that the equation of state must be of the form $\mu = \xi E_F$. Locally, this relates the

potential $U(\mathbf{r})$ to the local Fermi energy $E_F(\mathbf{r})$, given by the local density via $E_F = \frac{\hbar^2}{2m}(3\pi^2 n(\mathbf{r}))^{2/3}$.

$$\mu(\mathbf{r}) = \mu_0 - U(\mathbf{r}) = \xi E_F(\mathbf{r}) = \xi \frac{\hbar^2}{2m}(3\pi^2 n(\mathbf{r}))^{2/3}. \tag{8}$$

The density profile must thus be

$$n(\mathbf{r}) = \frac{1}{3\pi^2}\left(\frac{2m}{\hbar^2}\frac{1}{\xi}\left(\mu_0 - U(\mathbf{r})\right)\right)^{3/2} \tag{9}$$

which is just $1/\xi^{3/2}$ times the density profile of a non-interacting Fermi gas at zero temperature at the same global chemical potential μ_0. A measurement of the local density at the center of the trap where $U(\mathbf{r}) = 0$ yields μ_0/ξ, and a measurement of the potential $V_{\max}$ where the density vanishes yields $\mu_0 = V_{\max}$, thus allowing to determine the Bertsch parameter ξ. For harmonic trapping, where $U(\mathbf{r}) = \frac{1}{2}m\omega^2 r^2$ (anisotropic trapping can be dealt with as well), one can simply measure the size of the atom cloud, i.e. the radius R_μ where the density vanishes, to obtain $\mu_0 = \frac{1}{2}m\omega^2 R_\mu^2$, and the total atom number $N = \int \mathrm{d}^3 r\, n(\mathbf{r})$, related to μ_0 and ξ via $\mu_0 = \sqrt{\xi}\hbar\omega(3N)^{1/3} = \sqrt{\xi}E_{F,\mathrm{trap}}$, where $E_{F,\mathrm{trap}}$ is the Fermi energy of a non-interacting spin mixture with total number N in the same trap. Denoting with R_F the Fermi radius of such a non-interacting spin mixture, i.e. $\frac{1}{2}m\omega^2 R_F^2 = E_{F,\mathrm{trap}}$, we obtain a simple formula for $\xi = \left(\frac{R_\mu}{R_F}\right)^4$. It was used in [22] to obtain an estimate for ξ. However, this determination depends very sensitively on the size measurement R_μ, the trapping frequency and the atom number calibration. Of course, experiments can also create non-interacting Fermi gases with relative ease (either a spin-polarized sample or a weakly interacting gas far away from the Feshbach resonance), and ξ can be obtained by comparing the interacting and non-interacting radii (R_μ and R_F) and total numbers ($N_{\mathrm{non-int.}}$ and $N_{\mathrm{int.}}$) of atom clouds via $\xi = \left(\frac{R_\mu}{R_F}\right)^4 \left(\frac{N_{\mathrm{non-int.}}}{N_{\mathrm{int.}}}\right)^{2/3}$, which only involves relative quantities and is thus free from calibration errors. Of course, experiments are performed at finite temperature, which will lead to a systematic error in the measurement of ξ.

2˙1.2. Viral theorem for the trapped gas at unitarity. A simple Virial theorem holds for a trapped gas at unitarity, relating the total energy E_{Trap} of the gas to an average over the trapping potential [50, 54, 55]:

$$E_{\mathrm{Trap}} = N\left\langle U + \frac{1}{2}\mathbf{r}\cdot\nabla U\right\rangle \tag{10}$$

where $\langle \dots \rangle$ denotes a density-weighted $n(\mathbf{r})$. For a harmonic trapping potential, where $\mathbf{r}\cdot\nabla U = 2U$, it simplifies to

$$E_{\mathrm{Trap}} = 2N\langle U\rangle \tag{11}$$

The theorem directly follows from the scale invariance present at unitarity [54], where no interaction dependent length scale enters the description of the gas. One derivation [50] employs mechanical equilibrium $\nabla P = -n\nabla U$ and the general relation between the pressure and the energy density, Eq. 5. Applied to a local volume ΔV, the local energy density (the sum of kinetic and interaction energy densities) is given by $\mathcal{E} = \frac{3}{2}P$. The total energy is the integral over kinetic, interaction and potential energy densities, i.e. $E_{\mathrm{Trap}} = \int \mathrm{d}^3 r\ (\mathcal{E} + nU)$. Via

$$\int \mathrm{d}^3 r\, \mathcal{E} = \frac{3}{2}\int \mathrm{d}^3 r\, P = -\frac{1}{2}\int \mathrm{d}^3 r\, \mathbf{r}\cdot\nabla P = \frac{1}{2}\int \mathrm{d}^3 r\, n\, \mathbf{r}\cdot\nabla U \tag{12}$$

the Virial theorem follows. Away from unitarity, a more general Virial theorem holds (see below and [55, 56, 57]).

As for harmonic trapping, $\langle U\rangle = \frac{3}{2}m\omega_z^2\langle z^2\rangle$, one may thus simply measure the cloud size to determine the energy of the gas. The Virial theorem at unitarity has been demonstrated experimentally in [50].

The total energy of the trapped cloud not only determines how large the cloud is in the harmonic oscillator potential, but also how fast it expands after switching off the trap. The total energy of a trapped, interacting Fermi gas at or close to resonance was derived from measurements of the cloud size either in trap or after expansion [58, 59, 10, 60, 41, 61]. In the ENS experiment [62], the magnetic field was rapidly switched off to zero. In this case, the interaction energy could be removed before it had been converted to kinetic energy. By comparing the cloud's expansion with immediate or delayed magnetic field switching, the interaction energy was directly measured.

It is possible to obtain the entropy of the trapped gas from size or energy measurements. For this, the magnetic field is adiabatically (meaning isentropically) swept to transform the system into a weakly interacting Fermi gas. The observed size or energy in this regime yields the entropy through known relations for an ideal Fermi gas. This allows the determination of entropy as a function of energy for trapped gases [63]. The homogeneous equation of state obtained from this trap-averaged equation of state is however unreliable due to the necessary derivatives that would need to be taken. In addition, it is difficult to observe signatures of the superfluid phase transition in a trap-averaged equation of state, as only a narrow shell of the trapped atom cloud is critical. Local measurements as presented below are able to obtain the homogeneous equation of state and to directly observe the superfluid phase transition in the density profiles of the gas.

2˙2. *General thermodynamic relations.* – In the micro-canonical description of statistical mechanics, the energy E of the gas, given as a function of the entropy S, particle number N, volume V and scattering length a, serves as the thermodynamic potential that defines the temperature $T = \frac{\partial E}{\partial S}\big|_{N,V,a}$, the pressure $P = -\frac{\partial E}{\partial V}\big|_{S,N,a}$, and the chemical potential $\mu = \frac{\partial E}{\partial N}\big|_{S,V,a}$. The scattering length a can be viewed as yet another intensive thermodynamic variable. The change in the energy of the system as the scattering length is adiabatically varied is measured by the so-called contact [64, 57, 65, 53]. Such

an adiabatic change in a is possible experimentally via a Feshbach resonance through the change of an external magnetic field. We define the extensive contact $\mathcal{C}$ as the variable conjugate to the negative of the inverse scattering length $1/a$, i.e.

$$\mathcal{C} = -\left.\frac{\partial E}{\partial a^{-1}}\right|_{S,N,V} \tag{13}$$

The contact measures the probability for two particles to be within a short distance of each other (see below section **2**˙4) and is thus a positive quantity. The energy thus increases as a^{-1} is decreased. This is obvious at zero temperature, where for weak attractive interactions (a^{-1} large and negative), we have a Fermi gas with positive energy $E = \frac{3}{5}NE_F$, while in the regime where a^{-1} is large and positive, atoms are paired in tightly bound molecules of negative binding energy $E_B = -\hbar^2/ma^2$ and $E = \frac{N}{2}E_B < 0$. Including the contact as an extensive thermodynamic quantity, the first law of thermodynamics is written as

$$\mathrm{d}E = T\,\mathrm{d}S + \mu\,\mathrm{d}N - P\,\mathrm{d}V - \mathcal{C}\,\mathrm{d}a^{-1} \tag{14}$$

We have seen that the grand-canonical description of the gas with fixed chemical potential μ instead of fixed number N as well as fixed temperature T instead of fixed entropy S is well suited for the study of trapped atomic gases. The relevant thermodynamic potential is the grand-canonical potential

$$\Omega(T,\mu,V,a) \equiv E - TS - \mu N \tag{15}$$

with total derivative

$$\mathrm{d}\Omega = -S\,\mathrm{d}T - N\,\mathrm{d}\mu - P\,\mathrm{d}V - \mathcal{C}\,\mathrm{d}a^{-1}. \tag{16}$$

The contact is thus also written as $\mathcal{C} = -\left.\frac{\partial\Omega}{\partial a^{-1}}\right|_{T,\mu,V}$. Since V is the only extensive variable that Ω depends on, and since Ω itself is extensive, we have $\Omega(T,\mu,\alpha V,a) = \alpha\,\Omega(T,\mu,V,a)$ for any scaling factor α. It follows for the pressure that $P(T,\mu,a) = -\left.\frac{\partial\Omega}{\partial V}\right|_{T,\mu,a} = -\frac{\Omega}{V}$. This yields the fundamental relation

$$E = TS + \mu N - PV \tag{17}$$

Using the first law, we obtain for the total derivatives the Gibbs-Duhem equation

$$S\,\mathrm{d}T + N\,\mathrm{d}\mu - V\,\mathrm{d}P + \mathcal{C}\,\mathrm{d}a^{-1} = 0 \tag{18}$$

that provides an important relationship between the intensive variables of the gas.

2˙2.1. Obtaining the pressure from density profiles. In particular, for a trapped atom cloud at a given temperature and fixed, uniform scattering length, we obtain the equation for hydrostatic equilibrium

$$\mathrm{d}P = n\,\mathrm{d}\mu = -n\,\mathrm{d}U \tag{19}$$

since the local chemical potential $\mu(\mathbf{r}) = \mu_0 - U(\mathbf{r})$ and thus $\mathrm{d}\mu = -\mathrm{d}U$. The pressure at any given point in the trap thus simply results from integrating the density profile $n(U)$:

$$P(U) = \int_{-\infty}^{\mu} \mathrm{d}\mu'\, n(\mu') = \int_{U}^{\infty} \mathrm{d}U'\, n(U') \tag{20}$$

2˙2.2. "Magic formula" for harmonic trapping. In the case of a harmonic trap, there follows a simple relation [66, 67] between the pressure and the doubly integrated density profile $n_{1\mathrm{D}}(z) = \int \mathrm{d}x\mathrm{d}y\, n(x,y,z)$. We take for simplicity a cylindrically symmetric harmonic trap, $U(x,y,z) = \frac{1}{2}m\omega_\perp^2\rho^2 + \frac{1}{2}m\omega_z^2 z^2$ with $\rho^2 = x^2 + y^2$. We then have

$$n_{1\mathrm{D}}(z) = \int \mathrm{d}x\mathrm{d}y\, n(x,y,z) = 2\pi \int_0^\infty \mathrm{d}\rho\, \rho\, n(\rho,z) \tag{21}$$

On the other hand, for fixed z we have $\mathrm{d}U = m\omega_\perp^2\,\rho\,\mathrm{d}\rho$, so the local pressure $P(z) \equiv P(\mu_0 - U(0,0,z), T, a)$ at position $(0,0,z)$ in the trap is just given by

$$P(z) = \int_{U(0,0,z)}^{\infty} \mathrm{d}U'\, n(U') = m\omega_\perp^2 \int_0^\infty \mathrm{d}\rho\, \rho\, n(\rho,z) = \frac{m\omega_\perp^2}{2\pi}\, n_{1\mathrm{D}}(z) \tag{22}$$

The doubly integrated profile can be directly measured in experiments. Absorption images yield the column density $n_{2\mathrm{D}}(y,z) = \int \mathrm{d}x\, n(x,y,z)$, and the doubly integrated profile or line density is obtained via one more integration along the y-axis.

This relation has allowed a series of measurements of the equation of state in strongly interacting Fermi gases, for balanced and spin-imbalanced mixtures, at the Feshbach resonance and in the entire BEC-BCS crossover [35, 37]. In [35], the EoS of the balanced gas was determined in an iterative fashion. For every realization of the experiment, the temperature T was obtained from a co-trapped gas of weakly interacting bosons (^{7}Li), while the chemical potential μ was obtained from fits to the pressure profiles using the portion of the equation of state that was already known at high temperatures. Each cloud profile thus yielded a new portion of the equation of state now valid at lower temperatures. In [37], the equation of state of balanced and imbalanced spin mixtures was studied as a function of interaction strength at low temperatures, which will be discussed in section **2**˙4. We will now present an approach that yields the equation of state at unitarity with high accuracy [38] without relying on the assumption of harmonic trapping.

2˙3. *Universal Thermodynamics of the Unitary Fermi Gas.* – Initial measurements on the thermodynamics of strongly interacting Fermi gases have focused on trap averaged quantities [60, 61, 68] in which the superfluid transition was inherently difficult to observe. The transition is second order, and therefore singular behavior is expected only for second derivatives of the grand potential (or pressure). The local energy density is proportional to the pressure and thus already not sensitive to the transition, but trap averaging reduces any remaining sensitivity further, as only a narrow shell of the gas is critical. Even revealing the critical behavior through the study of *local* thermodynamic quantities is challenging. The emergence of the condensate of fermion pairs in a spin-balanced Fermi gas is accompanied by only minute changes in the density [69] (n is a first order derivative of the grand potential). Therefore, quantities that involve integration of the density over the local potential, such as the energy E [36] (see Eq. 11) and the pressure P [35] (see Eq. 22), are only weakly sensitive to the sudden variations in the thermodynamics of the gas that one expects near the superfluid phase transition [38].

A thermodynamic quantity involving the second derivative of the pressure P is the (isothermal) compressibility

$$\kappa \equiv -\frac{1}{V}\left.\frac{\partial V}{\partial P}\right|_{T,N,a} = \frac{1}{n}\left.\frac{\partial n}{\partial P}\right|_{T,a}, \tag{23}$$

the relative change of the gas density n due to a change in the pressure P. As the change in pressure is related to the change in chemical potential μ of the gas via $\mathrm{d}P = n\,\mathrm{d}\mu$ at constant temperature and scattering length,

$$\kappa = \frac{1}{n^2}\left.\frac{\partial^2 P}{\partial \mu^2}\right|_{T,a} \tag{24}$$

is a second derivative of the pressure (and the grand potential $\Omega = -PV$), and should thus provide a clear signature of the superfluid transition.

A high-precision measurement of the local compressibility, density and pressure across the superfluid phase transition in the unitary Fermi gas was reported in [38], using a trapped, two-spin mixture of fermionic ^{6}Li atoms at a Feshbach resonance [69, 70]. The combination of these three directly measurable, local quantities determines the entire thermodynamics of the homogeneous gas. The method is general and applies to other systems as well, such as Bose gases in three or two dimensions.

2˙3.1. Compressibility equation of state. At unitarity, the grand-canonical equation of state $\Omega(T, \mu, V)$ can be expressed via the pressure $P(\mu, T) = -\Omega/V$. Equivalently, replacing the pressure by the density $n = \frac{\partial P}{\partial \mu}|_T$, one can determine the density EoS $n(\mu, T)$.

The local gas density $n(U)$ can be directly measured as a function of the local potential U from in-situ absorption images of a trapped gas. In [38], the trapping potential was cylindrically symmetric, with harmonic confinement along the axial direction. This symmetry allows to find the 3D density via the inverse Abel transform of the measured

column density [42]. Other than cylindrical symmetry, no other assumption on the shape of the potential is made. Instead, the local potential is directly measured via the atomic density distribution and the accurately known harmonic potential along the axial direction of the atom trap.

The compressibility κ follows as the change of the density n with respect to the local potential U experienced by the trapped gas. As $\mathrm{d}\mu = -\mathrm{d}U$, the compressibility is

$$\kappa = -\frac{1}{n^2}\frac{\mathrm{d}n}{\mathrm{d}U}|_T. \tag{25}$$

The compressibility allows replacing the unknown chemical potential μ in the density EoS $n(\mu, T)$ by its known variation in the atom trap, yielding the equation of state $n(\kappa, T)$. Instead of the a priori unknown temperature, one can use the pressure $P(U) = \int_U^\infty \mathrm{d}U' n(U')$ [66, 67] (see Eq. 20). The resulting equation of state $n(\kappa, P)$ contains only quantities that can be directly obtained from the density distribution. This represents a crucial advantage over methods that require the input of additional thermodynamic quantities, such as the temperature T and the chemical potential μ, whose determination requires the use of a fitting procedure or an external thermometer, as in [36, 35].

The compressibility and the pressure is normalized by the respective quantities at the same local density for a non-interacting Fermi gas at $T = 0$, $\kappa_0 = \frac{3}{2}\frac{1}{nE_F}$ and $P_0 = \frac{2}{5}nE_F$, yielding

$$\tilde{\kappa} \equiv \frac{\kappa}{\kappa_0} = \frac{2}{3}\kappa\, nE_F \qquad \text{and} \qquad \tilde{p} \equiv \frac{P}{P_0} = \frac{5}{2}\frac{P}{nE_F}. \tag{26}$$

As discussed in the introduction, in the unitarity limit the thermodynamics is universal [33], all dimensionless thermodynamic quantities, such as $\tilde{\kappa}$, $\tilde{p}$, T/T_F, μ/k_BT etc. must directly depend on each other. Away from unitarity, an additional dependence on the interaction strength $1/k_Fa$ would appear. On resonance, however, $\tilde{\kappa}$ is a universal function of $\tilde{p}$ only. Every experimental profile $n(U)$, whatever the trapping potential, the total number of atoms or the temperature, must produce the same universal curve $\tilde{\kappa}$ versus $\tilde{p}$. By averaging many profiles, one obtains a low-noise determination of $\tilde{\kappa}(\tilde{p})$.

2˙3.2. Specific heat versus temperature - the Lambda transition in a gas. From the universal function $\tilde{\kappa}(\tilde{p})$ one can obtain *all* other thermodynamic quantities of the unitary gas. First of all, it allows to obtain the relation between the pressure thermometer $\tilde{p} = P/P_0$ and the normalized temperature T/T_F.

To obtain this relation, note that

$$\frac{\mathrm{d}\tilde{p}}{\mathrm{d}(T/T_F)} = -\frac{T_F^2}{T}\left.\frac{\partial\tilde{p}}{\partial T_F}\right|_T = -\frac{T_F}{T}\frac{3}{2}n\left.\frac{\partial\tilde{p}}{\partial n}\right|_T \tag{27}$$

involves the relative change in pressure with density and thus the measured compress-

ibility, as

$$n\left.\frac{\partial P/P_0}{\partial n}\right|_T = \frac{n}{P_0}\left.\frac{\partial P}{\partial n}\right|_T - \frac{nP}{P_0^2}\frac{\partial P_0}{\partial n} = \frac{5}{3}\left(\frac{\kappa_0}{\kappa} - \frac{P}{P_0}\right) \tag{28}$$

This gives the relation [38]

$$\frac{\mathrm{d}\tilde{p}}{\mathrm{d}(T/T_F)} = \frac{T_F}{T}\frac{5}{2}\left(\tilde{p} - \frac{1}{\tilde{\kappa}}\right) \tag{29}$$

The reduced temperature T/T_F thus follows by integration [38]

$$\frac{T}{T_F} = \left(\frac{T}{T_F}\right)_i \exp\left\{\frac{2}{5}\int_{\tilde{p}_i}^{\tilde{p}} \mathrm{d}\tilde{p}\frac{1}{\tilde{p} - \frac{1}{\tilde{\kappa}}}\right\}. \tag{30}$$

Here, $(T/T_F)_i$ is the normalized temperature at an initial normalized pressure $\tilde{p}_i$ that can be chosen to lie in the known high-temperature Boltzmann or Virial regime.

Furthermore, using $E = \frac{3}{2}PV$ valid at unitarity (Eq. 5), one can directly obtain the heat capacity per particle at constant volume [38],

$$\frac{C_V}{k_B N} \equiv \frac{1}{k_B N}\left.\frac{\partial E}{\partial T}\right|_{N,V} = \frac{3}{5}\frac{\mathrm{d}\tilde{p}}{\mathrm{d}(T/T_F)} = \frac{3}{2}\frac{T_F}{T}\left(\tilde{p} - \frac{1}{\tilde{\kappa}}\right). \tag{31}$$

Note that the last equation follows precisely because $\tilde{p}$ only depends on T/T_F and not on another dimensionless variable, such as $1/k_F a$ as would be the case away from unitarity.

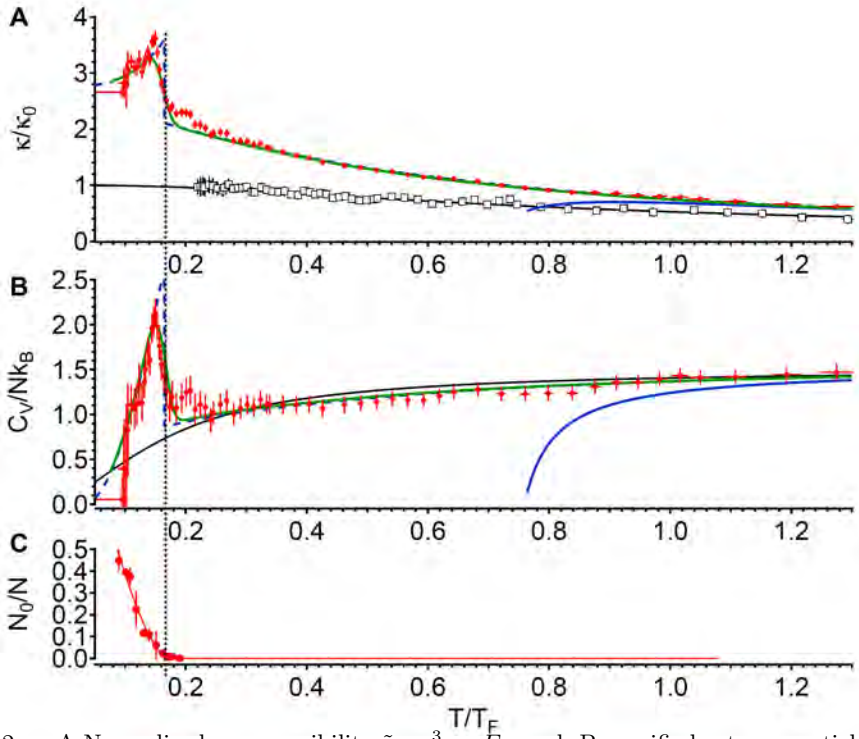

Fig. 2. – A Normalized compressibility $\tilde{\kappa} = \frac{3}{2}\kappa\, n\, E_F$ and B specific heat per particle C_V/Nk_B of a unitary Fermi gas versus reduced temperature T/T_F, shown in solid red circles. The black solid curve shows the theory for a non-interacting Fermi gas, the blue solid curve shows the third order Virial expansion for the unitary gas. Black open squares denote data for a non-interacting Fermi gas. C Condensate fraction at unitarity as determined from a rapid ramp to the molecular side of the Feshbach resonance. The onset of condensation coincides with the sudden rise of the specific heat. From [38].

Fig. 2 shows the normalized compressibility and the specific heat as a function of T/T_F. At high temperatures, the specific heat approaches that of a non-interacting Fermi gas and eventually $C_V = \frac{3}{2}Nk_B$, the value for a Boltzmann gas. A dramatic rise is observed around $T_c/T_F \approx 0.16$, followed by a steep drop at lower temperatures. Such a λ-shaped feature in the specific heat is characteristic of second order phase transitions, as in the famous λ-transition in ^{4}He [71]. Jumps in the specific heat are also well-known from superconductors [72] and ^{3}He [73]. Below T_c, the specific heat is expected to decrease as $\sim \exp(-\Delta_0/k_BT)$ due to the pairing gap Δ_0. At low temperatures $T \ll T_c$ the phonon contribution $\propto T^3$ dominates [74], but is not discernible at the resolution of the experiment.

The critical temperature T_c/T_F was determined directly from the density profiles, finding a sudden rise in the specific heat and the onset of condensation at $T_c/T_F = 0.167(13)$, in agreement with theoretical determinations [75, 74], and Monte-Carlo calculations which give $T_c/T_F = 0.173(6)$ [76] and 0.152(7) [77]. It disagrees with $T_c/T_F = 0.23(2)$ [78], but is close to a later determination of $T_c/T_F \lesssim 0.15(1)$ [79].

We note here that the low-temperature behavior of the equation of state is completely fixed by the value of the parameter ξ, as this fixes the speed of sound for phonons via

$$c_s = \sqrt{\frac{1}{m}\left.\frac{\partial P}{\partial n}\right|_S} \xrightarrow[T\to 0]{} \sqrt{\frac{\xi}{3}}\, v_F \tag{32}$$

where $v_F = \frac{\hbar k_F}{m}$ is the Fermi velocity. We have used $P = \xi P_0 = \frac{2}{5}\xi n E_F$ valid at low temperatures deep in the superfluid regime. The contribution of phonons to the specific heat is then

$$C_V = k_B \frac{2\pi^2}{15} V \left(\frac{k_B T}{\hbar c_s}\right)^3 \tag{33}$$

or in dimensionless form

$$\frac{C_V}{Nk_B} = \frac{\pi^4}{20}\left(\frac{3}{\xi}\right)^{3/2}\left(\frac{T}{T_F}\right)^3, \tag{34}$$

which indeed only depends on the parameter ξ.

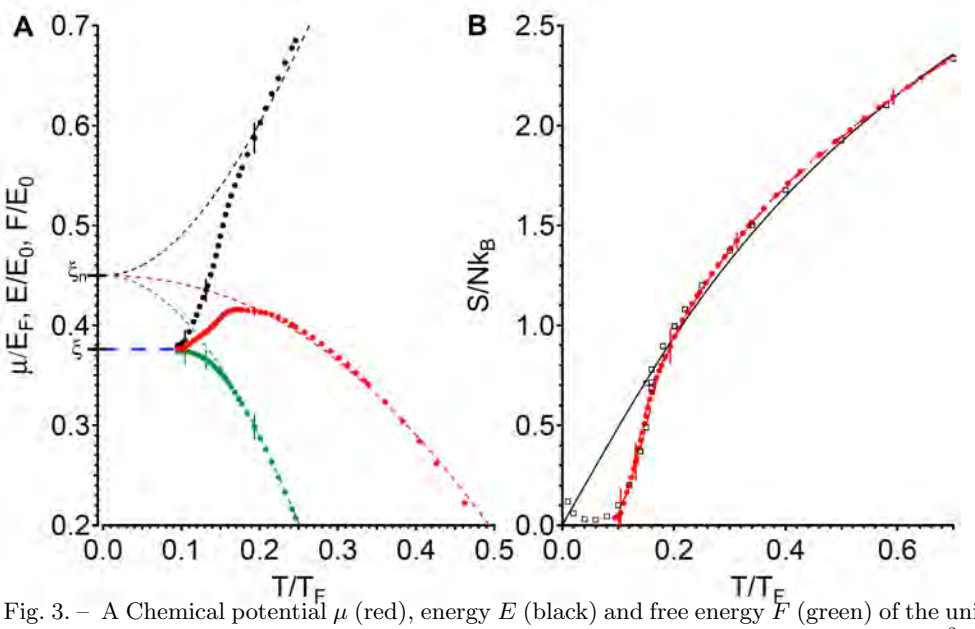

Fig. 3. – A Chemical potential μ (red), energy E (black) and free energy F (green) of the unitary Fermi gas versus T/T_F. μ is normalized by the Fermi energy E_F, E and F by $E_0 = \frac{3}{5}NE_F$. At high temperatures, all quantities approximately track those for a non-interacting Fermi gas, shifted by $\xi_n - 1$ (dashed lines). The peak in the chemical potential signals the onset of superfluidity. In the deeply superfluid regime at low temperatures, μ/E_F, E/E_0 and F/F_0 all approach ξ. B Entropy per particle. At high temperatures, the entropy closely tracks that of a non-interacting Fermi gas (solid line). Below $T/T_F = 0.1$, the entropy per particle reaches values $< 0.04\,k_B$. The open squares are from the self-consistent T-matrix calculation [74]. A few representative error bars are shown, representing one standard deviation. From [38].

2˙3.3. Chemical potential, energy and free energy. From the definition of the compressibility $\kappa = \frac{1}{n^2}\frac{\partial n}{\partial \mu}|_T$ one can obtain the reduced chemical potential μ/E_F as a function of the reduced temperature, see Fig. 3A. In terms of the normalized compressibility $\tilde{\kappa}$, viewed as a function of T/T_F, one has

$$\beta\mu = (\beta\mu)_i - \int_{T_i/T_F}^{T/T_F} \mathrm{d}(\tfrac{T}{T_F})\frac{1}{\tilde{\kappa}}\left(\frac{T_F}{T}\right)^2. \tag{35}$$

Alternatively, one can consider T/T_F as a function of $\tilde{p}$ and obtain

$$\beta\mu = (\beta\mu)_i + \frac{2}{5}\int_{\tilde{p}_i}^{\tilde{p}} \mathrm{d}\tilde{p}\,\frac{T_F}{T}\frac{1}{1-\tilde{\kappa}\tilde{p}}. \tag{36}$$

Around $T/T_F \sim 0.25$ to 1, the chemical potential is close to that of a non-interacting Fermi gas, shifted by $(\xi_n - 1)E_F$ due to interactions present already in the normal state, with $\xi_n \approx 0.45$. However, unlike a normal Fermi gas, the chemical potential attains a maximum of $\mu/E_F = 0.42(1)$ at $T/T_F = 0.171(10)$, and then decreases at lower temperatures. This is expected for a superfluid of paired fermions [74]. As the temperature is increased from zero in a superfluid, the first excitations that emerge are phonons. They increase the chemical potential μ. In addition, fermion pairs start to break and single fermions contribute increasingly to the chemical potential with increasing temperature. At T_c, μ/E_F must have a sharp change in slope, as observed, because $\mathrm{d}(\mu/E_F)/\mathrm{d}(T/T_F)$ involves the singular compressibility. At low temperatures, the reduced chemical potential μ/E_F saturates to the universal value ξ. As the internal energy E and the free energy F satisfy

$$E(T) > E(T=0) = \frac{3}{5}N\xi E_F = F(T=0) > F(T) \tag{37}$$

for all T, the reduced quantities $f_E \equiv \frac{5}{3}\frac{E}{NE_F} = \tilde{p}$ and $f_F \equiv \frac{5}{3}\frac{F}{NE_F} = \frac{5}{3}\frac{\mu}{E_F} - \frac{2}{3}\tilde{p}$ provide upper and lower bounds for ξ [80], shown in Fig. 3A. The determined value of ξ is $\xi = 0.376(5)$. A slight shift in the Feshbach resonance position, measured in [81], shifts ξ down by 1.6% to $\xi = 0.370(5)$[8], where the first error is the statistical uncertainty, while the second is the systematic error, estimated from the difference in the corrected values of μ/E_F, E/E_0 and F/E_0. This value is consistent with an upper bound $\xi < 0.383$ [82], is close to $\xi = 0.36(1)$ from a self-consistent T-matrix calculation [74], and agrees with $\xi = 0.367(9)$ from an epsilon expansion [83]. It lies below earlier estimates $\xi = 0.44(2)$ [84] and $\xi = 0.42(1)$ [85] via fixed-node quantum Monte-Carlo that provide upper bounds on ξ. The measurement agrees with several less accurate experimental determinations [52], but disagrees with the experimental value 0.415(10) that was used to calibrate the pressure in [35], shown in Fig. 4B.

2˙3.4. Entropy, density and pressure. From the energy, pressure and chemical potential, one can obtain the entropy $S = \frac{1}{T}(E + PV - \mu N)$ (see Eq. 17). Shown in Fig. 4B is the entropy per particle

$$\frac{S}{Nk_B} = \frac{T_F}{T}\left(\tilde{p} - \frac{\mu}{E_F}\right) \tag{38}$$

as a function of T/T_F. At high temperatures, S is close to the entropy of an ideal Fermi gas at the same T/T_F. Down to T_c, neither the non-interacting nor the unitary Fermi gas has $S/N \ll k_B$. Also, the specific heat C_V is not linear in T. Thus it is questionable to identify the normal regime as a Landau Fermi Liquid, although some thermodynamic quantities agree surprisingly well with the expectation for a Fermi liquid (see [35] and [38]). Below about $T/T_F = 0.17$ the entropy starts to strongly fall off compared to that of a non-interacting Fermi gas, indicating the freezing out of single-particle excitations due to formation of fermion pairs. At the critical point one obtains $S_c = 0.73(13)Nk_B$, in agreement with a calculation based on the self-consistent T-matrix approach [74].

From the chemical potential μ/E_F and $T/T_F = \frac{4\pi}{(3\pi^2)^{2/3}}\frac{1}{(n\lambda^3)^{2/3}}$, one can finally obtain the density EoS $n(\mu, T) \equiv \frac{1}{\lambda^3} f_n(\beta\mu)$. The pressure EoS follows as $P(\mu, T) \equiv \frac{k_B T}{\lambda^3} f_P(\beta\mu)$ with

$$f_P = \frac{2}{5}\frac{T_F}{T}\tilde{p}\, f_n(\beta\mu). \tag{39}$$

Fig. 4B shows the density and pressure normalized by their non-interacting counterparts at the same chemical potential and temperature. For the normal state, a Bold Diagrammatic Monte-Carlo calculation agrees well with the experiment [39].

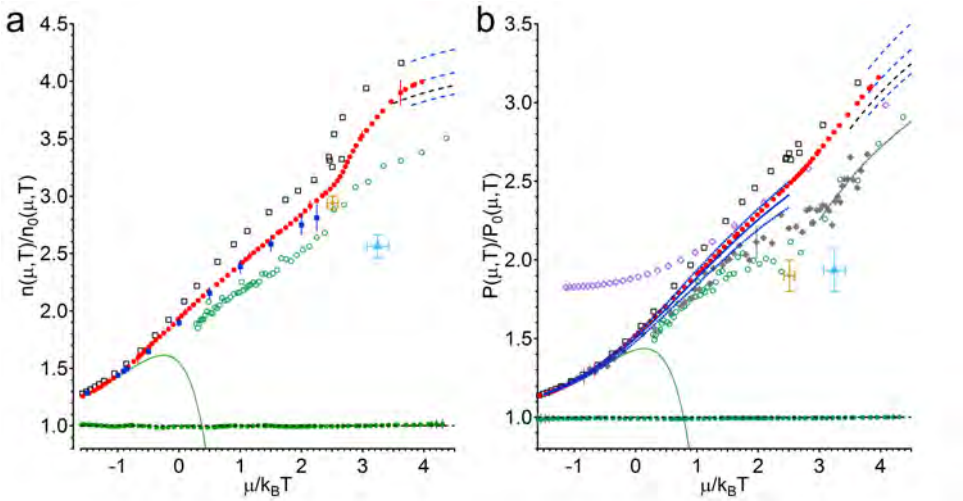

Fig. 4. – A Density and B pressure of a unitary Fermi gas versus μ/k_BT, normalized by the density and pressure of a non-interacting Fermi gas at the same chemical potential μ and temperature T. Red solid circles: experimental EoS. Dashed lines: low-temperature behavior with $\xi = 0.364, 0.376$ and 0.389. Black dashed line: low-temperature behavior from the ξ upper bound $\xi = 0.383$ [82]. Green open circles and black dashed line at 1.0: MIT experimental density and pressure, and theory for the ideal Fermi gas. Blue solid squares (blue band): Diagrammatic Monte-Carlo [39] for density (pressure). Solid green line: 3rd order Virial expansion. Open black squares: self-consistent T-matrix [74]. Open green circles: [78]. Orange star: [76]. Blue star: [77]. Solid diamonds: ENS experiment [35]. Open diamonds: Tokyo experiment [36]. From [38].

Thermal expansivity from Maxwell relation. Since $C_V/N = \frac{3}{2}\frac{1}{n}\left.\frac{\partial P}{\partial T}\right|_{N,V}$, we can make use of the relation

$$\left.\frac{\partial P}{\partial T}\right|_{N,V} = -\frac{\left(\frac{\partial V}{\partial T}\right)_{P,N}}{\left(\frac{\partial V}{\partial P}\right)_{T,N}} = \frac{\alpha}{\kappa} \tag{40}$$

where α is the thermal expansivity (the expansion coefficient) of the gas. This gives us for α the relation

$$\alpha = \frac{2}{3} n\kappa \frac{C_V}{N} = \frac{5}{2}\frac{1}{k_B T}\left(P\kappa - \frac{3}{5}\right) \tag{41}$$

Specific heat at constant pressure. Further use of thermodynamic relations yields the specific heat at constant pressure

$$\frac{C_P}{N} = \frac{C_V}{N} + \frac{T\alpha^2}{n\kappa} \tag{42}$$

$$= \frac{C_V}{N} + \frac{25}{4}\frac{1}{n\kappa T}\left(P\kappa - \frac{3}{5}\right)^2 \tag{43}$$

which reduces to the well-known expression $C_P/N = C_V/N + 1k_B$ in the classical limit where $P\kappa \to 1$ and $n\kappa\, k_B T \to 1$.

Speed of sound. The speed of sound c of the gas directly follows from the adiabatic change of pressure with density. As constant entropy per particle implies constant P/P_0, we have $mc^2 = \left.\frac{\partial P}{\partial n}\right|_{S,N} = \frac{P}{P_0}\frac{\partial P_0}{\partial n} = \frac{5}{3}\frac{P}{n}$. The speed of sound, normalized by the Fermi velocity v_F, is thus given by

$$\frac{c}{v_F} = \sqrt{\frac{5}{3}\frac{1}{m}\frac{P}{n}} = \sqrt{\frac{1}{3}\tilde{p}} \tag{44}$$

with the limiting value at zero temperature $\frac{c}{v_F} = \sqrt{\frac{\xi}{3}}$. The speed of sound as a function of temperature at unitarity was measured in [17] (see section **??**).

2˙4. *Equation of state in the BEC-BCS crossover - The contact.* – As we move away from unitarity and vary the scattering length a, the thermodynamic quantity governing the change of the thermodynamic quantities with a is the contact [49, 64, 57, 86, 53] $\mathcal{C} = -\frac{\partial E}{\partial a^{-1}}\big|_{S,N,V}$. From the known hamiltonian of the gas we can obtain an explicit expression for the contact via the Hellmann-Feynman theorem

$$\mathcal{C} = -\frac{\partial E}{\partial a^{-1}} = -\frac{\partial \langle H\rangle}{\partial a^{-1}} = -\left\langle \frac{\partial H}{\partial a^{-1}} \right\rangle, \tag{45}$$

where $\langle \dots \rangle$ can denote the expectation value in a given quantum state of the system or a thermal average in the canonical ensemble, with the derivative taken at constant entropy S. The hamiltonian is:

$$\begin{aligned} H = &\sum_{\sigma=\uparrow,\downarrow} \int \mathrm{d}^3 r \left(\frac{1}{2m} \nabla \psi_\sigma^\dagger(\mathbf{r}) \cdot \nabla \psi_\sigma(\mathbf{r}) \right) \\ &+ \int \mathrm{d}^3 r \mathrm{d}^3 r' v(\mathbf{r}-\mathbf{r}') \psi_\uparrow^\dagger(\mathbf{r}) \psi_\downarrow^\dagger(\mathbf{r}') \psi_\downarrow(\mathbf{r}') \psi_\uparrow(\mathbf{r}) \end{aligned} \tag{46}$$

Here $v(\mathbf{r}-\mathbf{r}')$ is the bare potential between two atoms in states $|\uparrow\rangle$ and $|\downarrow\rangle$ (not a low-energy effective interaction). $v(\mathbf{r})$ determines the scattering length, and varying the scattering length means in turn to vary properties of $v(\mathbf{r})$. Thanks to the low temperature and the diluteness of the gas, instead of inserting the true interatomic potential with short range $R \ll n^{-1/3}$ and $R \ll \lambda$, we may use a short-range contact interaction with large momentum cutoff $\Lambda \simeq 1/R$. The interaction part of the hamiltonian then simplifies to $\bar{g} \int \mathrm{d}^3 r\, \psi_\uparrow^\dagger(\mathbf{r}) \psi_\downarrow^\dagger(\mathbf{r}) \psi_\downarrow(\mathbf{r}) \psi_\uparrow(\mathbf{r})$. In order to obtain the same scattering length a as the true potential, the bare coupling strength $\bar{g}$ of the contact potential must be related to the measured low-energy coupling $g = \frac{4\pi\hbar^2 a}{m}$ via

$$\bar{g}^{-1} = g^{-1} - \int \frac{\mathrm{d}^3 k}{(2\pi)^3} \frac{1}{2\epsilon_k} = g^{-1} - \frac{m\Lambda}{2\pi^2\hbar^2} \tag{47}$$

with $\epsilon_k = \hbar^2 k^2/2m$ the single-particle energy, as can be found by solving the t-matrix equation [69]. Introducing the cutoff distance $r_0 \equiv \frac{\pi}{2\Lambda}$, this can be expressed equivalently through the bare scattering length $\bar{a} \equiv m\bar{g}/4\pi\hbar^2$ as

$$\bar{a}^{-1} = a^{-1} - r_0^{-1} \tag{48}$$

A variation in the inverse scattering length a^{-1} is thus equivalent to varying the inverse of the bare coupling strength of a contact interaction. We therefore obtain immediately:

$$\mathcal{C} = -\left.\frac{\partial E}{\partial a^{-1}}\right|_{S,N,V} = -\left\langle \frac{\partial H}{\partial \bar{a}^{-1}} \right\rangle = \frac{4\pi\hbar^2 V}{m} \bar{a}^2 \left\langle \psi_\uparrow^\dagger(0) \psi_\downarrow^\dagger(0) \psi_\downarrow(0) \psi_\uparrow(0) \right\rangle \tag{49}$$

The contact thus measures the probability for particles in $|\uparrow\rangle$ and $|\downarrow\rangle$ to be at the same point in space, i.e. the pair correlation function at zero distance.

Such a relation was first found in one dimension [87], where the pair distribution function was expressed in terms of the change of the gas energy with respect to the one-dimensional scattering length. In [88] the tail of the momentum distribution was also tied to this energy derivative. In three dimensions, such a connection was shown first for the weakly interacting Bose gas [89, 90]. For interacting bosonic or fermionic gases, the change in the energy at constant entropy and density determines the radiofrequency (RF) clock shift, as was shown in [91], where this change was related to the pair correlation function. The clock shift is the average shift of the radiofrequency spectrum with respect to the non-interacting case. It measures the change of the energy as the spins are rotated into a new spin state with new scattering properties [91, 92] - it therefore directly measures the contact. For strongly interacting Fermi gases, the relation was found in [49, 64], and independently in work on the RF clock shift [92]. The relation was also derived from the operator-product expansion in [57], who introduced the short-hand term *contact* for the quantity $C \equiv \frac{4\pi m}{\hbar^2}\mathcal{C}$. The latter quantity was introduced in [49, 64] as the *average contact intensity* that was shown to also govern the large momentum tails of the momentum distribution $n_{\mathbf{k}\sigma}$ for each spin state $\sigma = \uparrow, \downarrow$ in interacting gases:

$$n_{\mathbf{k}\sigma} \xrightarrow[|\mathbf{k}|\to\infty]{} \frac{C}{k^4} \tag{50}$$

This relation is general for contact interactions, and was demonstrated in a diagrammatic theory of the BEC-BCS crossover in [75]. To derive it, one considers that at very large momenta $k \gg k_F$ one probes physics at very short length scale $r \ll n^{-1/3}$, where at most two particles can be near each other. The scattering length a imposes the boundary condition for the wavefunction of two particles of opposite spin at $\mathbf{r}_1$ and $\mathbf{r}_2$ to depend as

$$\phi(\mathbf{r}_1, \mathbf{r}_2) \xrightarrow[\mathbf{r}_1\to\mathbf{r}_2]{} A\left(\frac{1}{r} - \frac{1}{a}\right) \tag{51}$$

on their distance $r = |\mathbf{r}_2 - \mathbf{r}_1|$ as r goes to zero. While A depends on all other particles and thus changes with the many-body state of the system, the dependence on r for small r only involves two-particle scattering. The limiting value is given when $r \to r_0$, the cutoff distance, and $\phi(\mathbf{r}_1, \mathbf{r}_2) = A\left(\frac{1}{r_0} - \frac{1}{a}\right) = -A/\bar{a}$. We have $\left\langle \psi_\uparrow^\dagger(\mathbf{r}_1)\psi_\downarrow^\dagger(\mathbf{r}_2)\psi_\downarrow(\mathbf{r}_2)\psi_\uparrow(\mathbf{r}_1)\right\rangle \xrightarrow[\mathbf{r}_1\to\mathbf{r}_2]{} |\phi(\mathbf{r}_1, \mathbf{r}_2)|^2$ and Eq. 49 thus immediately yields [49, 64]

$$\mathcal{C} = \frac{4\pi\hbar^2 V A^2}{m} \tag{52}$$

or $C = (4\pi)^2 V A^2$. On the other hand, the Fourier transform $\phi_{\mathbf{k}_1,\mathbf{k}_2}$ of $\phi(\mathbf{r}_1, \mathbf{r}_2)$ is dominated by the singular A/r term and will go like $\phi_{\mathbf{k},\mathbf{k}'} \simeq (2\pi)^3 A \frac{4\pi}{k^2}\delta(\mathbf{k} + \mathbf{k}')$ for high

momenta k. The momentum distribution is then

$$n_{\mathbf{k}\sigma} = \sum_{\mathbf{k}'} |\phi_{\mathbf{k},\mathbf{k}'}|^2 \xrightarrow[k\to\infty]{} \frac{(4\pi)^2 V A^2}{k^4} = \frac{C}{k^4} \tag{53}$$

As we deal with contact interactions, it is intuitive that the change in the energy with interaction strength is directly sensitive to the probability for two interacting particles to be at the same point in space. At the same time, at high momenta we are probing physics at short range, so that the tail of the momentum distribution should again be sensitive to pair correlations.

Although the system can be a complicated many-body state, at short enough distance scales the likelihood to find three or more particles nearby becomes negligible, and the behavior of pair correlations must be given by simple two-body physics alone, described at low energies by the scattering length. Only the overall scale of these short-range pair correlations is dependent on the many-body state in question.

It follows that the contact measures the number of pairs in a volume V that have distances smaller than a small distance s. Indeed, integrating the pair distribution function $\left\langle \psi_\uparrow^\dagger(\mathbf{r}_1)\psi_\downarrow^\dagger(\mathbf{r}_2)\psi_\downarrow(\mathbf{r}_2)\psi_\uparrow(\mathbf{r}_1)\right\rangle \xrightarrow[\mathbf{r}_1\to\mathbf{r}_2]{} |\phi(\mathbf{r}_1,\mathbf{r}_2)|^2 \approx \frac{A^2}{r^2}$ over a spherical volume of radius s, one finds [64]

$$N_{\text{pair}} = \frac{Cs}{4\pi} \tag{54}$$

For this result to hold, the distance s must be much smaller than the scattering length a, the interparticle distance $n^{-1/3}$ and the de Broglie wavelength λ, but still much larger than the cutoff distance r_0. Note that the number of pairs is proportional to the distance s, not to the volume $\propto s^3$ as one might expect, precisely because the probability to have pairs at distance s decreases as $1/s^2$.

Due to the divergent behavior of the two-body wavefunction $\phi(\mathbf{r}_1,\mathbf{r}_2) \to A\left(\frac{1}{r}-\frac{1}{a}\right) \to -\frac{A}{a}$, which causes $n_{k\sigma}$ to fall off as C/k^4 at high momenta, the kinetic energy E_{kin} as well as the potential energy E_{pot} each separately diverge (i.e. they depend on the cut-off):

$$E_{\text{kin}} = \sum_\sigma \int \frac{\mathrm{d}^3k}{(2\pi)^3} n_{k\sigma}\epsilon_k \to C\int \frac{\mathrm{d}^3k}{(2\pi)^3}\frac{\hbar^2}{mk^2} = C\frac{\hbar^2\Lambda}{2\pi^2 m} \tag{55}$$

$$E_{\text{pot}} = \bar{g}\left\langle \psi_\uparrow^\dagger\psi_\downarrow^\dagger\psi_\downarrow\psi_\uparrow\right\rangle = \bar{g}V|\phi(\mathbf{0},\mathbf{0})|^2 = \frac{\bar{g}}{\bar{a}^2}VA^2 = \frac{\hbar^2 C}{4\pi m a} - C\frac{\hbar^2\Lambda}{2\pi^2 m} \tag{56}$$

However, as we see, their *sum* is convergent, independent on the cutoff Λ and equal to the energy content of the many-body state [64]:

$$E = E_{\text{kin}} + E_{\text{pot}} = \sum_\sigma \int \frac{\mathrm{d}^3k}{(2\pi)^3}\frac{\hbar^2k^2}{2m}\left(n_{k\sigma} - \frac{C}{k^4}\right) + \frac{\hbar^2 C}{4\pi m a} \tag{57}$$

The relation is general for contact interactions. A similar equation also holds for Bose gases, provided the infinite-cutoff limit $\Lambda \to \infty$ exists [86]. For a (single-component) Bose gas, the spin-sum is omitted in the derivation above, and the interaction term is now (to avoid over-counting) $\frac{1}{2}\bar{g}\int \mathrm{d}^3 r\, \psi^\dagger\psi^\dagger\psi\psi$, resulting in $\frac{\hbar^2 C}{8\pi m a}$ instead of $\frac{\hbar^2 C}{4\pi m a}$ in the second term of Eq. 57, and also to a modified definition of $C = -\frac{8\pi m}{\hbar^2}\frac{\partial E}{\partial a^{-1}}$ that preserves the relation $n_k \to C/k^4$ at high momenta. The relation is thus

$$E_{\text{Bose gas}} = \int \frac{\mathrm{d}^3 k}{(2\pi)^3}\,\frac{\hbar^2 k^2}{2m}\left(n_k - \frac{C}{k^4}\right) + \frac{\hbar^2 C}{8\pi m a} \tag{58}$$

2̇4.1. Energy of molecular Bose-Einstein condensates. To obtain the energy of the gas in the molecular regime of the BEC-BCS crossover, we consider a Bose-Einstein condensate with repulsive interactions described by a scattering length a, at chemical potential μ. Within the mean-field approximation the free energy $G = E - \mu N$ is $G = -\frac{\mu^2 V}{2\bar{g}}$, and $N = -\frac{\partial G}{\partial \mu} = \frac{\mu V}{\bar{g}}$ so that $E = G + \mu N = N\frac{2\pi\hbar^2\bar{a}}{m}n$. G, E and N are all cutoff dependent within the mean-field approximation. The contact is $C = -\frac{8\pi m}{\hbar^2}\,\frac{\partial G}{\partial a^{-1}}\big|_{\mu,V} = \frac{m^2}{\hbar^4}\mu^2 V$. The fact that C is non-zero implies that the momentum distribution of the Bose gas must fall off as C/k^4, i.e. the atoms cannot all be Bose-condensed in the $\mathbf{k} = 0$ state, as the mean-field solution assumes. This is precisely the result of Bogoliubov theory, which shows that boson pairs are coherently excited out of the condensate into $\mathbf{k}, -\mathbf{k}$ pairs of non-zero momentum states. The resulting momentum distribution is given by [93]

$$n_k/V = \frac{\epsilon_k + \mu}{2E_k} - \frac{1}{2} \xrightarrow[k\to\infty]{} \frac{m^2}{\hbar^4}\frac{\mu^2}{k^4} = \frac{C/V}{k^4} \tag{59}$$

where $E_k = \sqrt{\epsilon_k^2 + 2\mu\epsilon_k}$ is the Bogoliubov spectrum. n_k indeed behaves as C/k^4 at large momenta, as it should be. The corrected energy of the Bose condensate, which takes into account the non-zero contact, is thus Eq. 58 with $C = \frac{m^2}{\hbar^4}\mu^2 V$. The integral over momenta in 58 converges, giving

$$E_{\text{BEC}} = -\frac{4}{5\pi^2}\mu\frac{V}{\xi^3} + \frac{m\mu^2 V}{8\pi\hbar^2 a} \tag{60}$$

with the healing length $\xi = \sqrt{\hbar^2/m\mu}$. Eliminating μ in favor of the particle number $N = \int_0^\mu \mathrm{d}\mu' \frac{1}{\mu'}\frac{\partial E}{\partial \mu'} = \frac{\mu V}{g} - \frac{4}{3\pi^2}\frac{V}{\xi^3}$ we recover the famous result by Lee, Huang and Yang [94, 95]

$$E_{\text{BEC}} = N\frac{2\pi\hbar^2 a n}{m}\left(1 + \frac{128}{15\sqrt{\pi}}\left(na^3\right)^{1/2} + \dots\right). \tag{61}$$

Expressed in terms of the particle number, the contact C for the Bose gas is

$$C_{\text{BEC}} = 16\pi^2 a^2 n N\left(1 + \frac{64}{3\sqrt{\pi}}\left(na^3\right)^{1/2} + \dots\right) \tag{62}$$

The number of boson pairs within a distance smaller than s behaves in leading order like Nna^2s, with the simple interpretation that each boson, traveling a short distance s, will collide with $\sim na^2s$ other atoms, as $4\pi a^2$ is the scattering cross section. To apply these formulas to a BEC of molecules, one simply replaces $N \to N/2$ by the number of fermion pairs in a gas of total fermion number N, $m \to 2m$ as the molecule mass is twice the fermion mass, and the scattering length between molecules $a \to a_d \approx 0.6a$ [96]. One also needs to add the binding energy $-\hbar^2/ma^2$ of $N/2$ molecules. The total energy is then

$$E_{\text{Mol. BEC}} = -\frac{N}{2}\frac{\hbar^2}{ma^2} + N\frac{\pi\hbar^2 a_d n}{4m}\left(1 + \frac{128}{15\sqrt{\pi}}\left(\frac{n}{2}a_d^3\right)^{1/2} + \dots\right) \tag{63}$$

For weak interactions, the contact is dominated by the first term, the binding energy of molecules, which contributes $C_{\text{mol}} = \frac{4\pi N}{a}$:

$$C_{\text{Mol. BEC}} = \frac{4\pi N}{a} + \pi^2 Nnaa_d\left(1 + \frac{64}{3\sqrt{\pi}}\left(\frac{n}{2}a_d^3\right)^{1/2} + \dots\right) \tag{64}$$

2˙4.2. Energy of weakly interacting Fermi gas. In the BCS-regime where $1/k_F a \to -\infty$, the energy of an equal spin mixture of fermions with a total number of atoms N is given by [94]

$$E = \frac{3}{5}NE_F\left(1 + \frac{10}{9\pi}k_F a + \frac{4}{21\pi^2}(11 - 2\ln 2)(k_F a)^2 + \dots\right). \tag{65}$$

The contact is dominated by the second term above, the mean-field (or Hartree) energy $N\pi\hbar^2 na/m$, leading to

$$C = 4\pi^2 Nna^2\left(1 + \frac{12}{35\pi}(11 - 2\ln 2)k_F a + \dots\right). \tag{66}$$

Note that Cooper pairing changes the ground state energy only by a minute piece $\propto \rho(E_F)\Delta^2$ where $\rho(E_F)$ is the density of states at the Fermi surface. Δ decays exponentially as $\exp(-\pi/2k_F|a|)$ for vanishing interaction strength while the mean-field energy only decays as $k_F a$. The contact is thus insensitive to Cooper pairing in the BCS regime.

2˙4.3. Near unitarity. Near unitarity, the energy can be expanded in the small parameter $1/k_F a$:

$$E = \frac{3}{5}NE_F\left(\xi - \frac{\zeta}{k_F a} + \dots\right) \tag{67}$$

where ξ is the Bertsch parameter and ζ is related to the contact via

$$C = \frac{6\pi\zeta}{5}Nk_F = V\frac{2\zeta}{5\pi}k_F^4 \tag{68}$$

Theoretical values for ζ are $\zeta \approx 0.8$ from a diagrammatic theory that calculates the full thermodynamics in the BEC-BCS crossover [75, 97], as well as the tails of the radiofrequency (RF) spectra [98] and that was used to determine the average RF cock shift in [99], $\zeta \approx 1$ from the slope of the ground-state energy versus interaction strength from Monte-Carlo calculations [85, 100] used in [92] to estimate the average RF clock shift on resonance, and $\zeta \approx 0.95$ from the study of the pair correlation function [101].

2˙4.4. Pressure relation. In the BEC-BCS crossover, the energy E normalized by the energy of a non-interacting Fermi gas E_0 at the same density is a universal function of T/T_F and $1/k_Fa$, or alternatively a universal function $f_E(s,x)$ of $s \equiv S/Nk_B$ and $x \equiv 1/k_Fa$:

$$E = E_0 f_E\left(\frac{S}{Nk_B}, \frac{1}{k_Fa}\right) \tag{69}$$

Derivatives of E at constant entropy and particle number will thus only involve derivatives with respect to the interaction parameter $1/k_Fa$. From this observation one can deduce a general relation between the energy, pressure and the contact [55]. The contact is the change of $-E$ with scattering length at constant entropy, atom number and volume:

$$\mathcal{C} = -\left.\frac{\partial E}{\partial a^{-1}}\right|_{S,N,V} = -\frac{1}{k_F} E_0 \frac{\partial f_E}{\partial x} \tag{70}$$

The pressure is the change in $-E$ with volume at constant entropy, atom number and scattering length:

$$P = -\left.\frac{\partial E}{\partial V}\right|_{S,N,a} = \frac{2}{3}\frac{E}{V} - E_0 \frac{\partial x}{\partial V}\frac{\partial f_E}{\partial x} = \frac{2}{3}\frac{E}{V} + \frac{1}{3}\frac{\mathcal{C}}{aV} \tag{71}$$

One finds the relation

$$E = \frac{3}{2}PV - \frac{1}{2}\frac{\mathcal{C}}{a}. \tag{72}$$

This is the generalized form, valid in the entire crossover, of the relation Eq. 5 found at unitarity. Along with $E - TS - \mu N = \Omega = -PV$, it follows for the entropy

$$S = \frac{1}{T}\left(\frac{5}{2}PV + \frac{1}{2}\frac{\mathcal{C}}{a} - \mu N\right) \tag{73}$$

2˙4.5. General Virial theorem. When the gas is confined in a trapping potential, we can use the relation between energy, pressure and contact in Eq. 72 in every local volume

ΔV, introducing the contact density $c(\mathbf{r}) = \mathcal{C}/\Delta V$. We have for the energy density $\mathcal{E}$, the sum of kinetic and interaction energy densities:

$$\mathcal{E} = \frac{3}{2}P - \frac{1}{2}\frac{c}{a} \tag{74}$$

The integral over $\frac{3}{2}P$ gives $N\left\langle \frac{1}{2}\mathbf{r}\cdot\nabla U\right\rangle$ (see Eq.12). The total energy of the trapped system $E_{\mathrm{Trap}} = \int \mathrm{d}^3 r\ (\mathcal{E}(\mathbf{r}) + nU(\mathbf{r}))$ is [55, 56]

$$E_{\mathrm{Trap}} = E_{\mathrm{kin}} + E_{\mathrm{int}} + E_{\mathrm{pot}} = N\left\langle U + \frac{1}{2}\mathbf{r}\cdot\nabla U\right\rangle - \frac{1}{2}\frac{\mathcal{C}}{a} \tag{75}$$

In the case of harmonic trapping, we have $N\left\langle \frac{1}{2}\mathbf{r}\cdot\nabla U\right\rangle = N\langle U\rangle = E_{\mathrm{pot}}$ so that one finds [55]

$$E_{\mathrm{kin}} + E_{\mathrm{int}} - E_{\mathrm{pot}} = -\frac{1}{2}\frac{\mathcal{C}}{a} \tag{76}$$

This Virial theorem generalizes the simpler relation found at unitarity. It was tested experimentally in [102] (see Fig. 5).

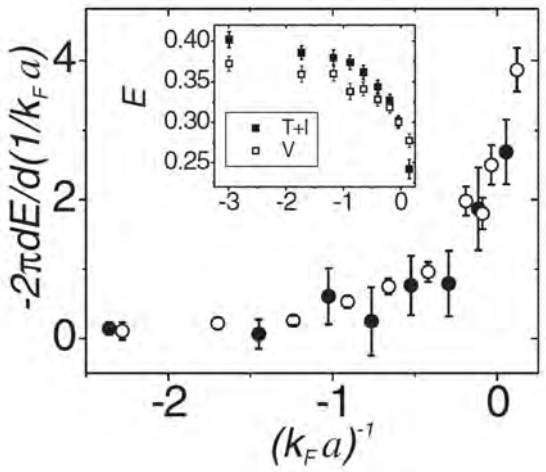

Fig. 5. – Testing the virial theorem. (Inset) The measured potential energy, E_{pot}, and release energy, $E_{\mathrm{kin}} + E_{\mathrm{int}}$, per particle in units of E_F are shown as a function of $1/k_F a$. (Main) Taking a discrete derivative of the inset data, it is found that $2\pi\frac{\mathrm{d}E}{\mathrm{d}(-(k_F a)^{-1})}$ agrees well with the average value of the contact obtained from measurements in Fig. 11. From [102].

2˙5. *Equation of state in the BEC-BCS crossover - Experiments.* – For a system with contact interactions, it is natural that many physical properties are directly tied to the probability for particles to be near each other, i.e. to the contact. We therefore find the contact in vastly different experimental contexts, from radiofrequency spectroscopy [20, 91, 92, 103, 102, 104], Bragg spectroscopy [105] and photoassociation [13], to measurements of the momentum distribution of the gas [106, 102], the variation of the system's energy with interaction strength [10, 102], the structure factor [107, 105, 108, 109], pair correlations [101], viscosity [110, 29] and generally the equation of state of the gas [37].

2˙5.1. Radiofrequency Spectroscopy. Radiofrequency (RF) spectroscopy has been an invaluable tool to detect correlations, interactions and pairing in strongly interacting Fermi gases [19, 20, 91, 111, 21, 22, 112, 113, 23, 24, 45]. In the typical setting, the gas is initially in a two-state mixture of (hyperfine) spin states, say $|1\rangle$ and $|2\rangle$. In RF spectroscopy, a short pulse (typically ~ 1 ms, much longer than the characteristic time $\hbar/E_F \sim 10\,\mu$s) transfers atoms from state $|2\rangle$, say, into a third, initially unoccupied spin state $|3\rangle$. In the absence of interactions the necessary RF frequency for resonant transfer is precisely known (atomic clocks are based on such hyperfine transitions). However, if states $|1\rangle$ and $|2\rangle$ interact, the RF photon needs to make up for the change in the interaction energy as atoms are transferred out of state $|2\rangle$ into the new state $|3\rangle$. The average frequency shift of an RF spectrum $I(\omega)$ is

$$\Omega_c = \langle\omega\rangle = \frac{\int \mathrm{d}\omega\, \omega\, I(\omega)}{\int \mathrm{d}\omega\, I(\omega)} \tag{77}$$

where the offset of the frequency ω is chosen for convenience to be the transition frequency of a single atom in the absence of interactions. Ω_c is also called the clock shift, as density-dependent interactions limit the accuracy of atomic clocks.

Absence of the clock shift in a two-state mixture of fermions. One might attempt to naively obtain the clock shift by taking the difference in energies of a state with N_1 atoms in state $|1\rangle$, N_2 atoms in state $|2\rangle$, versus a state where only $N_2 - 1$ atoms are in state $|2\rangle$, and one additional atom in state $|3\rangle$ - i.e., the difference in chemical potentials that an atom has in the final and the initial state. However, this simple accounting will generally fail, as these two states necessarily have different entropies and cannot be connected by a coherent interaction such as the RF drive. As a simple example, consider driving a transition from $|1\rangle$ to $|2\rangle$, with no third state involved. Let the coupling constant for scattering between states $|1\rangle$ and $|2\rangle$ be $g_{12} = 4\pi\hbar^2 a_{12}/m$, where a_{12} is the scattering length between the two states (note that there is no s-wave contact interaction between two fermions of the same spin). Ignoring the coherent nature of the RF coupling, simple accounting, say within mean-field, would find as the required frequency shift $\hbar\Omega_c = g_{12}(N_1-1)(N_2+1)/V - g_{12}N_1N_2/V \approx g_{12}(n_1-n_2)$, i.e. the difference in chemical potentials of $|1\rangle$ and $|2\rangle$. However, the correct result is zero (and for bosons it is twice as

large as the naive result [114, 91]). The RF frequency drive does not incoherently take out an atom from state $|1\rangle$ and puts it into state $|2\rangle$. Instead, it coherently rotates atoms in state $|1\rangle$ into a superposition state $|1,\theta\rangle = \cos\theta\,|1\rangle + \sin\theta\,|2\rangle$, while atoms in state $|2\rangle$ are at the same time rotated into the orthogonal superposition $|2,\theta\rangle = \cos\theta\,|2\rangle - \sin\theta\,|1\rangle$. We need to calculate the energy cost for this coherent rotation. The scattering length between the rotated states $|1,\theta\rangle$ and $|2,\theta\rangle$ is still equal to a (the scattering cross section is $4\pi a^2(\cos^2\theta + \sin^2\theta) = 4\pi a^2$). Also, the RF drive leaves the spatial part of the many-body wavefunction unchanged. As for s-wave contact interactions fermionic atoms only interact with orthogonal spin partners - and their number has not changed in the coherent drive - there is no change in the interaction energy at all under the influence of the RF drive. Consequently, there is no clock shift [91].

This absence of the clock shift for two-state mixtures of fermions makes fermionic gases highly attractive for atomic clocks. In [115], density-related clock shifts in a fermionic strontium clock were shown to be suppressed to a fractional uncertainty of 10^{-16}. The residual clock shifts were first attributed to s-wave clock shifts made possible by the inhomogeneous excitation of the trapped sample. Such inhomogeneous rotation can rotate spins at a different rate in different regions of the atom cloud, and when atoms having different spin orientations travel through the cloud and meet, they can collide as they are no longer spin-polarized. However, it was later shown that p-wave interactions are stronger than initially believed, and these might have dominated the residual clock shift [116, 117].

Clock shift for transitions to a third state. Generally, the clock shift can be obtained from the change in the interaction energy of the system per transferred particle as atoms are coherently rotated into a new spin state [91]:

$$\hbar\Omega_c = \left.\frac{\mathrm{d}E_{\mathrm{int}}}{\mathrm{dN}_2}\right|_S \tag{78}$$

where $\mathrm{d}N_2$ is the number of particles transferred from state $|2\rangle$ into the final state. Note that the coherent RF drive preserves entropy.

In the above case for an RF drive between $|1\rangle$ and $|2\rangle$, the interaction energy is invariant and the clock shift is zero. However, when one drives RF transitions from state $|2\rangle$ to a new final state $|3\rangle$ that has different interactions with the interacting partner state $|1\rangle$ than state $|2\rangle$, there will be a clock shift.

To treat this case, the interaction hamiltonian must now include possible interactions between all spins:

$$H_{\mathrm{int}} = \sum_{i<j} \int \mathrm{d}^3 r \mathrm{d}^3 r'\, v_{ij}(\mathbf{r}-\mathbf{r}')\psi_i^\dagger(\mathbf{r})\psi_j^\dagger(\mathbf{r}')\psi_j(\mathbf{r}')\psi_i(\mathbf{r}) \tag{79}$$

Here, $v_{ij}(\mathbf{r}-\mathbf{r}')$ is the bare potential between two atoms in state $|i\rangle$ and $|j\rangle$ (not a low-energy effective interaction). The (spatially uniform) RF field couples the states $|2\rangle$ and $|3\rangle$, and is represented by $H_{\rm rf}=\mathcal{B}(t)Y$ with the pseudospin-flip operator

$$Y = i\int \mathrm{d}^3r \left(\psi_3^\dagger(\mathbf{r})\psi_2(\mathbf{r}) - \psi_2^\dagger(\mathbf{r})\psi_3(\mathbf{r})\right), \tag{80}$$

where $\mathcal{B}(t)=2\omega_R\cos\omega t$, with ω_R the Rabi frequency. The RF clock shift is simply the change in energy per $|2\rangle$ atom required to rotate all $|2\rangle$ atoms infinitesimally into state $|\beta\rangle=\cos\theta\,|2\rangle+\sin\theta\,|3\rangle$. This rotation transforms the many-body state $|12\rangle$ into a state $|1\beta\rangle=e^{i\theta Y}\,|12\rangle$ of $|1\rangle$ and $|\beta\rangle$ atoms, with the same spatial many-particle wave function as $|12\rangle$. The energy difference of the two states is thus $\delta E=\langle 1\beta|\,H\,|1\beta\rangle-\langle 12|\,H\,|1\beta\rangle\to\frac{1}{2}\theta^2\,\langle 12|\,[[Y,H],Y]\,|12\rangle$ to second order in θ. Since the number of atoms δN_2 transferred from $|2\rangle$ to $|3\rangle$ is $N_2\theta^2$, we have for the clock shift [92]

$$\Omega_c = \frac{1}{2N_2}\,\langle 12|\,[[Y,H],Y]\,|12\rangle \tag{81}$$

a result valid for superfluid and normal phases. The general expression for the clock shift in terms of the interactions is

$$\Omega_c = \frac{1}{n_2}\int \mathrm{d}^3r\,[v_{13}(\mathbf{r})-v_{12}(\mathbf{r})]\left\langle\psi_1^\dagger(\mathbf{r})\psi_2^\dagger(\mathbf{0})\psi_2(\mathbf{0})\psi_1(\mathbf{r})\right\rangle \tag{82}$$

For short-range contact interactions with coupling constants $\bar{g}_{ij}=4\pi\hbar^2\bar{a}_{ij}/m$ and cut-off Λ as introduced above, one finds [92]

$$\Omega_c = \frac{1}{n_2}\,(\bar{g}_{13}-\bar{g}_{12})\left\langle\psi_1^\dagger(\mathbf{0})\psi_2^\dagger(\mathbf{0})\psi_2(\mathbf{0})\psi_1(\mathbf{0})\right\rangle \tag{83}$$

An immediate way to find this result is to observe via Hellmann-Feynman that $\delta E=\delta\,\langle H\rangle=\langle\delta H\rangle=\delta(\bar{g})\left\langle\Psi_1^\dagger\Psi_2^\dagger\Psi_2\Psi_1\right\rangle$, where $\delta(\bar{g})=\bar{g}_{13}-\bar{g}_{12}$ is the change in the bare coupling strength for a transferred atom. As before, the correlation function is given by the change of the energy density with $\bar{g}_{12}$ at constant entropy, $\left\langle\Psi_1^\dagger\Psi_2^\dagger\Psi_2\Psi_1\right\rangle=\partial E/\partial\bar{g}_{12}|_S$. Expressing the bare coupling strengths $\bar{g}_{ij}$ in terms of the renormalized coupling strengths and taking the cut-off distance r_0 to be independent of the states of the atoms, one finds, for scattering lengths much larger than r_0, [92, 99]

$$\Omega_c = \frac{1}{N_2}\left(\frac{1}{a_{13}}-\frac{1}{a_{12}}\right)\left.\frac{\partial E}{\partial a_{12}^{-1}}\right|_{S,N,V} = \left(\frac{1}{a_{12}}-\frac{1}{a_{13}}\right)\frac{\mathcal{C}}{N_2} \tag{84}$$

The RF clock shift thus directly measures the contact $\mathcal{C}$ of the gas per $|2\rangle$ atom times the change in the inverse scattering length. The result has the simple intuitive interpretation that on average, the RF photon has to make up for the change in the many-body energy

per $|2\rangle$ atom as the inverse scattering length is changed from a_{12}^{-1} to a_{13}^{-1}. This change in the energy occurs at constant entropy, as it should be for a coherent drive [91].

The formula explains why in the case of ^{6}Li brought quickly near the 1-2 Feshbach resonance, before molecule formation could occur, a near-zero clock shift was found [20]. The reason is that both a_{13} and a_{12} were large and comparable, suppressing the clock shift according to the formula 84. No divergence occurs if a_{13} or a_{12} become resonant, instead, if both are resonant, or generally if both are equal, the clock shift is zero. The spectrum is then trivially a delta-function centered at the "atomic", unshifted resonance, as the interaction energy does not change during spin-rotation.

For a molecular BEC, the energy is given by $-\frac{N}{2}E_B$ with $E_B = \hbar^2/ma_{12}^2$ and one finds

$$\Omega_c = 2E_B\,(1 - a_{12}/a_{13})\,. \tag{85}$$

The clock shift in the strongly interacting regime can be obtained from Monte-Carlo results for the ground-state energy [85] (see Fig. 6). To apply the result to experimental data, the data must be available in the entire frequency range, beyond a frequency scale $\sim \hbar/ma_{13}^2$, where there are significant contributions to the spectral weight [118, 119]. The next section shows why the clock shift is sensitive to these typically far-out wings of the RF spectrum.

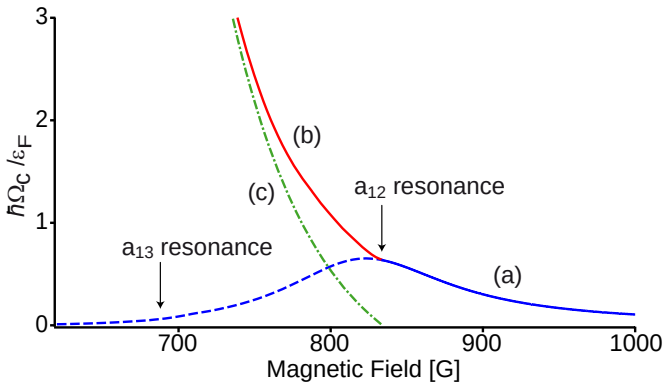

Fig. 6. – Calculated clock shift for a gas of ^{6}Li atoms at zero temperature as a function of magnetic field. The dashed-dot line (c) shows the result Eq. 85 for a non-interacting gas of molecules. Curve (b) is derived from the Monte-Carlo result [85] for the energy of a strongly interacting Fermi gas. The dashed part of curve (a), the difference between (b) and (c), is thus a measure of the many-body contribution to the shift below the 12 resonance. From [92].

In the case of ^{6}Li, the scattering length a_{13} is large (comparable to $1/k_F$) and negative in the entire resonant regime of a_{12}. In this case the clock shift near the Feshbach resonance will be on the order of the Fermi energy, and the spectral weight must necessarily be well localized around this energy scale, i.e. there will not be long tails in the

RF spectrum that would cause the clock shift to be very much larger than E_F. This is a favorable case for the application of the clock shift formula to extract the contact. An early experiment on RF spectroscopy in the strongly interacting regime was performed at the ^{6}Li 1-2 Feshbach resonance [120], and the spectra were indeed observed to be well localized, without long tails (see Fig. 7). The shift of the peak position from the unperturbed atomic resonance was initially interpreted as a possible signature of fermion pairing, but the previous discussion has shown that a shift is expected whenever there is a non-zero contact 6, i.e. whenever there are interactions in the gas. Indeed, no change in the trap-averaged RF spectrum was observed in [112] when imbalancing the spin populations beyond the Clogston-Chandrasekhar limit, where superfluidity and pairing are destroyed (see section **3**). The observed bimodality originates from trap-averaging, as clarified in [22, 118, 23, 121]: signals from the low-density wings of the cloud are unshifted, while signals closer to the center are shifted more strongly. Locally, there is only one single peak, as observed in [22, 23].

The data can thus serve as a direct measurement of the temperature- and interaction dependence of the trap-averaged contact of a strongly interacting Fermi gas. Since the spectra are observed to be rather symmetric, and $1/k_F a_{13} \approx 1$, the measured peak position will quite closely (within a factor of about two [99]) correspond to the average transition frequency, i.e. to the clock shift. Indeed, the interaction dependence of the peak position, qualitatively follows the trend obtained for the clockshift in Fig. 6. In particular, the peak position becomes density dependent in the strongly interacting regime and the BCS regime, as expected for the contact. In addition, the spectra show an increasing shift as the temperature is lowered (see Fig. 8), as expected from the temperature-dependence of the contact.

Locally resolved RF spectra of strongly interacting ^{6}Li at the 12-resonance have been obtained in [22], by applying a short pulse on the $|2\rangle \rightarrow |3\rangle$ transition and immediately imaging the density difference between states $|2\rangle$ and $|1\rangle$ in situ (see Fig. 9). Due to the strong final state interactions $a_{13} \sim 1/k_F$, the spectra were indeed well-localized in frequency. The clock-shift formula at the 12-resonance reads, in terms of $C = \frac{4\pi m}{\hbar^2}\mathcal{C}$ and $\zeta = 5/(6\pi)C/Nk_F$:

$$\Omega_c = -\frac{1}{2\pi}\frac{1}{k_F a_{13}}E_F\frac{C}{N_2 k_F} = -\frac{6}{5}\frac{1}{k_F a_{13}}E_F\zeta \tag{86}$$

The spectral peak in the center of the cloud occurred at $\hbar\Delta\omega = 0.48(4)E_F$. The expected clock-shift is $\Omega_c \approx 1.0E_F$, indeed within a factor of two equal to the peak position [99]. With low-noise spectra the clock shift itself, rather than the peak position, can be determined. Such local measurements of the RF clock-shift in the presence of strong final state interactions thus constitute an ideal probe of the contact. A single spectrum will yield the contact as a function of the reduced temperature T/T_F, which varies across the cloud together with the varying density. The entire shape of the spectra has been successfully described theoretically via a diagrammatic calculation that explicitly includes the final state interaction of the transferred atom with the state $|1\rangle$ medium [118, 119].

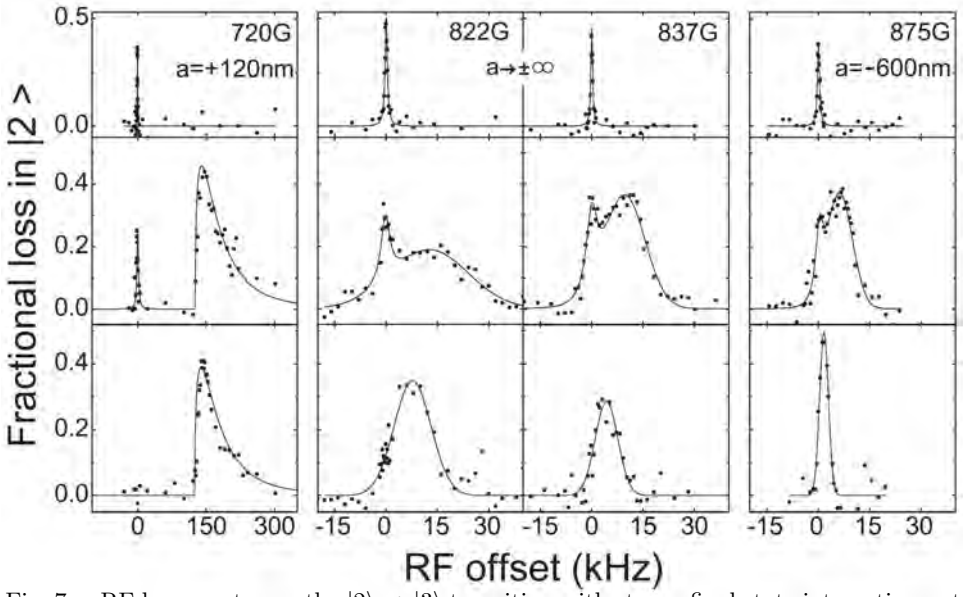

Fig. 7. – RF loss spectra on the $|2\rangle \rightarrow |3\rangle$ transition with strong final state interactions, starting with a 1-2-mixture at various magnetic fields and at different degrees of evaporative cooling. The RF offset is given relative to the atomic transition. Spectra in the molecular regime are observed for $B = 720\,\mathrm{G}$ (first column). Resonantly interacting Fermi gases are studied for $B = 822\,\mathrm{G}$ and $B = 837\,\mathrm{G}$ (second and third columns). The fourth column shows data at $B = 875\,\mathrm{G}$ on the BCS side of the Feshbach resonance. Temperature and Fermi energy decreases from the top row $T' \approx 6T_F$ ($T_F = 15\,\mu\mathrm{K}$), middle row $T' = 0.5T_F$ ($T_F = 3.4\,\mu\mathrm{K}$) to the bottom row, $T' < 0.2T_F$ ($T_F = 1.2\,\mu\mathrm{K}$). The temperature T' was measured in the BEC regime. The solid lines are introduced to guide the eye. From [21].

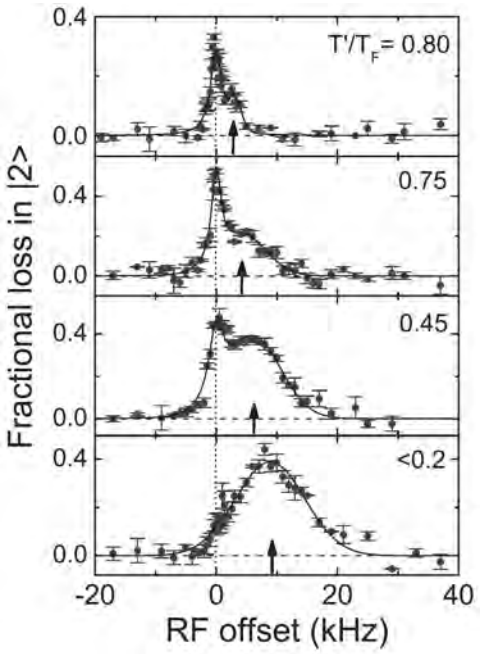

Fig. 8. – RF spectra measured close to the Feshbach resonance at $B = 837\,\mathrm{G}$ and $T_F = 2.5\,\mu K$ for different temperatures T' adjusted by controlled heating. The arrow marks the peak of the "interacting" feature, originating from a strong interaction shift due to the build-up of "contact", initially interpreted as a signal of fermion pairing. From [21].

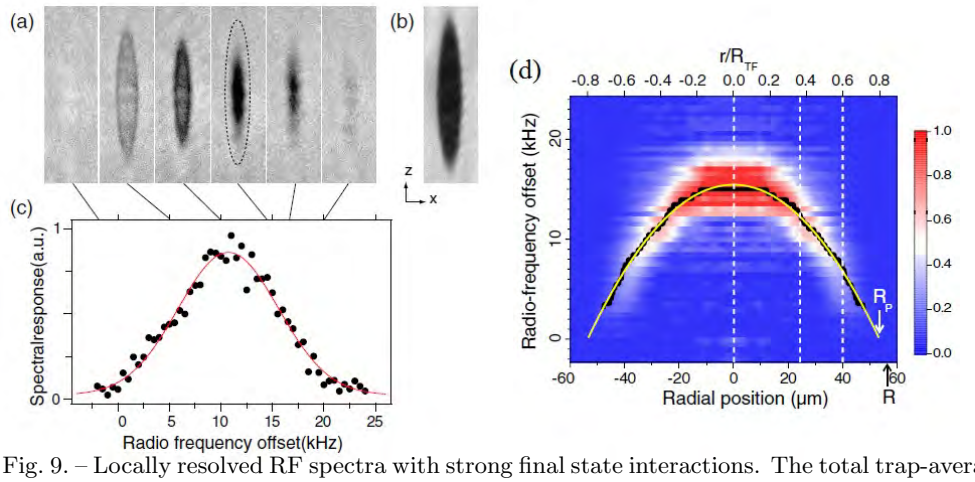

Fig. 9. – Locally resolved RF spectra with strong final state interactions. The total trap-averaged spectrum (c) is shown to originate from the summed response over equi-density shells (a) that each have their resonance shifted according to their local density. The total absorption of the cloud is shown in (b) as a reference. (d) reports the spectra as a function of radial position. Such localized RF spectra can become an ideal probe of the contact via the clock-shift formula. From [22].

Wings of the RF spectrum. The clock shift diverges for vanishing final state interactions ($a_{13} \to 0$), which hints at the fact that short-range physics on the order of r_0 must play an important role for the wings of the RF spectrum. Given the pseudospin-flip operator Y, the frequency dependent transition rate of atoms from state $|2\rangle$ to state $|3\rangle$ can be found by Fermi's Golden rule:

$$I(\omega) = 2\pi\hbar\omega_R^2 \sum_f |\langle f| Y |12\rangle|^2 \, \delta\left(\hbar\omega + E_{12} - E_f\right) \equiv 2\pi\hbar\omega_R^2 \tilde{I}(\omega) \tag{87}$$

where E_{12} is the initial energy of the gas mixture in states $|1\rangle$ and $|2\rangle$ and the sum includes all final eigenstates $|f\rangle$. We can express the mean clockshift as

$$\bar{\omega} = \frac{\int_{-\infty}^{\infty} \mathrm{d}\omega \, \omega I(\omega)}{\int_{-\infty}^{\infty} \mathrm{d}\omega \, I(\omega)} \equiv \omega_0 + \Omega_c \tag{88}$$

where $\omega_0 = \epsilon_3 - \epsilon_2$ is the bare energy difference of a single atom in state $|2\rangle$ and $|3\rangle$, due to the hyperfine plus Zeeman energy, and Ω_c is the clock shift. From the first moment of the spectrum, we rederive the result for the clock shift above [92],

$$\int_{-\infty}^{\infty} \mathrm{d}\omega \, \omega \tilde{I}(\omega) = \sum_f \left(E_f - E_{12}\right) |\langle f| Y |12\rangle|^2 \tag{89}$$

$$= \frac{1}{2} \langle 12| \left[[Y, H], Y\right] |12\rangle \tag{90}$$

Since state $|3\rangle$ is initially unoccupied,

$$\int_{-\infty}^{\infty} \mathrm{d}\omega \, \tilde{I}(\omega) = \int \mathrm{d}^3 r \, \mathrm{d}^3 r' \, \langle 12| \psi_2^\dagger(\mathbf{r}) \psi_3^\dagger(\mathbf{r}) \psi_3(\mathbf{r}') \psi_2(\mathbf{r}') |12\rangle \tag{91}$$

$$= N_2. \tag{92}$$

Taking the ratio of these expressions we thus again find Eq. 81 for the clock shift. We may now ask what part of the spectrum $I(\omega)$ might have the largest contribution to the average clockshift. We already know that the clockshift measures short-range correlations. It is thus natural to expect that processes resulting in atoms moving at high momenta, that can probe such short distance correlations, will have a large contribution. To see this, we can look at the final eigenstates $|f\rangle$ that are relevant for the spectrum. In a large box, momentum is a good quantum number and the possible final states can be written $|f\rangle \equiv c_{\mathbf{k},3}^\dagger |12(N-1), \lambda\rangle$ according to the momentum $\hbar\mathbf{k}$ of the free fermion in state $|3\rangle$ having energy $\epsilon_k = \hbar^2 k^2/2m$ (here we will ignore interactions of $|3\rangle$ with other states). The strongly interacting gas that was initially in state $|12\rangle$ will now be in $|12(N-1)\lambda\rangle$, a state with one missing fermion in state $|2\rangle$.The momentum -$\hbar\mathbf{k}$ can in principle be deposited into excitations in the mixture in a multitude of ways, leading to many possible eigenstates $|12(N-1), \lambda\rangle$ with eigenenergies ϵ_λ. However, at

high momenta k much larger than the Fermi momentum, corresponding to a wavelength much shorter than the interparticle distance, the hole is going to propagate without being affected by interactions, and its energy will be ϵ_k, just like that of the free particle in state $|3\rangle$. Only this one final state, $|12(N-1), \mathbf{k}\rangle$, then contributes for each $\mathbf{k}$. The total energy of the final state with one hole in the 12 mixture and a free particle in state $|3\rangle$ is then $E_f \approx E_{12} + 2\epsilon_k$ (compared to ϵ_k we can ignore the chemical potential difference μ between state $|3\rangle$ ($\mu_3 = 0$) and the 12-mixture). The matrix element $\langle f| Y |12\rangle$ reduces to $\langle 12(N-1), \mathbf{k}| c_{2,\mathbf{k}} |12\rangle$. The resonant RF photon will have an energy $\hbar\omega = 2\epsilon_k$, i.e. high momenta correspond to the wings of the RF spectrum. Since the final states are in this case uniquely determined by the momentum $\mathbf{k}$, we have the relation

$$\langle 12| c^\dagger_{2,\mathbf{k}} |12(N-1), \mathbf{k}\rangle \langle 12(N-1), \mathbf{k}| c_{2,\mathbf{k}} |12\rangle = \langle 12| c^\dagger_{2,\mathbf{k}} c_{2,\mathbf{k}} |12\rangle = n_{\mathbf{k}} \tag{93}$$

We then find for the spectrum:

$$\tilde{I}(\omega \to \infty) \approx \sum_k n_{\mathbf{k}}\, \delta(\omega - 2\epsilon_{\mathbf{k}}) \tag{94}$$

$$= \frac{1}{2}\, \rho(\epsilon_k)\, n_k \Big|_{\epsilon_k = \epsilon_k(\omega)} \tag{95}$$

Here, $\rho(\epsilon_k)$ is the free density of states, and $\epsilon_k(\omega) = \omega/2$. Since $n_k \to C/k^4$ at high momenta, we find, with $\rho(\epsilon_k) = \frac{1}{2\pi^2}\frac{mk}{\hbar^2}$:

$$\tilde{I}(\omega) \xrightarrow[\omega\to\infty]{} \frac{1}{4\pi^2} \left(\frac{\hbar^2}{m}\right)^{1/2} \frac{C}{\omega^{3/2}} \qquad (\text{for } a_{13} \approx 0) \tag{96}$$

A measurement of the tails of the RF spectrum thus yields the contact [122, 98, 123]. This result holds for frequencies large compared to the temperature and Fermi energy (all expressed in energy units), but small compared to the energy scale $\hbar^2/ma_{13}^2$ associated with final state interactions. At $\omega \gg \hbar^2/ma_{13}^2$, the wings of the RF spectrum decay with $1/\omega^{5/2}$, which yields a finite clock shift.

A good approximation for the RF spectrum, valid for all frequencies $\omega \ll \hbar^2/ma_{13}^2$, can be given in cases where the state $c_{2\mathbf{k}} |12\rangle$ has a well-defined energy, i.e. when the hole corresponds to a sharp quasi-particle. Then the simple expression Eq. 93 for the matrix element is still correct. The resonant RF photon now has an energy $\hbar\omega = E_k + \epsilon_k - \mu$, where E_k is the sharply defined energy difference between $|12(N-1)\rangle$ and $|12\rangle$ and μ is the chemical potential in the 12-mixture that the free atom in state $|3\rangle$ has given up. The spectrum then reads

$$\tilde{I}(\omega) = \frac{\rho(\epsilon_k)}{1 + \frac{\partial E_k}{\partial \epsilon_k}}\, n_k \Big|_{\epsilon_k = \epsilon_k(\omega)} \tag{97}$$

where again $\epsilon_k(\omega)$ solves the equation $\hbar\omega = E_k + \epsilon_k - \mu$ for ϵ_k. For a gas of tightly bound molecules, we have $\hbar\omega = 2\epsilon_k + |E_B|$, with $E_B = -\hbar^2/ma^2$ the molecular binding

energy, and, since $\phi(r) \propto e^{-r/a}$ we have $n_k = |\phi_k|^2 \propto (1+k^2a^2)^{-2} = (1+2\epsilon_k/|E_B|)^{-2} = (|E_B|/(\hbar\omega))^2$. The spectrum will thus be

$$\tilde{I}_{\rm BEC}(\omega) \propto \sqrt{\hbar\omega - |E_B|}\frac{1}{\omega^2}. \tag{98}$$

For the BEC-BCS crossover mean-field theory with well-defined quasi-particles, we have $1 + \frac{\partial E_k}{\partial \epsilon_k} = 1 + \xi_k/E_k = 2u_k^2$, and one finds

$$\tilde{I}_{\rm BEC-BCS}(\omega) = \frac{1}{2}N_p\ \rho(\epsilon_k)\,|\varphi_k|^2\Big|_{\epsilon_k=\epsilon_k(\omega)} \tag{99}$$

where $\varphi_k = v_k/(u_k\sqrt{N_p})$ is the Fourier transform of the pair wavefunction in the Leggett Ansatz, N_p the number of fermion pairs, $\epsilon(\omega) = \frac{1}{2\hbar\omega}(\hbar\omega - \hbar\omega_{\rm th})(\hbar\omega + \hbar\omega_{\rm th} + 2\mu)$ and $v_k^2/u_k^2\big|_{\epsilon_k=\epsilon(\omega)} = \Delta^2/(\hbar\omega)^2$. With $\rho(E_F) = 3N/4E_F$ the spectrum finally becomes

$$\tilde{I}_{\rm BEC-BCS}(\omega) = \frac{3}{8\sqrt{2}}\frac{N\,\Delta^2}{E_F^{3/2}}\frac{\sqrt{\hbar\omega - \hbar\omega_{\rm th}}}{\hbar^2\omega^2}\sqrt{1 + \frac{\omega_{\rm th}}{\omega} + \frac{2\mu}{\hbar\omega}} \tag{100}$$

In the BEC-limit, where $\Delta = \sqrt{\frac{16}{3\pi}}\frac{E_F}{\sqrt{k_F a}}$, this reduces to

$$\tilde{I}_{\rm BEC}(\omega) = \frac{2}{\pi}N_M\ \sqrt{|E_B|}\frac{\sqrt{\hbar\omega - |E_B|}}{\hbar^2\omega^2}. \tag{101}$$

This is exactly the dissociation spectrum of $N_M = N/2$ non-interacting molecules, consistent with Eq. 98. For high frequencies, from Eq. 96, we read off $C = 8\pi N_M/a$, which is just the contact for a gas of N_M non-interacting molecules found before directly from the energy $E = -N_M\hbar^2/ma^2$ (see Eq. 64).

In the BCS-limit, the result from basic BEC-BCS theory incorrectly predicts the contact to be $\propto N\Delta^2/E_F^2 k_F \propto Nk_F e^{-\pi/k_F|a|}$, which would imply that one could measure the BCS pairing gap via the wings of the RF spectrum, for example. Instead, we know from Eq. 66 that in the limit of weak interactions, the contact of the gas is dominated by the mean-field interaction, $C \propto Nna^2 \propto Nk_F(k_F a)^2$. This is exponentially larger than the result from the basic BEC-BCS theory. The reason for this failure is that the basic theory ignores interactions present already in the normal state, and thus completely misses the mean-field interaction in the gas.

A RF line shape demonstrating the universal tail is shown in Fig. 10b. The trap-averaged contact obtained from this measurement is compared to the result from the momentum distribution in Fig. 10. Also included in this graph are measurements via momentum-resolved radiofrequency spectroscopy, in which the atoms are momentum analyzed after the RF spin flip. This yields the trap-averaged spectral function $A(\mathbf{k}, \omega)$ whose frequency integral is the momentum distribution $n(k)$. This method of obtaining $n(k)$ does not require the interactions to be switched off via magnetic field sweeps, as in

the ballistic expansion method to be described next. The latter can yield a systematically lower apparent contact due to the finite sweep rate.

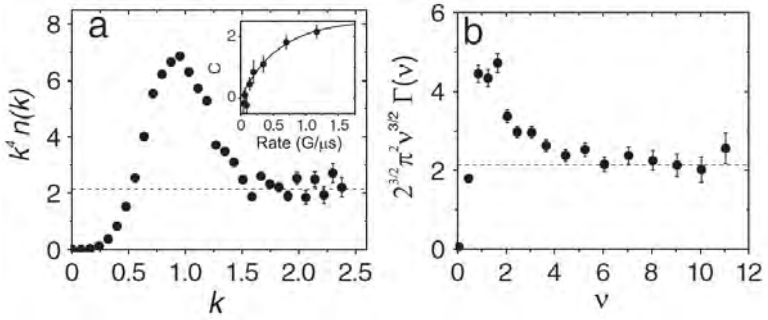

Fig. 10. – Extracting the contact from the momentum distribution and the RF line shape. a) Measured momentum distribution for a Fermi gas at $1/k_F a = -0.08 \pm 0.04$. The wavenumber k is given in units of k_F, and $n(k)$ has been multiplied by k^4. The dashed line corresponds to 2.2. The measured value of C depends on the rate of the magnetic field sweep that turns off the interactions. b) RF spectrum of a unitary Fermi gas. The spectrum is multiplied by $2^{3/2}\pi^2\nu^{3/2}$, which should asymptote to C for large ν. The dashed line corresponds to 2.1. From [102].

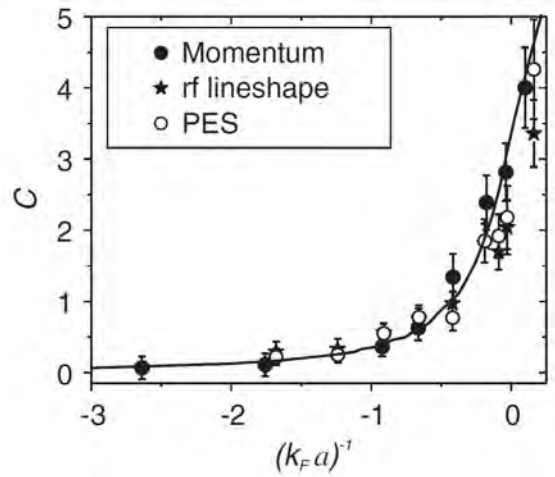

Fig. 11. – The trap-averaged contact is obtained via three different methods. Filled circles - from the wings of the momentum distribution. Open circles - from the wings of $n(k)$ as measured via momentum-resolved RF spectroscopy. Stars - from the wings of RF spectra. The line is a theory curve from [65]. From [102].

2˙5.2. Momentum distribution. The momentum distribution of the atoms in the cloud can be determined by releasing them from the trap and simultaneously switching the scattering length to zero. Such studies have been performed in both ^{40}K [106, 102] and ^{6}Li [62].

Far on the BCS side, one finds the momentum distribution of an ideal Fermi gas in a harmonic trap. On the BEC side, the momentum distribution approaches the squared magnitude of the molecular wave function's Fourier transform. The crossover region smoothly interpolates between these two limits. The modification of the momentum distribution due to the superfluid phase transition is too small to be discernable in these measurements [124].

The far wings of the momentum distribution display the universal tail $n_k = C/k^4$, and measurements of the wings of the momentum distribution thus directly yield the trap-averaged contact (see Fig. 11a)). The results are compared in Fig. 11 with results from RF spectroscopy.

2˙5.3. Photoassociation. As the contact measures the probability for two particles of opposite spin to be near each other, it will govern the rate of photoassociation to a tightly bound molecular state. This experiment was performed in [13], see Fig. 12 and its relation to the contact was demonstrated in [65].

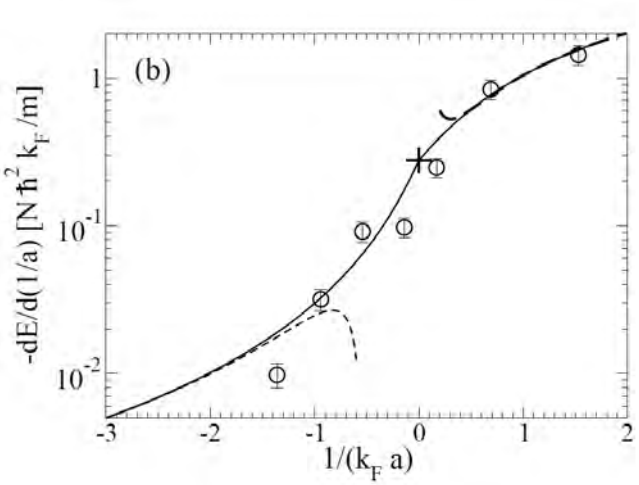

Fig. 12. – The trap-averaged contact $\mathcal{C} = -\mathrm{d}E/\mathrm{d}a^{-1}$ as determined from the photoassociation experiment in [13], from [65]. Solid line: Theoretical prediction combining the Lee-Huang-Yang formulas Eqs. 64, 66 in the weakly interacting regimes with an interpolation of the fixed-node Monte-Carlo results of [85, 101] in the strongly interacting regime. Dashed lines: Analytical predictions in the weakly interacting regimes. Circles: Experimental measurement of the number N_b of closed-channel molecules in a lithium gas [13], combined with the theory from [65] linking $\mathcal{C}$ to N_b.

In the photoassociation of two atoms into a bound molecule of electron spin singlet character, only the singlet admixture of the two-body wavefunction will contribute to the transfer. Near the Feshbach resonance of ^{6}Li, the continuum of scattering states, the so-called open channel, is predominantly triplet in character, while the closed channel molecular state causing the resonance is an electron singlet bound state. The Feshbach resonance mixes the closed channel molecular state with the continuum of scattering states in the open channel resulting in a "dressed" molecular state. The rate of photoassociation measures the closed-channel fraction of the many-body state, or in other words the number of closed-channel molecules N_b. This quantity was measured in [13] and it was verified that the closed channel contribution to the pair wave function is very small throughout the crossover region. It is the smallness of this closed channel fraction that allows for a description of the BEC-BCS crossover in ^{6}Li within an effective single-channel model whose single parameter is the scattering length a. However, it was pointed out in [65] that paradoxically the small number of closed channel molecules is directly related to the contact, i.e. a thermodynamic quantity of the single-channel model.

The reason is that the change in energy with scattering length in the two-channel model comes entirely from the change in energy of the closed-channel molecular state with magnetic field, which gives N_b:

$$\frac{\mathrm{d}E}{\mathrm{d}B} = \mu_b N_b \tag{102}$$

where $\epsilon(B)$ is defined relative to the energy of two unbound atoms at rest (the "threshold"), and μ_b is the difference in magnetic moments of the closed-channel molecular state and the open channel. So one has [65]

$$N_b = \left.\frac{\partial E}{\partial a^{-1}}\right|_S \frac{\mathrm{d}a^{-1}}{\mathrm{d}B}\frac{1}{\mu_b} \tag{103}$$

The derivative $\frac{\mathrm{d}a^{-1}}{\mathrm{d}B}$ is known from two-body physics. The relation between the experimental measurement of N_b and the contact is demonstrated in Fig. 12. For this comparison, a trap average of the local contact from the homogeneous equation of state was performed in order to take into account the spatial variation of the density in the trap.

As seen above, in basic BCS-theory, interactions in the normal state of the gas, such as in Eq. 66, are not taken into account and one finds the incorrect result that the contact is proportional to the square of the pairing gap, $C \propto \Delta^2$. This contribution decays exponentially with interaction strength, $C \propto \exp(-\pi/k_F|a|)$, while already the mean-field energy present already in the normal, non-superfluid Fermi gas contributes $C \propto Nna^2$. The contact as a function of interaction strength is thus not sensitive to the superfluid transition and many-body pairing. However, a possible strong variation as a function of temperature, near the critical temperature of superfluidity, might indicate the phase transition, just like the compressibility and specific heat strongly vary at the transition [38].

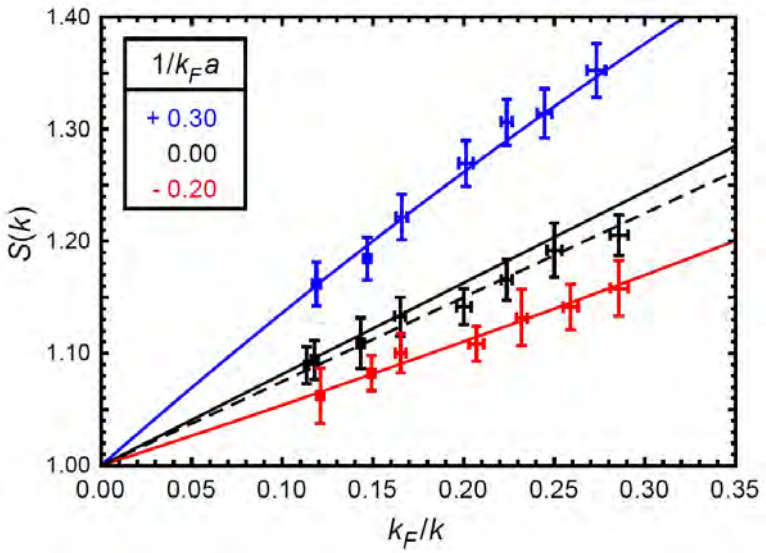

Fig. 13. – Universal dependence of the static structure factor for a strongly interacting Fermi gas. Measured and calculated static structure factor versus k_F/k for $1/k_F a = +0.3$, 0.0, and -0.2. The fitted slope on resonance yields $C/Nk_F = 3 \pm 0.12$ for the trap-averaged contact. From [108].

2˙5.4. Bragg specroscopy. As we have seen, for two points at short distance $r = |\mathbf{r}_1 - \mathbf{r}_2|$, the pair correlation function $\langle \hat{\rho}_\uparrow(\mathbf{r}_1)\hat{\rho}_\downarrow(\mathbf{r}_2)\rangle = \left\langle \psi^\dagger_\uparrow(\mathbf{r}_1)\psi^\dagger_\downarrow(\mathbf{r}_2)\psi_\downarrow(\mathbf{r}_2)\psi_\uparrow(\mathbf{r}_1)\right\rangle$ reduces to the two-body result $|\phi(\mathbf{r}_1,\mathbf{r}_2)|^2$, the probability of finding two particles (of opposite spin) at short range of each other. Its r-dependence is given by two-body physics (Eq. 51), only the prefactor depends on the many-body state via the contact [64]:

$$g^{(2)}_{\uparrow\downarrow}(r) = \frac{V^2}{N_\uparrow N_\downarrow}\left\langle \psi^\dagger_\uparrow(\mathbf{r}_1)\psi^\dagger_\downarrow(\mathbf{r}_2)\psi_\downarrow(\mathbf{r}_2)\psi_\uparrow(\mathbf{r}_1)\right\rangle \tag{104}$$

$$\xrightarrow[\mathbf{r}_1\to\mathbf{r}_2]{} \frac{V}{N}\frac{C}{4\pi^2 N}\left(\frac{1}{r^2}-\frac{2}{ar}\right) \tag{105}$$

$$= \frac{3}{4}\mathcal{I}\left(\frac{1}{k_F^2 r^2}-\frac{2}{k_F^2 ar}\right) \tag{106}$$

valid for $r \ll a$. Here, $\mathcal{I} = C/Nk_F$ is the dimensionless contact.

While pair correlations are difficult to measure directly, the Fourier transform of $g^{(2)}_{\uparrow\downarrow}$ is directly related to the static structure factor $S_{\uparrow\downarrow}(k)$ that is accessible to experimental measurement via Bragg spectroscopy [125]. This technique has been used to determine the static and dynamic structure factor of Bose-Einstein condensates [126, 127, 128, 129]. For strongly interacting Fermi gases it was applied in [105, 108].

In this method, atoms diffract of a moving light grating created by the intersection of two laser beams, of frequencies ω_1 and ω_2 and wavevectors $\mathbf{k}_{\mathrm{L}1}$ and $\mathbf{k}_{\mathrm{L}2}$. The coherent absorption of one photon from one laser beam and stimulated emission into the other laser beam - the first order Bragg scattering process - transfers a momentum $\mathbf{k} = \mathbf{k}_{\mathrm{L}2} - \mathbf{k}_{\mathrm{L}1}$ and an amount of energy $\hbar\omega = \omega_2 - \omega_1$ to the atom. The magnitude of the transferred momentum is $|\mathbf{k}| = 2\hbar k_L \sin(\theta/2)$, where k_L is the magnitude of the wave vector of the laser beams and θ the angle between them. For non-interacting atoms with initial momentum $\hbar\mathbf{q}$, the resonance condition is given by the Bragg condition $\hbar\omega = \epsilon_{q+k} - \epsilon_q = \hbar^2k^2/2m + \hbar\mathbf{q}\cdot\mathbf{k}/m$, which reflects energy and momentum conservation for a free particle. $\hbar\omega_r \equiv \hbar^2k^2/2m$ is the recoil energy associated with the transferred momentum $\hbar\mathbf{k}$, and $\hbar\mathbf{q}\cdot\mathbf{k}/m$ is simply the Doppler shift due to the motion of the atom relative to the grating. The process is thus Doppler sensitive and lends itself to the analysis of the momentum distribution of a non-interacting gas. For an interacting many-body system, however, there are a multitude of ways in which the Bragg momentum can be deposited in the atom cloud. Instead of outcoupling a given momentum class of atoms, one only observes a slight shift in the center-of-mass position of the cloud, after a given time T after the Bragg pulse. This shift is enough to deduce the strength of the system's response to the Bragg grating, which yields the static and dynamic structure factor.

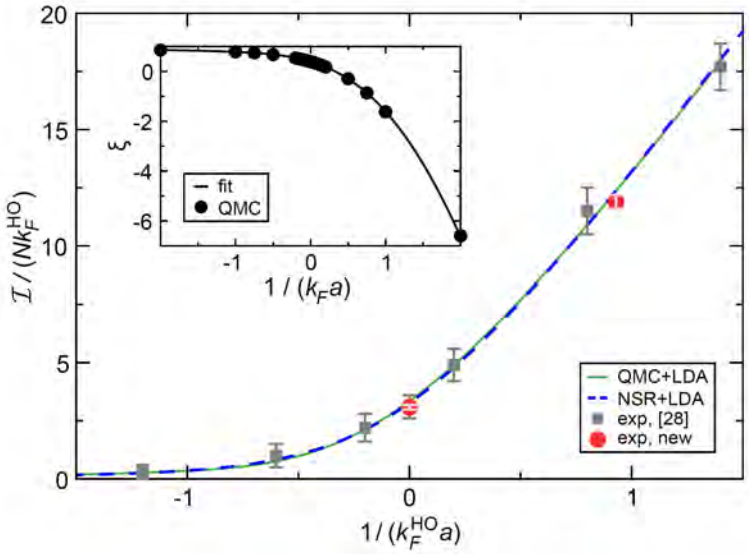

Fig. 14. – The trap-averaged contact as a function of $k_F^{\mathrm{HO}}a$, where k_F^{HO} is the trap-averaged Fermi wavevector. The red grey circles are experimental data from [108], the red data from [109]. Various theory curves are included for comparison (see [109]). At unitarity, the experimental result is $C/Nk_F^{\mathrm{HO}} = 3.06 \pm 0.08$ compared with the quantum Monte-Carlo value of 3.336 and the Nozières-Schmitt-Rink result of 3.26.

The operator associated with the Bragg pulse is $\hat{V}_{\text{Bragg}} = \frac{V}{2}\sum_\sigma \hat{\rho}^\dagger_\sigma(\mathbf{k})e^{-i\omega t}+\hat{\rho}^\dagger_\sigma(-\mathbf{k})e^{+i\omega t}$ where $\hat{\rho}_\sigma(\mathbf{k}) = \sum_q c^\dagger_{\sigma,\mathbf{q}+\mathbf{k}}c_{\sigma,\mathbf{q}}$ is the Fourier transform of the density operator of spin state σ at wave vector $\mathbf{k}$. Starting from an initial many-body state $|g\rangle$ with energy E_g, the excitation rate per particle is given by [127, 125]

$$\frac{2\pi}{N\hbar}\left(\frac{V}{2}\right)^2\sum_f\left|\langle f|\sum_\sigma\hat{\rho}^\dagger_\sigma(\mathbf{k})\,|g\rangle\right|^2\delta(\hbar\omega-(E_f-E_g)) = 2\pi\omega_R^2 S(\mathbf{k},\omega) \tag{107}$$

where, for an equal mixture of atoms in both spin states, as we assume here, the dynamic structure factor $S(\mathbf{k},\omega) = 2\left(S_{\uparrow\uparrow}(\mathbf{k},\omega)+S_{\uparrow\downarrow}(\mathbf{k},\omega)\right)$ and

$$S_{\sigma\sigma'}(\mathbf{k},\omega) = \sum_f \langle g|\,\hat{\rho}_\sigma(\mathbf{k})\,|f\rangle\,\langle f|\,\hat{\rho}^\dagger_{\sigma'}(\mathbf{k})\,|g\rangle\,\delta(\hbar\omega-(E_f-E_g)) \tag{108}$$

are the spin-parallel and spin-anti-parallel structure factors. The static structure factor $S_{\sigma\sigma'}(\mathbf{k})$ is obtained by integrating over all frequencies ω:

$$S_{\sigma\sigma'}(\mathbf{k}) = \frac{2}{N}\hbar\int_0^\infty \mathrm{d}\omega\, S_{\sigma\sigma'}(\mathbf{k},\omega) = \frac{2}{N}\,\langle g|\,\hat{\rho}_\sigma(\mathbf{k})\hat{\rho}^\dagger_{\sigma'}(\mathbf{k})\,|g\rangle \tag{109}$$

The spin-parallel and spin-anti-parallel static structure factors are directly related to the spin-parallel and spin-anti-parallel correlation functions $g_{\uparrow\uparrow}(r)$ and $g_{\uparrow\downarrow}(r)$ via a Fourier transform [125]:

$$\begin{aligned} S_{\uparrow\uparrow}(\mathbf{k}) &= 1+\frac{n}{2}\int \mathrm{d}^3r\,(g_{\uparrow\uparrow}(r)-1)\,e^{i\mathbf{k}\cdot\mathbf{r}} \\ S_{\uparrow\downarrow}(\mathbf{k}) &= \frac{n}{2}\int \mathrm{d}^3r\,(g_{\uparrow\downarrow}(r)-1)\,e^{i\mathbf{k}\cdot\mathbf{r}} \end{aligned} \tag{110}$$

which leads to $S(\mathbf{k}) = 1+n\int \mathrm{d}^3r\,(g(r)-1)\,e^{i\mathbf{k}\cdot\mathbf{r}}$ with $g(r) = (g_{\uparrow\uparrow}(r)+g_{\uparrow\downarrow}(r))/2$. At high momenta, and thus short distances, the spin-parallel structure factor is dominated by auto-correlation, and $S_{\uparrow\uparrow}\to 1$. The spin-anti-parallel structure factor at large momenta is directly sensitive to the probability for two opposite spin particles to be near each other - which is again measured by the contact.

Indeed, from Eq. 106 one obtains directly [125, 108]

$$S_{\uparrow\downarrow}(k\gg k_F) = \frac{I}{4}\frac{k_F}{k}\left(1-\frac{4}{\pi k_F a}\frac{k_F}{k}\right) \tag{111}$$

At unitarity, $S_{\uparrow\downarrow}(k)$ depends linearly on k_F/k, with a slope that directly yields the contact. The measurements of [108] shown in Fig. 13 directly show this universal behavior, and yield a trap-averaged contact of $C/Nk_F = 3\pm 0.12$.

The interaction dependence of the trap-averaged contact, as measured via Bragg spectroscopy [108], shows the qualitative features expected from the previous discussion

(see Fig. 14): The contact is large in the molecular regime, and gradually shrinks in the BCS regime.

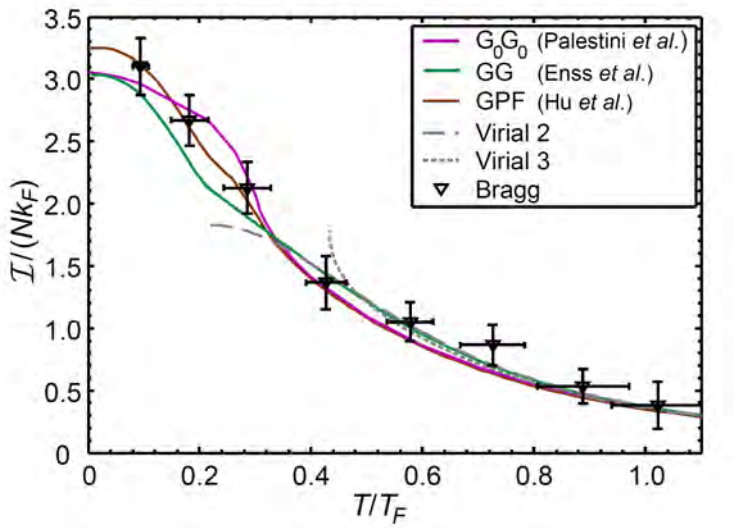

Fig. 15. – Temperature dependence of the trap-averaged contact obtained from Bragg spectroscopy. Solid lines are theoretical predictions (see [130]).

The temperature dependence of the (trap-averaged) contact was measured via Bragg spectroscopy in [130], see Fig. 15. The contact is seen to rise steadily as temperatures are decreased, showing the increasing pair correlations building up in the gas. This build-up starts already far above the superfluid transition. The value at the lowest measured temperatures is about $C = 3.1Nk_F$.

2˙5.5. Temperature dependence of the homogeneous contact. The contact depends on the state of matter of the gas and also on temperature. One may expect that the contact displays a significant change at the normal-to-superfluid transition, similar to the compressibility and specific heat. However, all of the previously discussed experimental determinations of the contact provided trap-averaged results. RF spectroscopy, momentum distribution, photoassociation, Bragg spectroscopy, etc., are typically applied to the entire trapped atom cloud. They are thus insensitive to the sudden change of local properties - the transition occurs only in a narrow shell within the three-dimensional cloud. The experiment in [104] overcomes this problem by selecting a central region in the cloud whose RF response is measured. This yields the contact for a nearly homogeneous gas. Fig. 16 shows such "localized" RF spectra, which again display the universal tail that allows to determine the contact.

Fig. 17 shows the experimentally measured contact as a function of temperature. Coming from high temperatures, the contact steadily grows in the normal phase. At

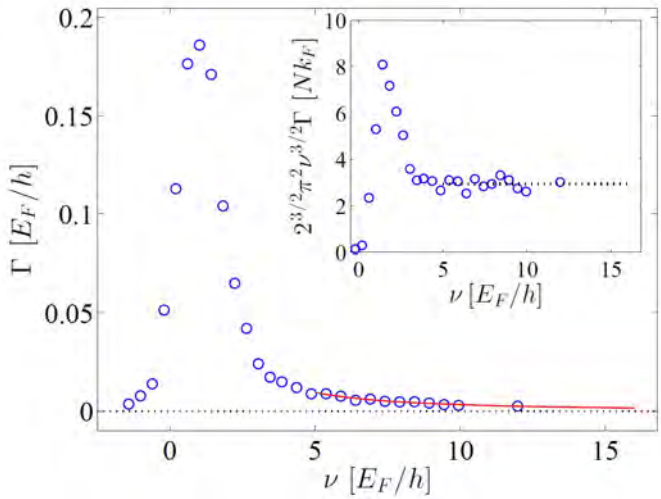

Fig. 16. – An RF spectrum for the unitary Fermi gas at $T/T_F = 0.25$. The red line is a fit to the expected $\propto C/\nu^{3/2}$ behavior at high frequencies ($\nu = \omega/2\pi$). The inset shows the same data multiplied by $\nu^{3/2}$, demonstrating the universal tail. From [104].

$T/T_F \approx 0.16$, close to the critical temperature found in [38], a sudden drop is observed. Theoretical predictions for the contact versus T/T_F differ substantially, from the summation of certain classes of Feynman diagrams [133, 110, 134] to lattice Monte-Carlo simulations [132]. The Bold Diagrammatic Monte-Carlo method, which compared excellently to experimental determinations of the equation of state [39, 38], shows a steadily increasing contact as T/T_F decreases, while Monte-Carlo calculations on the lattice predict the opposite trend in a certain temperature interval and 30% larger values. There is a clear need for further experiments on the homogeneous contact using the various available techniques, for example momentum-resolved RF spectroscopy [24, 102], as well as theoretical calculations in the superfluid phase.

2˙5.6. Collective oscillations. Collective oscillations of the trapped atom cloud have provided a rich source of information on the collisional properties of strongly interacting Fermi gases [135, 12, 25, 26, 136, 28]. In the context of equation of state measurements, one can distinguish between surface modes, that do not change the volume of the gas, and compressional modes that do. The latter type can thus serve as a sensitive probe of the equation of state.

Initial measurements [12, 25, 26] demonstrated a strong variation of compression mode frequencies in the BEC-BCS crossover, reflecting the variation of the density equation of state with interaction strength. In a high-precision version of this experiment [136] (see Fig. 18), the collective mode frequencies were shown to be inconsistent with mean-field theory, but consistent with the equation of state as calculated via Monte-Carlo calcu-

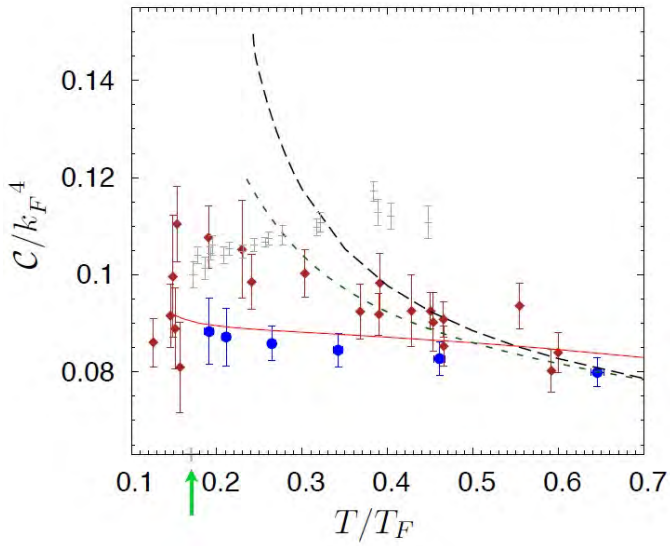

Fig. 17. – The contact of a nearly homogeneous sample of a unitary Fermi gas versus T/T_F at unitarity [104] (brown circles) is compared to a calculation from Bold Diagrammatic Monte-Carlo [131] (blue solid circles). Auxiliary Field Quantum Monte-Carlo results: Grey crosses [132]. From [131].

lations [85, 137]. Importantly, in the BEC-regime the data agreed with the prediction for collective oscillations deduced from Eq. 64 that includes the Lee-Huang-Yang beyond mean-field correction due to quantum depletion [135].

For highly elongated (cigar-shaped) atomic clouds in the hydrodynamic regime, collective mode frequencies can be directly tied to the equation of state. One exception is the lowest energy mode, the sloshing or dipole mode, where the cloud undergoes axial center-of-mass oscillations with a frequency always equal to the axial trapping frequency for a single atom. For harmonic trapping and pair-wise interactions one can show that such center-of-mass motion completely decouples from the relative motion of the particles and is thus insensitive to the state of the system. For a unitary Fermi gas in a harmonic trap, there exists a second exception, the lowest axial breathing mode, as found in [138]. Its oscillation frequency is independent of temperature and only a function of the aspect ratio, as has been checked experimentally [28]. However, the next higher axial mode, for which the deviation of the density has a node in the center of the cloud, is temperature dependent and can serve as a test of the unitary equation of state. The experiment was reported in [28] and provided a first independent check of the equation of state measured in [38].

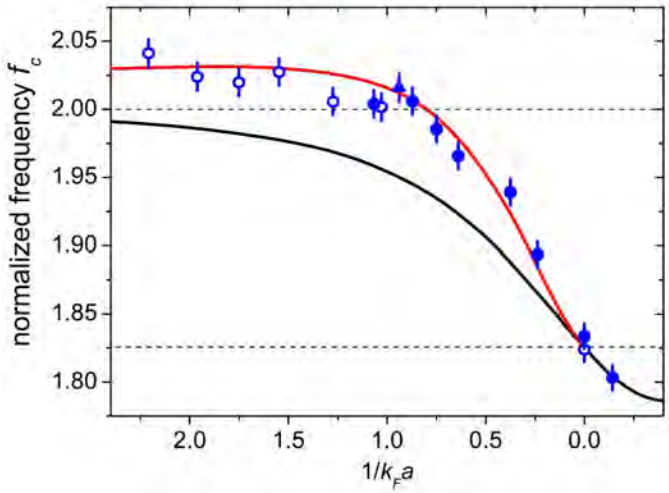

Fig. 18. – Radial compression mode frequency of an elongated atom cloud, normalized by the radial trapping frequency as a function of interaction strength. The theory curves refer to mean-field BCS theory (lower curve) and the quantum Monte-Carlo calculations (upper curve) [85, 137]. The horizontal dashed lines indicate the values for the BEC limit ($f_c = 2$) and the unitarity limit ($f_c = \sqrt{10/3} = 1.826$). From [136].

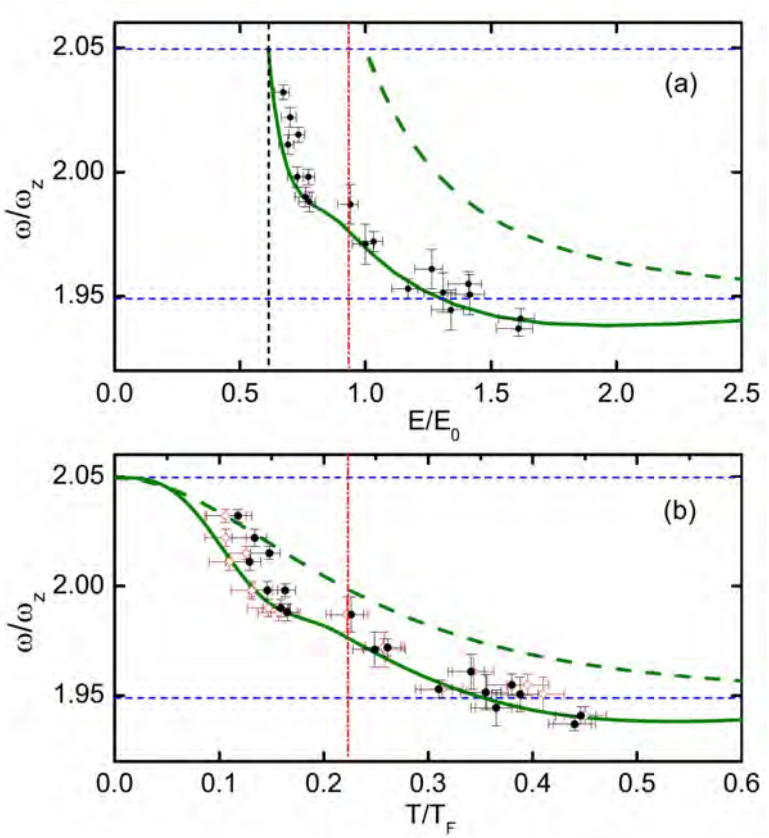

Fig. 19. – Temperature dependence of the nodal axial breathing mode frequency. The experimental data are shown as a function of (a) the measured energy parameter E/E_0, and (b) the temperature scale T/T_F. The theoretical curves (solid lines) are based on the EOS in [38]. This EOS is also used to extract T/T_F from the measured profile in two different ways: The filled symbols in (b) result from a direct conversion of E/E_0 to T/T_F, while the open symbols result from fitting the cloud profiles. Dashed curves: Mode frequencies that would result from the EOS of an ideal Fermi gas. Thin horizontal lines: $T = 0$ superfluid limit ($\omega/\omega_z = \sqrt{21/5}$) and the classical hydrodynamic limit ($\omega/\omega_z = \sqrt{19/5}$). In (a) the dashed vertical line indicates the $T = 0$ ground state with $E/E_0 = \sqrt{\xi} = 0.613(3)$, while the dash-dotted vertical lines in (a) and (b) indicate the critical energy $E/E_0 = 0.934(39)$ and temperature $T_c/T_F = 0.223(15)$ for a trapped gas. From [28].

2˙5.7. The equation of state in the BEC-BCS crossover. In [37], the equation of state in the BEC-BCS crossover was directly obtained from the density profiles of a harmonically trapped gas via the "magic formula" Eq. 22 relating the local pressure to the column density. The gas was determined to be at temperatures $T/T_F = 0.03(3)$, much lower than the critical temperature for superfluidity in the explored regime, justifying the assumption of zero temperature made in the analysis. In the superfluid regime, a spin-imbalanced gas consists of a central core at equal densities, surrounded by a normal mixture at unequal densities [40, 41, 139, 42]. Such a mixture thus allows for the study of the balanced superfluid in the center, while the normal wings are used for thermometry and to obtain the chemical potential. Thermometry was performed on the non-interacting wings of the spin-imbalanced Fermi gas [139]. The chemical potentials of the majority and minority cloud were directly obtained from the measured cloud sizes and the knowledge of the energy of a single minority atom immersed in a Fermi sea [45]. The outcome of the analysis is a zero-temperature equation of state for the two-component Fermi gas in the BEC-BCS crossover. Focussing here on the results for the balanced superfluid, the study directly gave the pressure $P(\mu, a)$ as a function of chemical potential and scattering length. The results are reported using the normalized quantity $h_S(\delta) = P(\mu, a)/(2P_0(\mu))$, the ratio of the pressure of the interacting system to the pressure of the non-interacting system, as a function of the normalized interaction strength $\delta \equiv \frac{\hbar}{\sqrt{2m\mu}a}$ that plays the role, in the grand-canonical ensemble, of $1/k_F a$ in the canonical ensemble. This function is shown in Fig. 20. In the BEC-regime, the measurement is consistent with the Lee-Huang-Yang result Eq. 64, and in the BCS regime it approaches the Lee-Yang formula Eq. 66. Furthermore, the data yielded a value of the local, homogeneous contact corresponding to $\zeta = 0.93(5)$ (i.e. $C/Nk_F = 3.5(2)$), in good agreement to other experimental and theoretical values. It is remarkable that the trapping potential, that was often regarded as a nuisance in ultracold atom experiments, has turned out to provide the key method to obtain the homogeneous equation of state - in principle from one single experimental image.

2˙6. *Condensation energy.* – The superfluid state is favored with respect to the normal state when its free energy F_S is smaller than the free energy F_N of the normal state. The difference E_c can be defined as the *condensation energy.* In BCS theory, the condensation energy is directly related to the pairing gap Δ as (see section **??**)

$$E_c = F_S - F_N = -\frac{1}{2}\rho(E_F)\Delta^2 = -\frac{3}{8}N\frac{\Delta^2}{E_F} \tag{112}$$

At zero temperature, we have $E_{S,N} = \frac{3}{5}NE_F\xi_{S,N}(1/k_F a)$, where the subscript S and N denote the superfluid and normal state, respectively. In the BCS regime, the condensation energy is thus related to $\xi_N - \xi_S$ via

$$\xi_N - \xi_S = \frac{5}{8}\left(\frac{\Delta}{E_F}\right)^2 \tag{113}$$

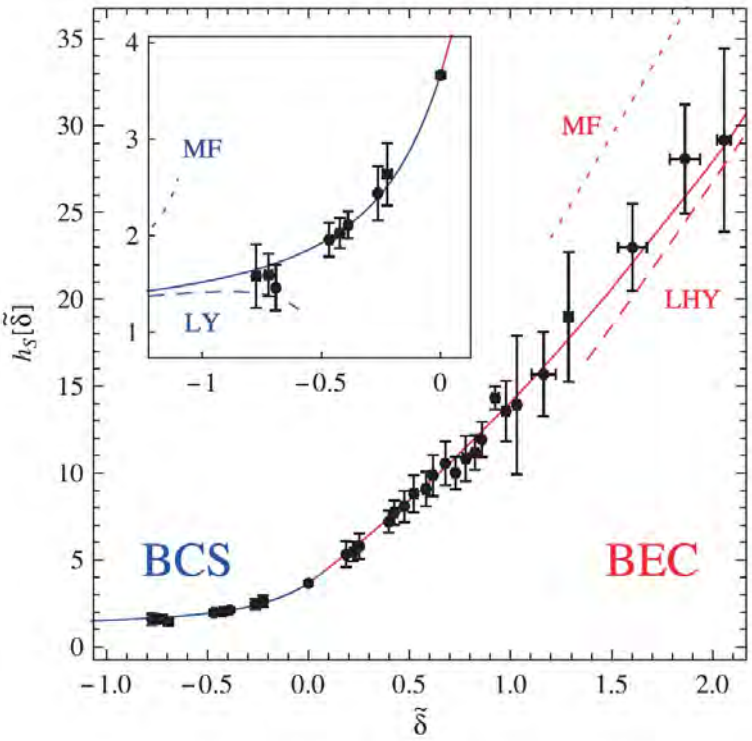

Fig. 20. – Equation of state in the BEC-BCS crossover. *black circles* data; *blue and red solid lines*: Padé expansion. Comparison with analytical expansions: MF: mean-field, LY: Lee-Yang, LHY: Lee-Huang-Yang. From [37].

This relation between $\xi_N - \xi_S$ and the gap is strictly valid only the BCS limit, and generally, as pointed out in [140], one rather has a more complicated relation

$$\xi_N - \xi_S = \frac{5}{8}\left(\frac{\Delta}{E_F}\right)^2 f(\Delta/E_F) \tag{114}$$

with an unknown function $f(\Delta/E_F)$. It is argued in [140] that $f(0) = 1$ to recover the BCS limit, and f should only receive corrections from unity starting with $(\Delta/E_F)^2$. At unitarity a moderate 25% correction to the simpler BCS relation is expected. The relation can be tested for its validity (see Fig. 21). ξ_N can be obtained by extrapolating the equation of state of the normal state either from temperature above T_c to $T = 0$ [35, 38] or from large spin imbalance to zero imbalance [140] (see section **3**). The pairing gap Δ has been measured in RF spectroscopy [23] (see Fig. 22). Comparison shows that the simple BCS expression 114 is still in excellent agreement up to $1/k_F a \approx 0.5$. This is on the BEC side of the resonance but still in the regime where $\mu > 0$. Here, pairing is a

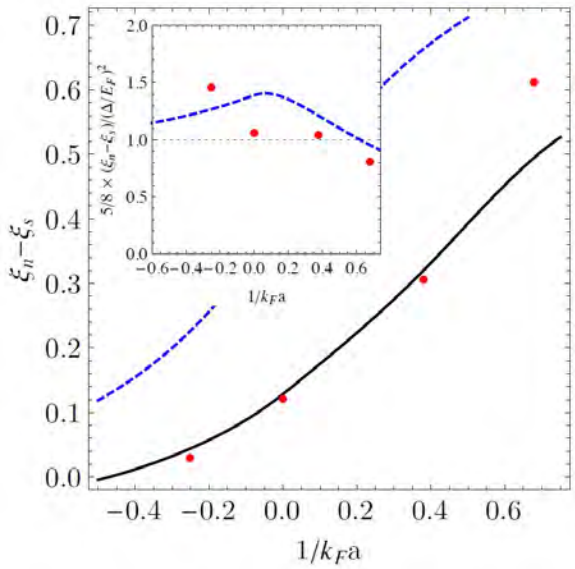

Fig. 21. – Condensation energy in the BEC-BCS crossover. Main panel: Dimensionless condensation energy $\xi_N - \xi_S$ versus interaction strength $1/k_F a$ (solid black line). In red points, BCS expression $\frac{5}{8}(\Delta/E_F)^2$ using the values of Δ measured in [23]. *Dashed blue line* Mean-field BCS theory. *Solid black line* Fixed node Monte-Carlo calculation. Inset: Ratio of the condensation energy $\xi_N - \xi_S$ to $\frac{5}{8}(\Delta/E_F)^2$. From [140].

many-body affair, with a minimum single-particle excitation energy at finite momentum given by the pairing gap Δ. This might give a qualitative explanation why the BCS relation (that has $f = 1$) still works in the strongly interacting regime.

2˙7. *The normal state above T_c: Pseudo-gap phase, Fermi liquid, or Fermi gas?*. – Of considerable interest is the state of the system close to, but above the critical temperature for superfluidity. Does fermion pairing occur already above T_c, i.e. is there a "pseudo-gap" phase of preformed Cooper pairs [141, 142]? Or is the gas a Fermi liquid, with well-defined quasi-particles [35, 143]? Or is the gas in fact too "hot" at temperatures at and above T_c to speak of a Fermi liquid? After all, T_c is a fair fraction of the Fermi energy, and the Fermi surface is likely significantly broadened by thermal effects. This question is a subject of current debate, as we discuss below. It is of relevance to the regime of high-temperature superconductors above but close to T_c, the so-called "Nernst" regime, where it is believed that pairing and strong phase fluctuations with well-defined vortices may exist [144]. This is however only a small part of the region in the high-T_c phase diagram known as the "pseudo-gap", a phenomenon that persists at temperatures much larger than T_c and that is unrelated to pairing, but rather related to the nearby Mott insulating state [145].

In the BCS-regime, pairing and superfluidity occur together. T_c is just given by the temperature of pair formation. However, in the BEC regime, it is natural to have pairing without superfluidity: Molecules can first form at a temperature on the order of the binding energy E_B, before they condense at much lower temperatures given by the criterion for Bose-Einstein condensation, which yields $T_c \approx T_F$. Thus on the BEC-side above T_c we expect to find a normal Bose gas of molecules, while in the BCS regime one should find a Fermi liquid of unpaired quasi-particles above T_c. Pairing above T_c in the BEC-regime is however simply a two-particle effect. The question of interest is whether many-body pairing, that requires the presence of the surrounding Fermi gas, may persist in the strongly interacting regime above T_c. Such BCS-type many-body pairing would be characterized by a pairing gap Δ^*, and the lowest single-fermion excitations of the gas at that pairing energy would have non-zero momentum.

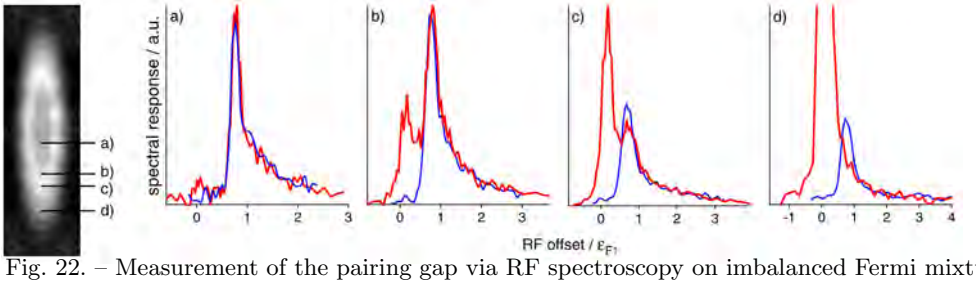

Fig. 22. – Measurement of the pairing gap via RF spectroscopy on imbalanced Fermi mixtures. The spectrum in a), from the balanced superfluid in the center of the trap, reveals an energy shift with respect to the bare atomic frequency (at 0 rf offset). In b) some majority atoms spatially coexist with superfluid pairs. Two peaks result, and the peak difference yields the pairing gap. Further out, in c) and d), one enters the polaronic regime (see section **3**). From [23].

The superfluid pairing gap was observed in localized RF spectroscopy [23], where a small population of quasi-particles was induced by spin-imbalance. In this way, both the spectrum of pairs and the spectrum of unpaired quasi-particles was detected at the same local position, and the difference in peak positions yielded the pairing gap (see Fig. 22). A balanced mixture did not reveal such double-peaks for any temperature, and the spectra above T_c were observed to acquire a width comparable to the Fermi energy. This speaks against a standard Fermi liquid picture, but rather than confirming an exotic non-Fermi liquid scenario this is likely due to the fact that $T_c \approx 0.17 T_F$ is a substantial fraction of T_F and thermal effects are important. Pauli blocking will not be effective at protecting quasi-particles at temperatures larger than a few percent of T_F. Also, the strong interactions at unitarity imply a short mean-free path on the order of the interparticle distance, and thus quasi-particle energies are likely to be ill-defined, with an energy width that could be comparable to the Fermi energy. The short mean-free path is reflected in the low viscosity of the gas above T_c [29, 146, 110], and in the low spin diffusivity on the order of $\hbar/m$ [30, 147, 148].

Momentum-resolved RF spectroscopy was employed to investigate the possibility of pairing above T_c [142]. Gap-like features and the associated "back-bending" of the dispersion *near* k_F, away from the chemical potential, were observed as a function of momentum (see Fig. 23). Note that back-bending *far from* k_F, with small but non-zero spectral weight, is predicted to be a universal feature of Fermi gases with contact interactions in all phases, normal and superfluid. It is a direct consequence of the $1/k^4$-tail in the momentum distribution associated with non-zero contact, as discussed above. Such a tail is indeed observed in the experiment [142], with back-bending persisting up to very high temperatures, even when the near-k_F behavior no longer exhibits the pseudo-gap-like behavior. The spectra are broadened to about the Fermi energy, possibly due to an interplay of temperature, short mean-free path and trap-averaging. Momentum-resolved spectra of a homogeneous sample will be of great value in the interpretation of the gap-like back-bending.

In weakly coupled layers of quasi-two-dimensional Fermi gases, evidence for similar back-bending was found [149] and the evolution of pairing from three to two dimensions was studied [150]. However, the interpretation of back-bending revealing a pseudo-gap is challenged by a theory that only includes a high-temperature Virial expansion and reproduces the qualitative features of the measurements [151].

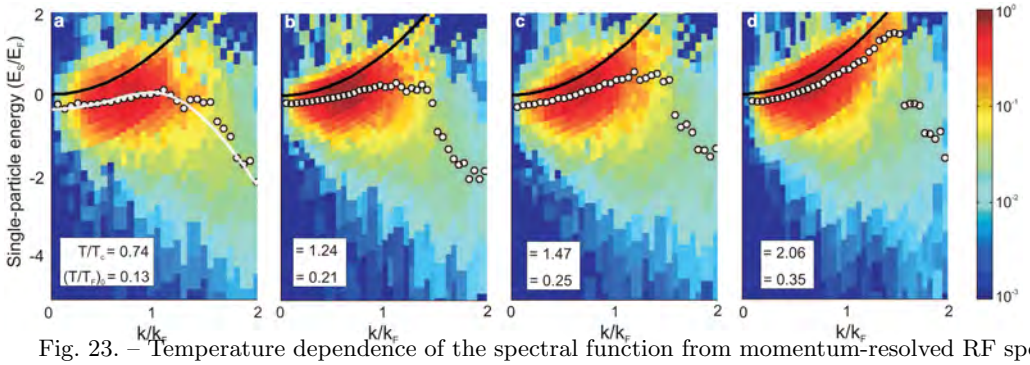

Fig. 23. – Temperature dependence of the spectral function from momentum-resolved RF spectroscopy. Spectra are shown for Fermi gases at four different temperatures at an interaction strength $1/k_F a \approx 0.15$. The intensity plots show the fraction of out-coupled atoms as a function of their single-particle energy (normalized to the trap-averaged E_F) and momentum (normalized to the trap-averaged k_F), where $E = 0$ corresponds to a particle at rest. The black curve is the quadratic dispersion expected for a free particle. The white curve is a fit to a BCS-like dispersion with back-bending. From [142].

As an argument in favor of the Fermi liquid scenario, measurements of the equation of state have revealed that surprisingly, the pressure, normalized by the pressure of a non-interacting Fermi gas at the same chemical potential, is to a high degree linear in $(k_B T/\mu)^2$, a property one would associate with Fermi liquid behavior [35, 38]. However, at the elevated temperatures above T_c, already a non-interacting Fermi gas would deviate

from this behavior, displaying a slope that varies with temperature [38]. Also, as argued above, quasi-particles might not have well-defined energies due to finite temperature and strong interactions that imply a short mean-free path and thus a short quasi-particle lifetime. The observed behavior seems to be a coincidence, related to the quadratic dependence of the chemical potential on temperature, and it does not persist when the temperature is normalized by the Fermi temperature, instead of the chemical potential [152, 38]. Still, a Fermi liquid picture was shown to explain the momentum resolved RF spectra quite satisfactorily [143], and the width of the spectra was recovered despite the assumption of long-lived quasi-particles and attributed instead to temperature, trap inhomogeneity and measurement resolution.

One way to very clearly bring out Fermi liquid behavior in a strongly interacting Fermi gas is to work with spin-imbalanced mixtures above the Clogston-Chandrasekhar limit of superfluidity [40]. A single spin down impurity immersed in a Fermi sea, the Fermi polaron [153, 154, 155, 156], possesses definite quasi-particle properties, a long lifetime, a sharply defined energy [45] and an effective mass [44]. As the number of impurities increases and the gas becomes less highly imbalanced, the energy of the minority spins does not significantly change [45], implying that a Fermi liquid description of non-interacting, well-defined quasi-particles is valid in this regime. Indeed, the equation of state of such imbalanced Fermi mixtures at near-zero temperature is excellently described within a Fermi liquid picture [34, 35, 37, 143]. Since there is no phase transition between the regime of high imbalance and low temperature $T \ll T_F$ and the balanced Fermi gas above T_c, this spin-imbalanced Fermi liquid must smoothly evolve to the spin-balanced state above T_c that may or may not contain preformed pairs. The study of this evolution is subject of current experiments.

A quantity that directly indicates pairing is the spin susceptibility χ_s of the gas [157]. Quantum Monte-Carlo studies see clear evidence of preformed Cooper pairs in a downturn of the spin-susceptibility before the superfluid critical temperature is reached [158, 159]. The spin susceptibility of the superfluid Fermi gas in the BEC-BCS crossover has been obtained experimentally via the detection of spin fluctuations [160]. As expected, the spin susceptibility was strongly suppressed in the superfluid regime. On resonance, for a condensate fraction of 35%, it was found $\chi_{\rm SF} = 0.28(6)\chi_0$, where $\chi_0 = 3n/2E_F$ the spin susceptibility of a non-interacting Fermi gas. However, also the interacting normal state retained significant suppression of spin fluctuations due to the strong attractive interactions. The spin susceptibility for a normal spin-imbalanced Fermi gas has been measured via the equation of state in [143], and the data was extrapolated to the spin-balanced case. On resonance, the result was $\chi_n = 0.54\chi_0$, about a factor of two larger than in the superfluid regime of [160]. The temperature dependence of the spin susceptibility was obtained from spin transport as the ratio of spin conductivity to spin diffusivity [30]. At high temperature $T \gg T_F$, the spin susceptibility χ closely tracked the compressibility κ in accord with the result for a Boltzmann gas, where $\chi = n^2\kappa$. Below $T \simeq T_F$, the susceptibility was seen to decrease below $n^2\kappa$, as expected for a Fermi liquid where spin- and density-response each come with their own Landau parameters. A further sudden decrease in χ was not observed down to $T/T_F = 0.2$ within the signal

to noise of the experiment, rather arguing for the Fermi liquid side. A precision measurement of the temperature dependence of the spin susceptibility would reveal whether the decrease to the superfluid value occurs at or already above T_c, and might provide insight into the question of the pseudogap for a resonant Fermi gas.

3. – Fermionic Superfluidity with Spin Imbalance

The question of superfluidity in the presence of spin imbalance is almost as old as BCS theory itself. Bardeen, Cooper and Schrieffer described the superconducting state as a condensate of pairs of electrons carrying opposite spin. But what is then the fate of a spin-imbalanced mixture? In this case, not every majority atom can find a minority partner to pair with. Will the gas still be superfluid? If so, are the excess fermions tolerated inside the gas of pairs or are they expelled from the superfluid? If superfluidity breaks down, what is the nature of the strongly interacting, imbalanced normal mixture left behind? The question is relevant to various fields of physics were fermion mixtures coexist at unequal populations, for example in nuclei but also in the core of neutron stars. Here, a quark superfluid (or color superfluid) is predicted to exist [161] that is neutral, and therefore must contain unequal densities of quarks.

Imbalanced superfluidity is difficult to study in conventional superconductors. To induce spin imbalance, one would apply a magnetic field, but that is expelled from the superconductor because of the Meissner effect. In ultracold atomic gases, one can freely choose the population in the two (hyperfine) spin states. This opens up an entirely new avenue for studying fermionic superfluids.

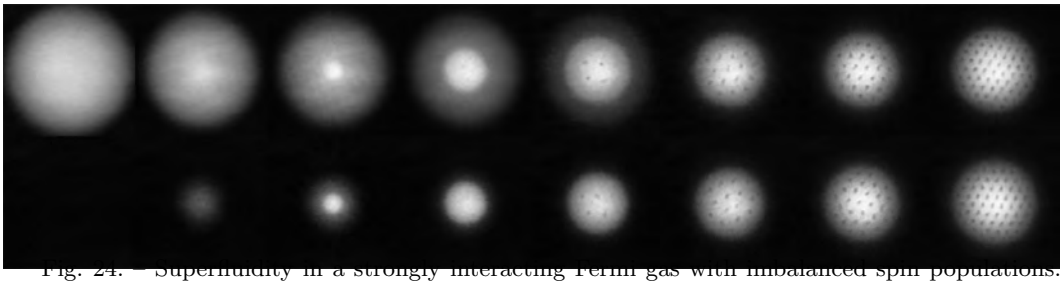

Fig. 24. – Superfluidity in a strongly interacting Fermi gas with imbalanced spin populations. Vortices mark the region of superfluidity. The population imbalance $(N_\uparrow - N_\downarrow)/(N_\uparrow + N_\downarrow)$ was (from left to right) 100, 90, 80, 62, 28, 18, 10 and 0%. From [40].

In the following we discuss the major findings for imbalanced Fermi mixtures. The creation of spin imbalanced fermionic superfluids and the determination of the equation of state of imbalanced Fermi gases can be considered a major success of ultracold atom experiments [40, 41, 42, 43, 34, 45, 35, 35]. The superfluid state was found to be robust against spin imbalance in the strongly interacting regime [40, 41] (see Fig. 24). At a critical population imbalance, that depends on the interaction strength, the superfluid

state was found to break down [40, 44]. This was the observation of the Clogston-Chandrasekhar (CC) limit of superfluidity, also known as the Pauli limit. Thus, in spin-imbalanced Fermi gases, there is no longer a smooth crossover between the BEC- and the BCS regime. Instead, a first order transition takes place: If the attractive interactions become too weak, the superfluid state becomes normal. This is in contrast to the spin-balanced case, where superfluidity occurs for arbitrarily small interactions. The stronger the imbalance, the smaller is the window of superfluidity. The phase diagram of imbalanced Fermi mixtures is much richer than for the balanced case. At low temperatures, the superfluid state requires equal spin densities, and phase separates from the normal state in a trap [40, 41, 162, 42, 43]. Accordingly, the density difference jumps, a direct consequence of the first order transition due to the Pauli limit. The first order transition at zero temperature continues as a first order phase transition at finite temperature, up to a critical point, where it becomes second order [163, 43]. Here, the density difference evolves continuously across the superfluid to normal transition.

At high imbalance, the system is normal down to the lowest temperatures realized so far, and behaves as a Fermi liquid [45, 44, 35, 37, 143]. In the limit of high imbalance there is one minority atom "swimming in the Fermi sea" [164] of majority atoms. This is the Fermi polaron [165, 166, 155, 167, 168], an impurity dressed by the surrounding fermionic bath, that has a well-defined energy $E_\downarrow$ and an effective mass m^*. Apart from mass-balanced, strongly interacting Fermi gases in 3D [45, 44], it has also been observed in unequal Fermi mixtures of two different fermionic species of atoms, ^{6}Li and ^{40}K [47], as well as in mass-balanced mixtures in two dimensions [46].

As always when symmetries are broken, one obtains new insights also for the symmetric state. Indeed, the study of imbalanced mixtures has improved our understanding of the balanced case. It enabled the direct observation of the formation of the superfluid without a rapid ramp to the BEC-side [139, 42] (see section **??**). Imbalance also offered a way to directly measure temperature in the strongly interacting regime, by using the fully polarized majority wings of the density distribution as a thermometer [139, 43, 35, 37]. This solved a long-standing problem of strongly interacting Fermi gases, where no simple thermometry had been available before, and enabled the determination of the equation of state of balanced and imbalanced Fermi mixtures.

3˙1. *Chandrasekhar-Clogston limit.* – If magnetic fields do enter a superconductor, the BCS state of electron pairs should be fragile as the field tends to align the spins. Following this thought, Chandrasekhar [169] and independently Clogston [170] derived an upper limit for the critical magnetic field of a superconductor: Once the energy gain for aligning the electron spins is larger than the energy gain from pairing opposite spins, Cooper pairs must break and the system should turn normal. This is the Pauli or Chandrasekhar-Clogston limit of superconductivity. The first-order superfluid-to-normal transition was studied by Sarma [171]. In 1964, Fulde and Ferrell [172], and independently Larkin and Ovchinnikov [173] found that not all the pairs necessarily break at once, but that there exists a novel superfluid state that tolerates a certain amount of majority spins if the remaining Cooper pairs are allowed to have a common non-zero momentum (FFLO or

LOFF state). The order parameter is thus not constant, but corresponds to a traveling (FF state) or standing (LO state) wave, and majority spins can reside in its nodes without energy penalty. The number of nodes is given by the number difference between the spin states. Forty years later, the debate about the ground state of imbalanced superfluidity is still not settled. The problem arises in condensed matter, where exotic superconductors were found [174, 175, 176] that are essentially Pauli limited, in nuclear physics in the study of superfluid pairing of quarks at unequal Fermi energies [161], and in atomic physics, were the advent of ultracold atomic Fermi gases presented a new opportunity to study imbalanced superfluidity [40, 41, 44].

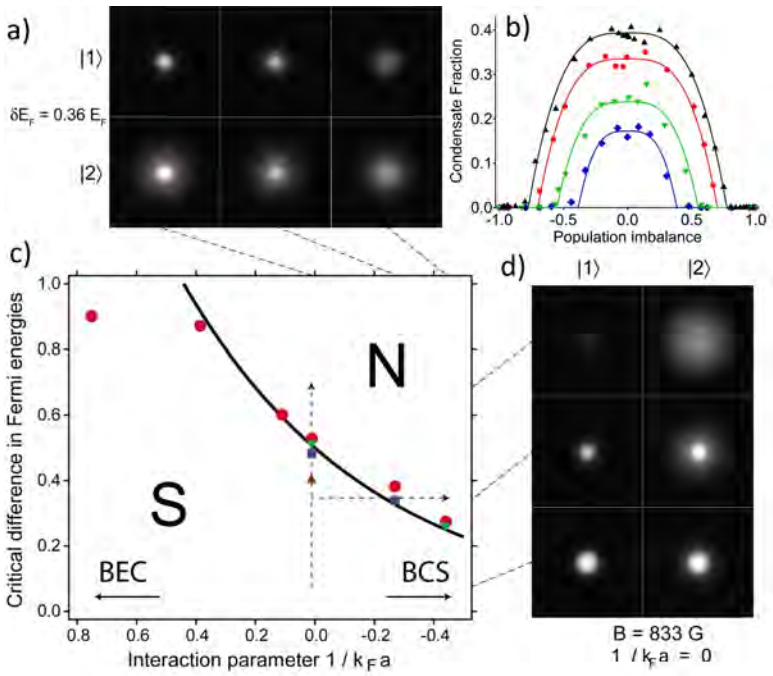

Fig. 25. – Clogston-Chandrasekhar limit of superfluidity. The critical Fermi energy mismatch δE_F between the two spin states at the superfluid-to-normal transition shown in c) is observed in the condensate fraction for varying interaction strength at fixed δE_F (a), and at fixed interaction strength and varying δE_F (d). b) Window of superfluidity as obtained from the condensate fraction at $1/k_F a = 0.11$ (triangles pointing up), $1/k_F a = 0$ (resonance, circles), $1/k_F a = -0.27$ (BCS-side, triangles pointing down), $1/k_F a = -0.44$ (diamonds). From [40].

To derive the CC limit, we need to compare the free energy $F(h)$ of the normal and the superfluid state in the presence of a "magnetic field" $h = (\mu_\uparrow - \mu_\downarrow)/2$. For zero field, the superfluid state is the ground state, but there will be a critical field - the CC limit -, beyond which the normal state has lower free energy than the superfluid. For illustration of the effect, we focus on the weakly interacting BCS regime, work at zero temperature and neglect the attractive mean-field (Hartree) interaction between opposite spins present already in the normal state. This will lead to an overestimate of the critical field, as it neglects attractive interaction present in the normal state that lowers its free energy. A balanced fermionic superfluid has free energy $F_S = F_N(0) - \frac{1}{2}\rho(E_F)\Delta^2$, lower than the free energy of the balanced normal gas at $h = 0$ by the condensation energy $\frac{1}{2}\rho(E_F)\Delta^2$ (see section **??**). The free energy of the normal state as a function of h is

$$\begin{aligned} F_N(h) &= -\frac{4}{15}\rho(1)\left(\mu_\uparrow^{5/2} + \mu_\downarrow^{5/2}\right) \\ &= F_N(0)\frac{1}{2}\left\{\left(1+\frac{h}{E_F}\right)^{5/2} + \left(1-\frac{h}{E_F}\right)^{5/2}\right\} \\ &\approx F_N(0) - \rho(E_F)h^2 \end{aligned} \tag{115}$$

where we have set $\mu_\uparrow = E_F + h$, $\mu_\downarrow = E_F - h$ and $F_N(0) = -\frac{8}{15}\rho(E_F)E_F^2$ in this approximation. We immediately obtain the critical "magnetic field"

$$h_{\rm CC} = \frac{1}{\sqrt{2}}\Delta \tag{116}$$

In superconductors, this corresponds to about 18.5 Tesla for a T_c of 10 K, much larger than the typical critical field H_{c2} where superconductivity breaks down due to the orbital effect of the magnetic field - the generation of vortices. The Pauli limit is thus not observable in conventional superconductors, but heavy fermion superconductors or layered superconductors may be in the Pauli limited regime [177]. For strongly interacting Fermi gases, where Δ approaches the Fermi energy, the critical field will be a substantial fraction of E_F, and the window of superfluidity as a function of the field h will be wide.

In atom traps, the control parameter is not the field h but the atom numbers $N_\uparrow$ and $N_\downarrow$ in each spin species. For a given equation of state that relates densities to chemical potentials and temperature, the field h is implicitly given as a function of $N_\uparrow$ and $N_\downarrow$. In the trap, the local chemical potentials depend on the trapping potential as $\mu_\sigma = \mu_{0,\sigma} - U(\mathbf{r})$ and thus the field $h(\mathbf{r}) = \frac{1}{2}(\mu_\uparrow(\mathbf{r}) - \mu_\downarrow(\mathbf{r})) = \frac{1}{2}(\mu_{0,\uparrow} - \mu_{0,\downarrow})$ is *constant* throughout the trap. However, the pairing gap $\Delta(\mathbf{r})$ depends on the local density. In the BCS limit, including the correction to the BCS result due to density fluctuations [178], one has $\Delta(\mathbf{r}) = \left(\frac{2}{e}\right)^{7/3}\mu(\mathbf{r})e^{-\pi/2k_F(\mathbf{r})|a|}$. Densities depend on the local chemical potential as $n_\sigma(\mathbf{r}) = n_\sigma(\mu_{0,\uparrow} - U(\mathbf{r}), \mu_{0,\downarrow} - U(\mathbf{r}), T, a)$. Accordingly, the Clogston-Chandrasekhar limit will be reached for a specific value of the trapping potential $U(\mathbf{r})$ where $\Delta(\mathbf{r}) \approx \sqrt{2}\, h_{\rm CC}$. This first order superfluid to normal transition thus occurs

at a certain equipotential shell in the cloud and will leave its trace in the density profiles, as shown in section **??**.

To directly demonstrate the robustness of superfluidity in the strongly interacting regime, the MIT group studied spin imbalanced Fermi mixtures in the presence of a stirring beam. The part of the mixture that was still superfluid despite the imbalance revealed a lattice of quantized vortices (see Fig. 24).

The window of superfluidity was determined from the number of vortices as a function of imbalance, as well as from condensate fraction measurements as in section **??** (see Fig. 25). Superfluidity was shown to be robust in the strongly interacting regime. At the Feshbach resonance, superfluidity was quenched at a critical population imbalance $P = (N_\uparrow - N_\downarrow)/(N_\uparrow + N_\downarrow)$ of about $P_c = 75\%$. This critical value agrees with the phase diagram obtained later by the ENS group [37]. A Monte-Carlo study obtains $P_c = 77\%$ [154]. BCS mean-field theory overestimates the critical population difference to $P_c = 92\%$ as it neglects interactions in the normal state, that make it more favorable at large fields h compared to the superfluid state. The experiments by the Rice group [41, 162] did not observe a critical population difference, and it was concluded that the critical imbalance was close to 100% at resonance. The reason for the discrepancy with the MIT results was later found to be due to the rapid evaporation sequence used at Rice [147, 179]. Slow spin transport, as observed in [30, 180], resulted in a non-equilibrium mixture.

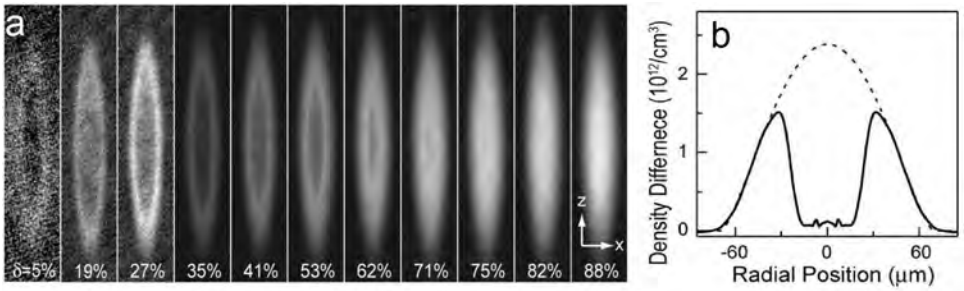

Fig. 26. – Phase separation in an imbalanced spin mixture. a) In-situ column density difference between the majority and minority species for various population differences $\delta = (N_\uparrow - N_\downarrow)/(N_\uparrow + N_\downarrow)$. Below an imbalance of $\delta < 75\%$, a central depletion indicates the fully paired superfluid, surrounded by a normal shell. b) Density difference as a function of radial position. The central core has equal spin densities. From [42].

3˙2. *Phase separation.* – Within BCS theory, at zero temperature, the superfluid state is expected to be fully paired. Excess fermions will require an energy of at least the pairing gap Δ to reside within the superfluid, so at low temperatures their presence should be exponentially suppressed. In contrast, beyond the Clogston-Chandrasekhar limit, the normal state will have imbalanced spin densities. The first order transition from the balanced superfluid to the imbalanced normal state should be signalled by a

jump in the density difference. First hints for phase separation between the normal and superfluid phase were seen in [40, 41]. Using tomographic techniques, a sharp separation between a superfluid core and a partially polarized normal phase was found in [42] (see Fig. 26). The jump in the density difference was observed in [43], directly demonstrating the first order nature of the phase transition. At higher temperatures, the signature of the first order transition disappears at a tricritical point (Fig. 27). The results are in good agreement with theoretical calculations [154, **?**]. In the BEC regime, the sharp first order transition including the jump in the density difference ceases to exist. One then deals with a strongly interacting Bose-Fermi mixture, where majority atoms are expelled from the condensate due to strong repulsive interactions [181]. However, for weaker interactions majority atoms can enter the superfluid and there will thus be a "magnetized superfluid" on the BEC-side of the phase diagram [182].

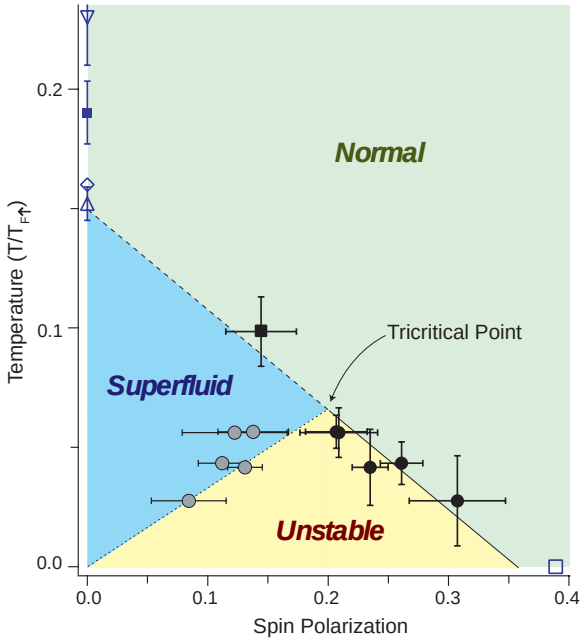

Fig. 27. – Phase diagram for a homogeneous spin-polarized Fermi gas with resonant interactions. Below the tricritical point first order phase boundaries are observed. The polarization jumps from the value in the superfluid (gray solid circles) to the higher value in the normal phase (black solid circles). Above the tricritical point, no abrupt change in spin polarization is observed. The phase transition was determined from the onset of pair condensation (black square). The blue open symbols show theoretical predictions for the critical temperature of a homogeneous equal mixture. From [43].

3˙3. *Limit of high imbalance - the Fermi Polaron.* – The fate of a single impurity interacting with its environment determines the low-temperature behavior of many condensed

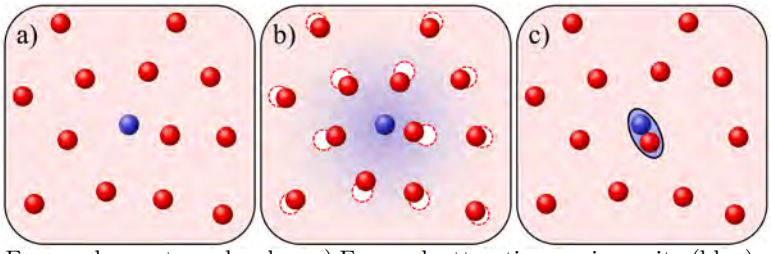

Fig. 28. – From polarons to molecules. a) For weak attraction, an impurity (blue) experiences the mean field of the medium (red). b) For stronger attraction, the impurity surrounds itself with a localized cloud of environment atoms, forming a polaron. c) For strong attraction, molecules form despite Pauli blocking from the environment. From [45].

matter systems. A well-known example is given by an electron moving in a crystal lattice, displacing nearby ions and thus creating a localized polarization. The electron, together with its surrounding cloud of lattice distortions, phonons, forms the lattice polaron [183]. It is a quasiparticle with an energy and mass that differ from that of the bare electron.

In the limit of highly imbalanced spin mixtures, one can study a novel kind of polaron problem, a spin down impurity immersed in a spin up Fermi sea - the Fermi polaron. This particle holds the key to the quantitative understanding of the phase diagram of imbalanced Fermi mixtures [166, 154, 112, 184, 155, 99, 185, 186, 153, 168, 187, 156]. Unlike in liquid ^{3}He, the s-wave interactions between the impurities and the spin up atoms in this novel spin-imbalanced Fermi liquid are attractive, and tunable via Feshbach resonances. Fig. 28 depicts the scenario for a single impurity: For weak attraction the impurity propagates freely in the spin up medium of density $n_\uparrow = k_F^3/6\pi^2$ (Fig. 28c). It merely experiences the familiar mean field energy shift $E_\downarrow = 4\pi\hbar^2 a n_\uparrow/m$. However, as the attractive interaction grows, the impurity can undergo momentum changing collisions with environment atoms, and thus starts to attract its surroundings. The impurity "dressed" with the localized cloud of scattered fermions constitutes the Fermi polaron (Fig. 28b). Dressing becomes important once the mean free path $\sim 1/n_\uparrow a^2$ of the impurity in the medium becomes comparable to the distance $\sim 1/k_F$ between environment particles or when $(k_F a)^2 \sim 1$. Collisions then reduce the impurity's probability of free propagation, the quasiparticle residue Z, from unity and shift its energy $E_\downarrow$ away from the simple mean field result. This polaronic state is stable until, for very strong attraction, the spin down impurity will bind exactly one spin up atom, thus forming a tightly bound molecule (Fig. 28a). This molecule is itself a dressed impurity, albeit a bosonic one [153].

The properties of the polaron were studied via RF spectroscopy that provided the polaron energy [45] (see Fig. 29), via collective excitations that provided the effective mass m^* [44] and via thermodynamic measurements that provided the full equation of state of imbalanced Fermi mixtures [34, 35, 37, 143]. These experiments have demonstrated

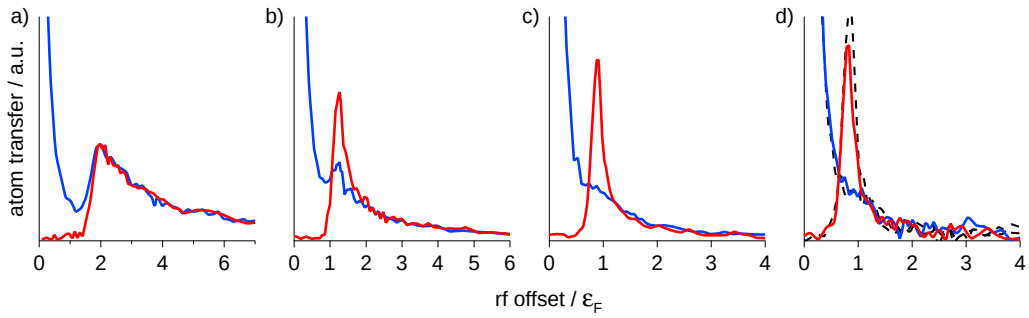

Fig. 29. – RF spectroscopy on Fermi polarons. Shown are spatially resolved, 3D reconstructed rf spectra of the majority (blue, state $|1\rangle$) and impurity (red, state $|3\rangle$) component in a highly imbalanced spin-mixture. a) Molecular limit, b), c) Emergence of the polaron, a distinct peak exclusively in the minority component. d) At unitarity, the peak dominates the impurity spectrum. The interaction strengths $1/k_F a$ were a) 0.76(2) b) 0.43(1) c) 0.20(1), d) 0 (Unitarity). From [45].

the quasi-particle nature of the spin impurity, as predicted in theoretical work [166, 154, 155, 99, 153, 168, 187, 156]. The dispersion law of the impurity follows that of a free particle with renormalized parameters:

$$\epsilon_{k,\downarrow}(p) = E_\downarrow + \frac{\hbar^2 k^2}{2m^*} + \dots \tag{117}$$

Here, $E_\downarrow$ is an energy shift with respect to the vacuum, due to the interaction of the impurity with the Fermi sea of spin up atoms. At unitarity, the shift must necessarily be a numerical constant A times the spin up Fermi energy $\mu_\uparrow = E_{F,\uparrow}$, as this sets the only available energy scale at low temperature $T \ll E_{F,\uparrow}$. The experiment [45] is consistent with the theoretical value $A = -0.615\dots$ from diagrammatic Monte-Carlo calculations [168] and the analytical result [156].

Remarkably, the theoretical calculations for the polaron can be well approximated by a variational ansatz due to F. Chevy [166] that captures the essential properties of the polaron:

$$|\Psi\rangle = \varphi_0 \, |\mathbf{0}\rangle_\downarrow \, |FS\rangle_\uparrow + \sum_{|\mathbf{q}|<k_F<|\mathbf{k}|} \varphi_{\mathbf{kq}} c^\dagger_{\mathbf{k}\uparrow} c_{\mathbf{q}\uparrow} \, |\mathbf{q}-\mathbf{k}\rangle_\downarrow \, |FS\rangle_\uparrow \tag{118}$$

The first part describes an impurity with a well-defined wavevector ($\mathbf{k}_\downarrow = \mathbf{0}$) that is not localized and free to propagate in the Fermi sea of up spins $|FS\rangle_\uparrow$. In the second part the impurity particle recoils off environment particles that are scattered out of the Fermi sea and leave holes behind. This describes the dressing of the impurity with particle-hole excitations. The probability of free propagation is given by the first, unperturbed part,

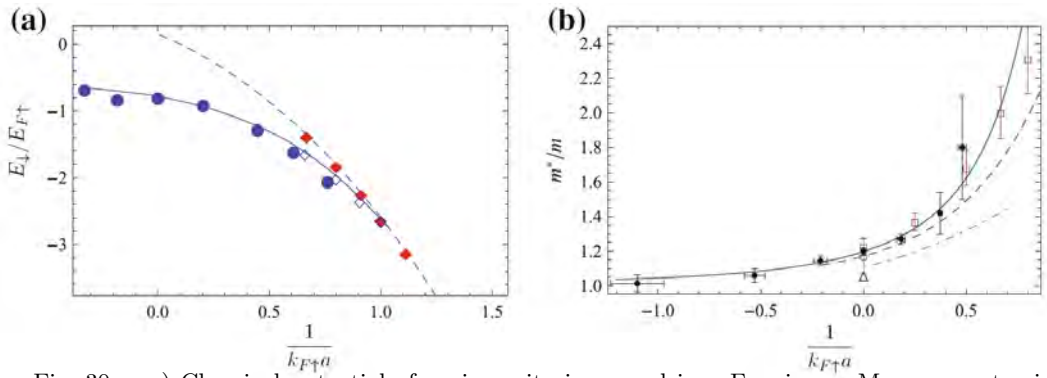

Fig. 30. – a) Chemical potential of an impurity immersed in a Fermi sea. Measurements via RF spectroscopy at MIT [45] (circles) are compared to theoretical predictions for polaron and molecule energies. *Full (empty) diamonds* Monte-Carlo simulations of the molecule (polaron). *Full (dashed) line*, variational Ansatz for the polaron [166, 155] and molecule [189, 190, 182]. b) Effective mass of the Fermi polaron in the BEC-BCS crossover measured at ENS [37] (*black dots*). *Blue dashed line* calculation from [155], *red open squares* [168], *green dot-dashed line* [186], and *blue solid line* [190]. Measurements from density profile analysis (*blue triangle* [34]) and collective modes study (*brown empty circle* [44]). From [53].

$Z = |\varphi_0|^2$. The two portions of $|\Psi\rangle$ give rise to two distinct features of the impurity rf spectrum $\Gamma(\omega)$, measured in [45] (see Fig. 29):

$$\Gamma(\omega) = 2\pi\hbar\Omega_R^2 \, Z\delta(\hbar\omega + E_\downarrow) + \Gamma_{\text{incoh.}}(\omega) \tag{119}$$

The first part in $|\Psi\rangle$ contributes, according to Fermi's Golden Rule, a coherent narrow quasiparticle peak $\propto Z\delta(\hbar\omega + E_\downarrow)$ to the minority spectrum. Its position is a direct measure of the polaron energy $E_\downarrow$, its integral gives the quasiparticle residue Z. The particle-hole excitations in the second part give rise to an incoherent background $\Gamma_{\text{incoh.}}(\omega)$. For large detuning the spectrum decays like $C/\omega^{3/2}$, where C is the contact of the polaron (see section **2**˙4). For theoretical studies of polaron RF spectra see e.g. [187, 188]. In the weakly interacting regime, the coherent part leads to coherent Rabi oscillations of the impurity during the RF pulse. The Rabi frequency provides a direct way to measure the quasi-particle residue Z [47, 46].

In a trap, the polaron will oscillate in an effective potential given by the combination of the bare trapping potential $U(\mathbf{r})$ and the interaction term $AE_{F,\uparrow}(\mathbf{r})$, where the Fermi energy of the spin up atoms is itself spatially varying according to $E_{F,\uparrow} = E^0_{F,\uparrow} - U(\mathbf{r})$. The effective potential is thus $(1-A)U(\mathbf{r})$, and the polaron oscillation frequency will be

$$\omega^*_{x,y,z} = \omega_{x,y,z}\sqrt{\frac{m}{m^*}(1-A)} \tag{120}$$

where $\omega_{x,y,z}$ are the bare trapping frequencies for a single atom in the potential $U(\mathbf{r})$. With the knowledge of A (from RF spectroscopy [45] or directly from theory), the measurement of the impurity's oscillation frequency gives access to the polaron mass m^*. The experiment has been performed at the ENS [44], and the resulting effective mass at unitarity was $m^* = 1.17(10)m$, consistent with theoretical calculations. Figure 30 summarizes the polaron properties obtained from RF spectra, collective excitations and thermodynamic measurements. In the BEC regime beyond a critical interaction strength of $1/k_F a \sim 0.9$, the polaron becomes unstable towards the formation of a molecule [168]. This transition is apparent in the evolution of RF spectra [45] (Fig. 29). Repulsive and attractive Fermi Polarons have been observed in a mass-imbalanced mixture of ^{6}Li and ^{40}K [47] as well as in a mass-balanced mixture of ^{40}K in two dimensions [46].

3˙4. *Fermi liquid of polarons.* – As we move away from the limit of a single impurity and add more spin down atoms to the spin up Fermi sea, we encounter a strongly interacting Fermi mixture. Still, it was found via RF spectroscopy [45] that the energy shift of the minority species depends only weakly on the impurity concentration. In other words, polarons appear to interact weakly. This is precisely the situation Landau describes: A normal, possibly strongly interacting fermionic system will behave as a weakly interacting gas of quasi-particles, a Fermi liquid. While in a typical scenario the nature of the quasi-particles might be obscure, in the present case it appears that the quasi-particles are simply polarons. It is natural that a dilute gas of spin down impurities will be weakly interacting if the characteristic distance between impurities $1/k_{F,\downarrow}$ is much larger than the distance between majority spins. Then, each impurity will be surrounded by its own dressing cloud of majority spins and polarons will not overlap. They should thus behave as a weakly interacting Fermi gas. This intuitive picture was confirmed in Monte-Carlo calculations [154] and analytic studies of the equation of state [191]. It was found that in the limit of a small number of impurities, the gas can be described as a non-interacting mixture of an undressed Fermi sea of majority spins and a Fermi sea of polarons with the renormalized energy and mass found for a single impurity above. In the next section we describe measurements of the full equation of state of imbalanced Fermi mixtures, including the Fermi liquid regime.

3˙5. *Thermodynamics of spin-imbalanced Fermi mixtures.* – In the presence of spin-imbalance, we have two separate chemical potentials $\mu_\uparrow$ for spin up and $\mu_\downarrow$ for the spin down species, that are the thermodynamic variables conjugate to the atom numbers $N_\uparrow$ and $N_\downarrow$. The first law of thermodynamics for the variation of the energy $E(T, N_\uparrow, N_\downarrow, V, a)$ is now written

$$\mathrm{d}E = T\,\mathrm{d}S + \mu_\uparrow\,\mathrm{d}N_\uparrow + \mu_\downarrow\,\mathrm{d}N_\downarrow - P\,\mathrm{d}V - \mathcal{C}\,\mathrm{d}a^{-1} \tag{121}$$

The grand potential $\Omega(T, \mu_\downarrow, \mu_\uparrow, V, a) = E - TS - \mu_\uparrow N_\uparrow - \mu_\downarrow N_\downarrow$ has total derivative

$$\mathrm{d}\Omega = -S\,\mathrm{d}T - \mathcal{C}\,\mathrm{d}a^{-1} - N_\uparrow\,\mathrm{d}\,\mu_\uparrow - N_\downarrow\,\mathrm{d}\,\mu_\downarrow \tag{122}$$

which generalizes Eq. 16 for spin-imbalanced species. $\Omega = -PV$ still holds, as V is still the only extensive variable that Ω depends on. We obtain the Gibbs-Duhem equation for spin-imbalanced gases

$$S\,\mathrm{d}T + N_\uparrow\,\mathrm{d}\mu_\uparrow + N_\downarrow\,\mathrm{d}\mu_\downarrow - V\,\mathrm{d}P + \mathcal{C}\,\mathrm{d}a^{-1} = 0 \tag{123}$$

In the local density approximation, we may again relate the local quantities, such as the local densities $n_\sigma(\mathbf{r})$ and the local pressure $P(\mathbf{r})$ from the equation of state for the homogeneous system. As in the case of a balanced mixture (see section **2**), the local chemical potentials are simply shifted by the trapping potential $U(\mathbf{r})$, that for simplicity we assume to be identical for the two spin states. Thus $\mu_\sigma = \mu_{0,\sigma} - U(\mathbf{r})$, and therefore $\mathrm{d}\mu_\uparrow = \mathrm{d}\mu_\downarrow$, i.e. the chemical potentials of spin up and spin down change in exactly the same way in the trap (if the trapping potentials are different, the changes are still related to each other in a known way if the trapping potentials are known). One then finds for a trapped atom cloud at given temperature and fixed, uniform scattering length

$$\mathrm{d}P = n_\uparrow\,\mathrm{d}\mu_\uparrow + n_\downarrow\,\mathrm{d}\mu_\downarrow = -n\mathrm{d}U \tag{124}$$

where $n = n_\uparrow + n_\downarrow$ is the total density. This is identical to the relation found before for balanced gases, and thus one again finds Eq. 20

$$P(U) = \int_U^\infty \mathrm{d}U'\, n(U') \tag{125}$$

The "magic formula" for the pressure in a harmonic trap is still valid in the presence of imbalance [66, 67, 35, 37]:

$$P(z) = P(\mu_\uparrow(z), \mu_\downarrow(z), T, a) = \frac{m\omega_\perp^2}{2\pi}\, n_{1\mathrm{D}}(z) = \frac{m\omega_\perp^2}{2\pi}\,(n_{\uparrow,1\mathrm{D}}(z) + n_{\downarrow,1\mathrm{D}}(z)) \tag{126}$$

As in the balanced case, measurements of the doubly integrated total density are directly related to the local pressure in the gas at the local chemical potential $\mu_\sigma(z) = \mu_{0,\sigma} - U(0,0,z)$. If the global chemical potentials $\mu_{0,\sigma}$, the temperature T, and the scattering length a are known, one obtains the *homogeneous* equation of state of the spin-imbalanced mixture [34, 35, 37] in a wide range of chemical potentials, $\mu_\uparrow = -\infty \ldots \mu_{0,\uparrow}$ and $\mu_\downarrow = -\infty \ldots \mu_{0,\downarrow}$. As in the balanced case, the trap is not a nuisance but the key tool that allows to obtain the equation of state - in principle, in a single shot of the experiment. Averaging of many such determinations results in a low-noise experimental equation of state.

3˙5.1. Equation of state at unitarity. At unitarity and at zero temperature, the energy of the gas can only depend on the two available energy scales, the Fermi energies $E_{F\sigma} = \hbar^2/2m(6\pi^2 n_\sigma)^{2/3}$. This allows to write for the energy density $\mathcal{E} = E/V$ [184]

$$\mathcal{E}(n_\uparrow, n_\downarrow) = \frac{3}{5} n_\uparrow E_{F\uparrow}\, g\left(\frac{n_\downarrow}{n_\uparrow}\right)^{5/3} \tag{127}$$

with a universal function $g(x)$ of the density ratio $x = n_\downarrow/n_\uparrow$. From this expression, one finds a simple relation between the chemical potentials $\mu_\sigma = \partial\mathcal{E}/\partial n_\sigma$

$$\mu_\uparrow = E_{F\uparrow}\, g(x)^{5/3} - \frac{n_\downarrow}{n_\uparrow}\mu_\downarrow \tag{128}$$

and the energy density takes on the simple form

$$\mathcal{E} = \frac{3}{5}\left(n_\uparrow\mu_\uparrow + n_\downarrow\mu_\downarrow\right) \tag{129}$$

As $\Omega = E - \mu_\uparrow N_\uparrow - \mu_\downarrow N_\downarrow = -PV$, one again finds $P = \frac{2}{3}E/V$ as in the balanced case on resonance. In terms of the universal function $g(x)$, one has:

$$g(x)^{5/3} = \frac{\mu_\uparrow}{E_{F\uparrow}}\,(1 + xy) \tag{130}$$

where $y = \mu_\downarrow/\mu_\uparrow$ is the chemical potential ratio. Within the local density approximation, the local chemical potentials are given by $\mu_\sigma(\mathbf{r}) = \mu_{0,\sigma} - U(\mathbf{r})$, with the global chemical potentials $\mu_{0,\sigma}$ for each species. In the outer wings of the atom mixture one simply has a non-interacting Fermi gas of only majority atoms. One can therefore directly obtain the majority global chemical potential from the radius of the majority cloud $R_\uparrow$, i.e. $\mu_{0,\uparrow} = U(R_\uparrow)$. The minority global chemical potential $\mu_{0,\downarrow}$ can be obtained by noting that the last majority atom at the outermost wing of the minority cloud is a polaron, and thus $\mu_{0,\downarrow} = AE_{F\uparrow}(R_\downarrow) = A(U(R_\uparrow) - U(R_\downarrow))$. This method was employed in [166] and [184] to estimate the polaron energy from the experimental cloud radii measured in [139]. Alternatively, if the central part of the mixture is superfluid, we know from the balanced equation of state that $\mathcal{E} = \frac{3}{5}\xi n E_F$, where n and E_F are the total density and Fermi energy, and since $n_\uparrow = n_\downarrow$ this implies $\mu_{0,\uparrow} + \mu_{0,\downarrow} = 2\xi E_F(0)$, where $E_F(0)$ is the Fermi energy in the center of the trap. This analysis also provides a link between the polaron energy parameter A, the Bertsch parameter ξ and the experimental quantities $E_F(0)$, $R_\uparrow$ and $R_\downarrow$. The Bertsch parameter ξ can be obtained directly from the normalized compressibilities $\tilde{\kappa} = \kappa/\kappa_0 = \mathrm{d}E_{F\uparrow}/\mathrm{d}U$ of the majority species in the fully polarized normal wings where $\tilde{\kappa} = 1$ and in the superfluid region where $\tilde{\kappa} = 1/\xi$.

The equation of state of spin-imbalanced Fermi gases in the form of the universal function $g(x)$ was directly measured from the density profiles of the trapped gas in [34], following the proposal in [184] (see Fig. 31). The density was obtained via an inverse Abel transform of the measured column density [42]. As known from previous studies at MIT [40, 139, 42, 43], three distinct phases are found: A superfluid region at equal spin densities in the core at small distances from the trap center, followed by a normal mixed region at unequal densities, and beyond the minority cloud radius $R_\downarrow$ a region of a fully polarized normal gas of majority atoms. In Fig. 31a, the normal-to-superfluid transition is directly visible as the boundary between the spin-balanced region at equal densities and the imbalanced region. The jump in the density difference marks the first-order transition [43]. The universal function $g(x)$ was obtained from only five independent

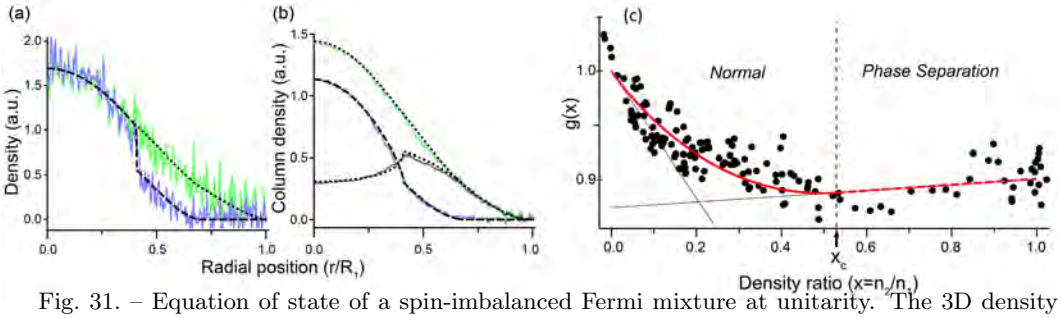

Fig. 31. – Equation of state of a spin-imbalanced Fermi mixture at unitarity. The 3D density profiles (a) obtained via an inverse Abel transform from the measured column density profiles (b) (at population imbalance of 44%) directly yield the equation of state (c) for spin-imbalanced Fermi gases. The normal-to-superfluid transition at $x = n_\uparrow/n_\downarrow \equiv n_2/n_1 = 0.53(5)$. From [34].

measurements. The form of $g(x)$ is constrained by the limiting cases: In the superfluid region where $(\mu_\uparrow + \mu_\downarrow)/2 = \xi E_{F\uparrow}$, $\mu_\uparrow/E_{F\uparrow} = 2\xi/(1+y)$ and thus $g(1) = (2\xi)^{3/5}$; in a fully polarized ($x = 0$) non-interacting Fermi gas one has $\mu_\uparrow = E_{F\uparrow}$ and $g(0) = 1$. The critical chemical potential ratio y_c above which the superfluid forms was found to be $y_c = 0.03(2)$, at a critical density ratio $x = 0.53(5)$. The polaron energy was estimated to be $y_c = A = -0.58(5)$ from a Thomas-Fermi fit to $g(x)$, and $y_c = A = -0.69(8)$ from the measured cloud radii, assuming $\xi = 0.42(1)$, which is however slightly larger than the current value $\xi = 0.37(1)$. The values for A are in good agreement with later studies via RF spectroscopy. The experiment yielded good agreement with a Fermi liquid description of the normal mixed state.

A later experiment by the ENS group [35] yielded a low-noise equation of state for imbalanced gases, making use of the "magic formula" relating the pressure to the doubly integrated density n_{1D}, and working in the grand- ensemble of fixed chemical potentials (see Fig. 32). In the superfluid region with $\mu_s = (\mu_\uparrow + \mu_\downarrow)/2$ the pressure is

$$P(\mu_\uparrow, \mu_\downarrow) = \frac{1}{15\pi^2}\left(\frac{m}{\xi\hbar^2}\right)^{3/2}(\mu_\uparrow + \mu_\downarrow)^{5/2} \tag{131}$$

while in the Fermi liquid region good agreement was found, as in [34], assuming a non-interacting Fermi gas of majority atoms coexisting with a Fermi liquid of polarons with renormalized energy and mass. The corresponding pressure is

$$P(\mu_\uparrow, \mu_\downarrow) = \frac{1}{15\pi^2}\left[\left(\frac{m}{\hbar^2}\right)^{3/2}\mu_\uparrow^{5/2} + \left(\frac{m^*}{\hbar^2}\right)^{3/2}(\mu_\downarrow - E_\downarrow)^{5/2}\right] \tag{132}$$

In terms of the energy density, this can be expressed in the canonical form as a Landau-

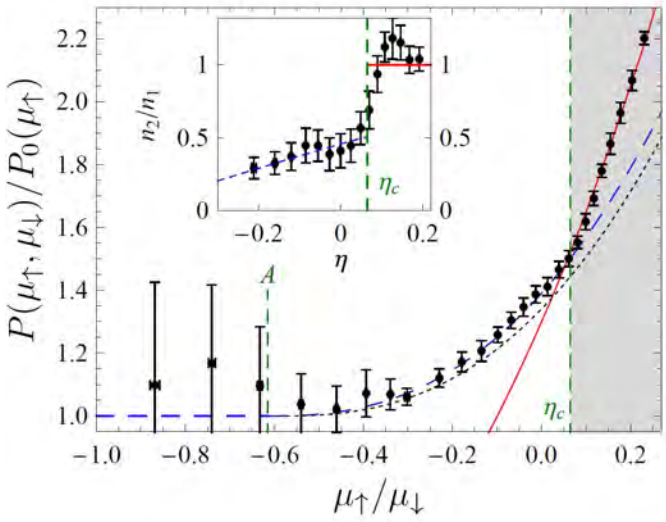

Fig. 32. – Equation of state of a spin-imbalanced Fermi mixture at unitarity (black dots). $P_0(\mu_\uparrow)$ is the pressure of a non-interacting Fermi gas at a chemical potential $\mu_\uparrow$. The red solid line is the superfluid equation of state, the blue dashed line is the ideal Fermi liquid equation 132 with $A = -0.615$, $m^* = 1.20\,m$ and the black dotted line is the Monte-Carlo calculation from [154]. η corresponds to $y = \mu_\uparrow/\mu_\downarrow$ in the text. From [35].

Pomeranchuk functional [154, 186, 191]

$$\mathcal{E}(n_\uparrow, n_\downarrow) = \frac{3}{5} n_\uparrow E_{F\uparrow} \left(1 + \frac{5A}{3}x + \frac{m}{m^*}x^{5/3} + Fx^2\right) \tag{133}$$

The first term is the majority Fermi energy, the second is the polaron energy shift, the third is the Fermi energy of a non-interacting gas of polarons with effective mass m^*, and the fourth describes an effective interaction between polarons. The interaction term was found in Monte-Carlo calculations [186], the analytic expression $F = \frac{5}{9}\left(\frac{\mathrm{d}E_\downarrow}{\mathrm{d}\mu_\uparrow}\right)^2$ was found in [191] and shown in [192] to be due to the induced interaction between minority atoms through interaction with the majority spins.

Assuming $\xi_s = 0.42(1)$, the experiment in [35] agreed excellently with the theoretical value for the polaron energy $A = -0.615$ and found $m^*/m = 1.20(2)$, in agreement with theory [156, 153]. It is remarkable that the simple expression 132 works well even for a large number of minority atoms, close to the superfluid-to-normal transition. One can expect that the majority Fermi sea will eventually experience dressing by the minority cloud so that the energy and mass of majority atoms will also be renormalized. The work was extended to interaction strengths in the BEC and BCS regime in [37], and the Fermi liquid picture for the mixed region confirmed in detail in [143].

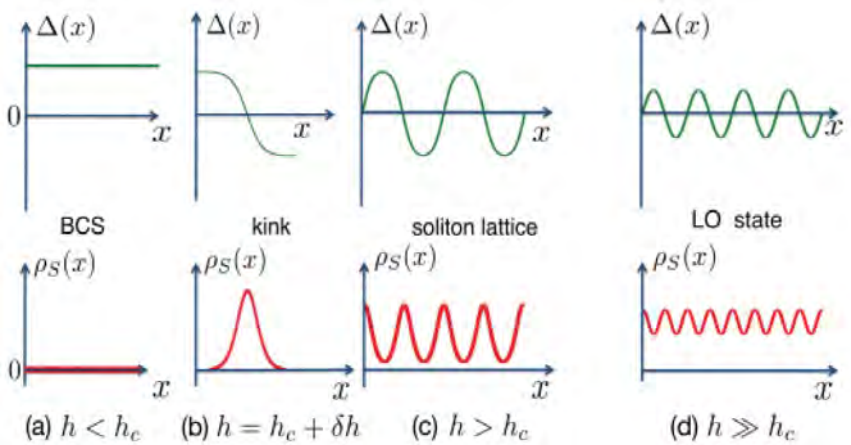

Fig. 33. – Evolution from the uniform superfluid to the Larkin-Ovchinnikov state via solitons and soliton trains, as a function of the chemical potential difference. The top row shows the pairing gap $\Delta(x)$, the bottom row the excess spin density $\rho_S(x)$. a) Below $h < h_c$, the uniform superfluid is favored. b) For one unpaired atom (per transverse area), at h slightly above h_c, $\Delta(x)$ develops a soliton kink. c) Soliton lattice at small imbalance. d) LO state at $h \gg h_c$, $\Delta(x)$ is sinusoidal. Note that $\rho_S(x)$ peaks where $\Delta(x)$ vanishes. From [193].

3˙6. *Prospects for observing the FFLO state.* – The Clogston-Chandrasekhar limit of superfluidity at a critical field $h_{\rm CC} \approx \Delta/\sqrt{2}$ (in the BCS limit) assumed a homogeneous pairing amplitude Δ. Fulde and Ferrell [172], and independently Larkin and Ovchinnikov [173] proposed a new superfluid ground state in the presence of a magnetic field that allows for an inhomogeneous order parameter, $\Delta(\mathbf{r})$. Fulde and Ferrell (FF) considered a state with $\Delta(\mathbf{r}) = \Delta_0 e^{i\mathbf{Q}\cdot\mathbf{r}}$ corresponding to Cooper pairs that are condensed at finite momentum $\mathbf{Q}$. This yielded a lower free energy than the BCS and normal state at $h = \Delta/\sqrt{2}$. Larkin and Ovchinnikov (LO) introduced a standing wave, an equal superposition of left- and right-moving Cooper pairs, or in other words a sinusoidally varying order parameter such as $\Delta(\mathbf{r}) = \Delta_0 \cos(Qx)$. This was energetically more favorable than the FF state. The magnitude of the order parameter is here spatially varying, as is the spin density $n_\uparrow - n_\downarrow$, which is concentrated at the nodes of the gap. This is natural in a local density approximation, as near $\Delta \approx 0$ it does not cost extra energy to place an excess particle.

In the limit of very small population imbalance, the LO state evolves into a train of domain walls, a soliton train [194] (see Fig 33 and [195, 196, 193] and references therein). The limit of a single soliton, where the order parameter switches sign once - corresponding to a phase shift of π -, has famous connections to quantum field theory [197], the Su-Schrieffer-Heeger model of Polyacetylene [198], and Josephson π-junctions. The spin density is concentrated at the soliton. In 1D, it is well-known that a single soliton provides exactly one bound state per spin [197], and it is in this bound state that the

excess spin resides. The energy cost for forming a soliton in one dimension is [194] $\frac{2}{\pi}\Delta_0$, where Δ_0 is the magnitude of the order parameter far away from the soliton, given by the BCS result for the uniform system. The critical magnetic field h at which it becomes energetically favorable to form the soliton is $h_c = \frac{2}{\pi}\Delta_0 = 0.637\ldots\Delta_0$, smaller than the CC limit $\Delta_0/\sqrt{2} = 0.707\ldots\Delta_0$. A calculation in three dimensions [199] gives a critical field of $h_c = 0.67\ldots\Delta_0$. The LO state is thus more robust than the uniform superfluid and the normal state, at least in the window $h_c < h < h_{\rm CC}$, but probably even up to $h \approx 0.84\Delta_0$.

The range of magnetic fields in which inhomogeneous superconductivity is predicted to be stable is narrow. In typical atom traps with harmonic confinement, the interesting range would only encompass a narrow shell of the entire superfluid, as $h/\Delta(\mathbf{r})$ varies in the trap. However, one prospect is to produce Fermi mixtures in a uniform box potential, as was demonstrated with bosons in [200]. This would allow tuning the density difference and therefore the chemical potential difference to the right value and enable the observation of the LO state.

Another exciting prospect is the creation of the FFLO state as a non-equilibrium excited state of the superfluid, in a regime where the ground state is still uniform. Solitary waves in a fermionic superfluid have been observed after phase-imprinting in an experiment at MIT [201], and in the presence of imbalance, they should offer bound states for majority spins. It might be possible to engineer entire soliton trains in the presence of spin imbalance. These would realize the LO state as a metastable excited state. Although this would not realize the FFLO state as the ground state of the system, the philosophy here is not different from what has applied for Bose-Einstein condensation - it is, after all, an excited metastable state of the absolute ground state of a collection of alkali atoms - the solid.

4. – Conclusion and Perspectives

This chapter presented a review of many of the experimental achievements in the study of fermionic superfluidity in ultracold atomic gases. The strong interactions induced by the Feshbach resonance mechanism enabled the realization of crossover superfluids in atomic Fermi gases that lie in between the limit of Bose-Einstein condensation of tightly bound fermion pairs to Bardeen-Cooper-Schrieffer superfluidity of long-range Cooper pairs. These gases provide an ideal realization of Fermi mixtures interacting via a contact potential, and therefore make direct contact to many-body theories. Spectroscopic tools and thermodynamic measurements have reached a precision that allows to validate or discard existing theories of interacting fermions that are used in many other contexts in physics. For example, a full-fledged theory of the equation of state of neutron matter must, at its core, contain the physics of strongly interacting fermions with s-wave contact interactions. If here it does not overlap with experimental results from ultracold Fermi gases, it must be modified. Thermodynamic measurements have played a crucial role for validating the bold diagrammatic Monte-Carlo method [39] that allows to sample the space of Feynman diagrams - a novel method where the fermion sign problem turns into

a sign blessing [167], making the sum of all Feynman diagrams convergent.

An intriguing question is whether the strongly interacting Fermi gas at unitarity has a weakly interacting gravity dual [202, 203, 204]. Thus far, we do not even know the wave equation governing the resonant Fermi gas. Through the study of solitons [205, 206, 201] and phonon-soliton scattering, one might be able to "guess" the properties of the underlying wave equation. If scattering is observed to be reflectionless, there is hope for the existence of a non-interacting dual theory.

Spin-imbalanced mixtures of strongly interacting fermions represent a novel system that has no weakly interacting counterpart in condensed matter physics. Their study has revealed a complex phase diagram with first- and second order transitions separated by a tricritical line [43]; a superfluid phase at equal spin densities phase separated from a normal mixed phase [40, 41, 42, 34, 35]; a novel attractive Fermi liquid whose quasiparticles can be studied "in isolation" in the limit of a single spin impurity immersed in a Fermi sea - the Fermi polaron [45, 44, 35, 37, 47, 46]; a transition line from a Fermi liquid of polarons to a "magnetized" superfluid in the BEC regime where fermions and bosonic molecules coexist [181]. Furthermore, there is hope to observe the long-sought Fulde-Ferrell-Larkin-Ovchinnikov state of non-zero momentum Cooper pairs, more specifically the LO state in the limit of small imbalance. Here it represents trains of solitons that each carry excess atoms in Andreev bound states. Solitons have already been observed in balanced superfluids and found to be long-lived [201].

Novel fermionic systems offer the prospect of observing new states of matter and to gain further insight into many-body physics. Atomic gases allow the realization of high-spin mixtures of fermions [207, 208] that offer the prospect of realizing exotic states of matter, such as a "color" superfluid [209]. In addition, one may create mixtures of fermions with another species. Mixtures between two fermionic species (e.g. ^{6}Li and ^{40}K) may allow the study of pairing and superfluidity where the pairs are made from atoms with different masses [210, 211]. Hydrodynamics caused by strong interactions in a ^{6}Li-^{40}K mixture [212], as well as attractive and repulsive polarons [47] have already been observed. Bose-Fermi mixtures have been used to study how the addition of fermionic atoms affects the bosonic superfluid-to-Mott-insulator transition [213, 214]. Also intriguing is the study of boson-mediated interactions between fermions [215, 216]. Interspecies Feshbach resonances between fermionic and bosonic atoms have been identified [217, 218, 219], and heteronuclear molecules observed in ^{40}K^{87}Rb [220, 221], ^{23}Na^{40}K [222] and ^{23}Na^{6}Li [223].

Another direction is the study of lower-dimensional Fermi gases, that has already revealed pairing in 1D [224, 225, 226, 227, 228] and 2D [149, 229, 150] and polarons in 2D gases [46, 230]. Fermionic superfluids in 1D optical lattices should realize ideal models of layered superconductors. In a single two-dimensional layer, the physics of the Berezinskii-Kosterlitz-Thouless (BKT) transition of proliferating vortex pairs, and the interplay with fragile fermion pairing will be an interesting future topic. An exciting avenue is the preparation of systems with a precisely controlled number of fermions. The odd-even effect due to pairing [227] as well as the interaction of a single spin down atom with a Fermi sea [228] has been studied by adding one atom at a time.

Experiments on Fermi gases in 3D optical lattices [231, 232, 233, 234, 235, 236], equipped with single-site-resolution imaging [237, 238, 239] are on the verge of becoming ideal testbeds for the Fermi Hubbard model. At low temperatures, the system should be antiferromagnetic, and at lower filling, it may show d-wave superfluidity, and should help to elucidate the nature of pairing in high-temperature superconductors. A mixture of a Fermi gas, e.g. ^{40}K, representing itinerant electrons, and another species, e.g. ^{23}Na, that can represent localized impurities in an optical lattice might allow realization of a Kondo-correlated state [240, 241].

An exciting prospect is the observation of p-wave superfluidity and topological states of matter in ultracold Fermi gases. p-wave Feshbach resonances have been observed [242, 243, 244, 245], and p-wave molecules have been produced [246]. However, the lifetime of the gas at such resonances was limited as three-body collisions are no longer suppressed, a feature that was so crucial for the stability near s-wave resonances. A novel way to create effective p-wave, i.e. single-band, interactions between fermions is to induce synthetic spin-orbit coupling [247]. In this method, laser fields provide momentum-dependent coupling of two (hyperfine) spin states of the atom. Spin-orbit coupling lies at the heart of topological states of matter [248, 249]. Laser-induced spin-orbit coupling has been realized for Fermi gases [250, 251, 252]. In combination with an s-wave Feshbach resonance, spin-orbit coupling leads to effective p-wave (and higher order partial wave) collisions and p-wave pairing. Spin-orbit coupled superfluids have been shown to be topological and they will feature Majorana fermions inside vortex cores [253, 254]. Feshbach molecules in the presence of spin-orbit coupling have been created [**?**, 255, 252], however the lifetimes were short and heating was severe. Novel methods to realize strong effective spin-orbit coupling and large magnetic fields in optical lattices [256, 257, 258] do not rely on near-resonant laser beams and might allow realization of topological states of fermionic matter, from quantum Hall states to topological superfluidity.

Finally, the realization of Fermi gases with strong dipolar interactions is currently one of the major avenues towards novel exotic many-body states. Fermi gases with magnetic dipolar interactions have been cooled to quantum degeneracy [259, 260]. In Erbium, a high density, long-lived dipolar Fermi gas was achieved with a dipolar interaction energy of about 1% of the Fermi energy [260]. In parallel, a highly promising route is the creation of ultracold fermionic molecules with tunable, strong electric dipole moment. In a pioneering experiment at JILA, a high-phase space density gas of ultracold fermionic ground-state molecules of ^{40}K^{87}Rb was formed [261] from loosely bound Feshbach molecules. The method was independently used at Innsbruck to create ultracold bosonic ground-state molecules of Cs_2 [262]. Chemical reactions limited the lifetime of the molecular gas in the bulk [263], but long lifetimes in an optical lattices at moderate filling were achieved [264]. Dipolar collisions have been studied in the bulk [265]. Coherent spin dynamics, driven by dipolar interactions, have been observed in a 3D optical lattice [266], demonstrating the utility of dipolar molecules to realize models of quantum magnetism. For possible p-wave superfluidity in a bulk gas, chemically stable molecules would be required. Possible candidates among bialkalis are NaK and KCs. NaK features a strong dipole moment of 2.7 Debye. Ultracold fermionic Feshbach molecules of ^{23}Na^{40}K

have been created [222]. A stable Fermi gas of fermionic dipolar molecules of NaK would feature a dipolar interaction energy that can reach up to several ten percent of the Fermi energy and would dominate the many-body physics of the gas, possibly leading to p-wave superfluidity.

The multitude of novel systems already in preparation is remarkable. The techniques to control and manipulate cold atoms are in place. The field is ready to embark on new adventures, and exotic states of matter are already on the horizon.

* * *

Work on ultracold fermions at MIT has been a tremendous team effort, and I am deeply grateful to the past and present collaborators who have shared both the excitement and the hard work. First and foremost I would like to thank Wolfgang Ketterle, who introduced me to ultracold Fermi gases as an infinitely rich research field in 2001 and who later, in Dave Pritchard's words, "handed the keys to the family car" to me when I became Assistant Professor at MIT in 2007. The family car is "BEC1", the first sodium BEC apparatus, still under ultra-high vacuum for now twenty years. I would also like to express my thanks to Jamil R. Abo-Shaeer, Peyman Ahmadi, Waseem Bakr, Lawrence W. Cheuk, Kai Dieckmann, Thomas Gersdorf, Axel Görlitz, Elmer Guardado-Sanchez, Subhadeep Gupta, Zoran Hadzibabic, Wenjie Ji, Andrew J. Kerman, Mark J. Ku, Katherine Lawrence, Huanqian Loh, Thomas Lompe, Biswaroop Mukherjee, Matthew Nichols, Melih Okan, Jeewoo W. Park, Sebastian M.F. Raupach, Vinary Ramasesh, Giacomo Roati, Ibon Santiago, Ariel Sommer, Andre Schirotzek, Christian H. Schunck, Yong-Il Shin, Claudiu A. Stan, Sebastian Will, Cheng-Hsun Wu, Zoe Z. Yan, Tarik Yefsah, and Hao Zhang. I would like to thank the National Science Foundation, the Air Force Office of Scientific Research, the Army Research Office, the Office of Naval Research, DARPA, the Alfred P. Sloan foundation, and the David and Lucile Packard Foundation for their encouragement and financial support of this work.

REFERENCES

[1] STWALLEY W. C., *Phys. Rev. Lett.*, **37** (1976) 1628.
[2] TIESINGA E., VERHAAR B. and STOOF H., *Phys. Rev. A*, **47** (1993) 4114.
[3] INOUYE S., ANDREWS M. R., STENGER J., MIESNER H. J., STAMPER-KURN D. M. and KETTERLE W., *Nature*, **392** (1998) 151.
[4] COURTEILLE P., FREELAND R., HEINZEN D., VAN ABEELEN F. and VERHAAR B., *Phys. Rev. Lett.*, **81** (1998) 69.
[5] GREINER M., REGAL C. A. and JIN D. S., *Nature*, **426** (2003) 537.
[6] JOCHIM S., BARTENSTEIN M., ALTMEYER A., HENDL G., RIEDL S., CHIN C., HECKER-DENSCHLAG J. and GRIMM R., *Science*, **302** (2003) 2101.
[7] ZWIERLEIN M., STAN C., SCHUNCK C., RAUPACH S., GUPTA S., HADZIBABIC Z. and KETTERLE W., *Phys. Rev. Lett.*, **91** (2003) 250401.
[8] REGAL C. A., GREINER M. and JIN D. S., *Phys. Rev. Lett.*, **92** (2004) 040403.
[9] ZWIERLEIN M., STAN C., SCHUNCK C., RAUPACH S., KERMAN A. and KETTERLE W., *Phys. Rev. Lett.*, **92** (2004) 120403.
[10] BARTENSTEIN M., ALTMEYER A., RIEDL S., JOCHIM S., CHIN C., HECKER-DENSCHLAG J. and GRIMM R., *Phys. Rev. Lett.*, **92** (2004) 120401.
[11] BOURDEL T., KHAYKOVICH L., CUBIZOLLES J., ZHANG J., CHEVY F., TEICHMANN M., TARRUELL L., KOKKELMANS S. and SALOMON C., *Phys. Rev. Lett.*, **93** (2004) 050401.
[12] KINAST J., HEMMER S., GEHM M., TURLAPOV A. and THOMAS J. E., *Phys. Rev. Lett.*, **92** (2004) 150402.
[13] PARTRIDGE G. B., STRECKER K. E., KAMAR R. I., JACK M. W. and HULET R. G., *Phys. Rev. Lett.*, **95** (2005) 020404.

[14] ZWIERLEIN M. W., ABO-SHAEER J. R., SCHIROTZEK A., SCHUNCK C. H. and KETTERLE W., *Nature*, **435** (2005) 1047.
[15] MILLER D. E., CHIN J. K., STAN C. A., LIU Y., SETIAWAN W., SANNER C. and KETTERLE W., *Phys. Rev. Lett.*, **99** (2007) 070402.
[16] RIEDL S., GUAJARDO E. R. S., KOHSTALL C., DENSCHLAG J. H. and GRIMM R., *New Journal of Physics*, **13** (2011) 035003.
[17] SIDORENKOV L. A., TEY M. K., GRIMM R., HOU Y.-H., PITAEVSKII L. and STRINGARI S., *Nature*, **498** (2013) 78.
[18] STADLER D., KRINNER S., MEINEKE J., BRANTUT J.-P. and ESSLINGER T., *Nature*, **491** (2012) 736.
[19] REGAL C. A. and JIN D. S., *Phys. Rev. Lett.*, **90** (2003) 230404.
[20] GUPTA S., HADZIBABIC Z., ZWIERLEIN M., STAN C., DIECKMANN K., SCHUNCK C., KEMPEN E. V., VERHAAR B. and KETTERLE W., *Science*, **300** (2003) 1723.
[21] CHIN C., BARTENSTEIN M., ALTMEYER A., RIEDL S., JOCHIM S., HECKER-DENSCHLAG J. and GRIMM R., *Science*, **305** (2004) 1128.
[22] SHIN Y., SCHUNCK C. H., SCHIROTZEK A. and KETTERLE W., *Phys. Rev. Lett.*, **99** (2007) 090403.
[23] SCHIROTZEK A., SHIN Y., SCHUNCK C. H. and KETTERLE W., *Phys. Rev. Lett.*, **101** (2008) 140403.
[24] STEWART J. T., GAEBLER J. P. and JIN D. S., *Nature*, **454** (2008) 744.
[25] KINAST J., TURLAPOV A. and THOMAS J. E., *Phys. Rev. A*, **70** (2004) 051401.
[26] BARTENSTEIN M., ALTMEYER A., RIEDL S., JOCHIM S., CHIN C., HECKER-DENSCHLAG J. and GRIMM R., *Phys. Rev. Lett.*, **92** (2004) 203201.
[27] GRIMM R., *Ultracold fermi gases in the bec-bcs crossover: a review from the innsbruck perspective*, in *Ultracold Fermi Gases, Proceedings of the International School of Physics "Enrico Fermi", Course CLXIV, Varenna, 20 - 30 June 2006*, edited by INGUSCIO M., KETTERLE W. and SALOMON C. (IOS Press, Amsterdam) 2008.
[28] TEY M. K., SIDORENKOV L. A., GUAJARDO E. R. S., GRIMM R., KU M. J. H., ZWIERLEIN M. W., HOU Y.-H., PITAEVSKII L. and STRINGARI S., *Phys. Rev. Lett.*, **110** (2013) 055303.
[29] CAO C., ELLIOTT E., JOSEPH J., WU H., PETRICKA J., SCHÄFER T. and THOMAS J. E., *Science*, **331** (2011) 58.
[30] SOMMER A., KU M., ROATI G. and ZWIERLEIN M. W., *Nature*, **472** (2011) 201.
[31] KOVTUN P. K., SON D. T. and STARINETS A. O., *Phys. Rev. Lett.*, **94** (2005) 111601.
[32] SCHAFER T. and TEANEY D., *Rep. Prog. Phys.*, **72** (2009) 126001.
[33] HO T.-L., *Phys. Rev. Lett.*, **92** (2004) 090402.
[34] SHIN Y.-I., *Phys. Rev. A*, **77** (2008) 041603.
[35] NASCIMBÈNE S., NAVON N., JIANG K. J., CHEVY F. and SALOMON C., *Nature*, **463** (2010) 1057.
[36] HORIKOSHI M., NAKAJIMA S., UEDA M. and MUKAIYAMA T., *Science*, **327** (2010) 442.
[37] NAVON N., NASCIMBENE S., CHEVY F. and SALOMON C., *Science*, **328** (2010) 729.
[38] KU M. J. H., SOMMER A. T., CHEUK L. W. and ZWIERLEIN M. W., *Science*, **335** (2012) 563.
[39] VAN HOUCKE K., WERNER F., KOZIK E., PROKOF/'EV N., SVISTUNOV B., KU M. J. H., SOMMER A. T., CHEUK L. W., SCHIROTZEK A. and ZWIERLEIN M. W., *Nat Phys*, **8** (2012) 366.
[40] ZWIERLEIN M. W., SCHIROTZEK A., SCHUNCK C. H. and KETTERLE W., *Science*, **311** (2006) 492.
[41] PARTRIDGE G. B., LI W., KAMAR R. I., LIAO Y. and HULET R. G., *Science*, **311** (2006) 503.

[42] SHIN Y., ZWIERLEIN M., SCHUNCK C., SCHIROTZEK A. and KETTERLE W., *Phys. Rev. Lett.*, **97** (2006) 030401.
[43] SHIN Y., SCHUNCK C., SCHIROTZEK A. and KETTERLE W., *Nature*, **451** (2007) 689.
[44] NASCIMBENE S., NAVON N., JIANG K. J., TARRUELL L., TEICHMANN M., MCKEEVER J., CHEVY F. and SALOMON C., *Phys. Rev. Lett.*, **103** (2009) 170402.
[45] SCHIROTZEK A., WU C.-H., SOMMER A. and ZWIERLEIN M. W., *Phys. Rev. Lett.*, **102** (2009) 230402.
[46] KOSCHORRECK M., PERTOT D., VOGT E., FROHLICH B., FELD M. and KÖHL M., *Nature*, **485** (2012) 619.
[47] KOHSTALL C., ZACCANTI M., JAG M., TRENKWALDER A., MASSIGNAN P., BRUUN G. M., SCHRECK F. and GRIMM R., *Nature*, **485** (2012) 615.
[48] ALFORD M. G., SCHMITT A., RAJAGOPAL K. and SCHAFER T., *Rev. Mod. Phys.*, **80** (2008) 1455.
[49] TAN S., *Annals of Physics*, **323** (2008, preprint arXiv:0508320 (2005)) 2971.
[50] THOMAS J. E., KINAST J. and TURLAPOV A., *Phys. Rev. Lett.*, **95** (2005) 120402.
[51] BERTSCH G., *Proceedings of the tenth international conference on recent progress in many-body theories*, presented at *Recent progress in many-body theories*, edited by BISHOP R., GERNOTH K. A., WALET N. R. and XIAN Y. (World Scientific, Seattle) 2000.
[52] GIORGINI S., PITAEVSKII L. P. and STRINGARI S., *Rev. Mod. Phys.*, **80** (2008) 1215.
[53] ZWERGER W. (Ed.), *The BCS-BEC crossover and the unitary Fermi gas*, Vol. 836 (Springer) 2011.
[54] WERNER F. and CASTIN Y., *Phys. Rev. A*, **74** (2006) 053604.
[55] TAN S., *Annals of Physics*, **323** (2008) 2987.
[56] WERNER F., *Phys. Rev. A*, **78** (2008) 025601.
[57] BRAATEN E. and PLATTER L., *Phys. Rev. Lett.*, **100** (2008) 205301.
[58] O'HARA K. M., HEMMER S. L., GEHM M. E., GRANADE S. R. and THOMAS J. E., *Science*, **298** (2002) 2179.
[59] GEHM M. E., HEMMER S. L., GRANADE S. R., O'HARA K. M. and THOMAS J. E., *Phys. Rev. A*, **68** (2003) 011401.
[60] KINAST J., TURLAPOV A., THOMAS J. E., CHEN Q., STAJIC J. and LEVIN K., *Science*, **307** (2005) 1296.
[61] STEWART J. T., GAEBLER J. P., REGAL C. A. and JIN D. S., *Phys. Rev. Lett.*, **97** (2006) 220406.
[62] BOURDEL T., CUBIZOLLES J., KHAYKOVICH L., MAGALH, K. M. F. AND AES, KOKKELMANS S. J. J. M. F., SHLYAPNIKOV G. V. and SALOMON C., *Phys. Rev. Lett.*, **91** (2003) 020402.
[63] LUO L., CLANCY B., JOSEPH J., KINAST J. and THOMAS J. E., *Phys. Rev. Lett.*, **98** (2007) 080402.
[64] TAN S., *Annals of Physics*, **323** (2008, preprint arXiv:0505200 (2005)) 2952.
[65] WERNER F., TARRUELL L. and CASTIN Y., *The European Physical Journal B - Condensed Matter and Complex Systems*, **68** (2009) 401.
[66] CHENG C.-H. and YIP S.-K., *Phys. Rev. B*, **75** (2007) 014526.
[67] HO T.-L. and ZHOU Q., *Nat Phys*, **6** (2010) 131.
[68] LUO L. and THOMAS J., *J. Low Temp. Phys.*, **154** (2009) 1.
[69] KETTERLE W. and ZWIERLEIN M., *Making, probing and understanding ultracold Fermi gases*, in *Ultracold Fermi Gases, Proceedings of the International School of Physics "Enrico Fermi", Course CLXIV, Varenna, 20 - 30 June 2006.*, edited by INGUSCIO M., KETTERLE W. and SALOMON C. (IOS Press, Amsterdam.) 2008.
[70] BLOCH I., DALIBARD J. and ZWERGER W., *Rev. Mod. Phys.*, **80** (2008) 885.
[71] KEESOM W. H. and KEESOM M. A. P., *Physica*, **1** (1934) 128.

[72] TINKHAM M., *Introduction to Superconductivity*, second edition Edition (Dover, Mineola, New York) 2004.
[73] VOLLHARDT D., W P. and "OLFLE, *The Superfluid Phases of Helium 3* (Taylor & Francis, London) 1990.
[74] HAUSSMANN R., RANTNER W., CERRITO S. and ZWERGER W., *Phys. Rev. A*, **75** (2007) 023610.
[75] HAUSSMANN R., *Phys. Rev. B*, **49** (1994) 12975.
[76] GOULKO O. and WINGATE M., *Phys. Rev. A*, **82** (2010) 053621.
[77] BUROVSKI E., PROKOF'EV N., SVISTUNOV B. and TROYER M., *Phys. Rev. Lett.*, **96** (2006) 160402.
[78] BULGAC A., DRUT J. E. and MAGIERSKI P., *Phys. Rev. Lett.*, **96** (2006) 090404.
[79] BULGAC A., DRUT, JOAQUIN E. and MAGIERSKI P., *Phys. Rev. A*, **78** (2008) 023625.
[80] CASTIN Y. and WERNER F., *Preprint arXiv:1103.2851*, (2011) .
[81] ZÜRN G., LOMPE T., WENZ A. N., JOCHIM S., JULIENNE P. S. and HUTSON J. M., *Phys. Rev. Lett.*, **110** (2013) 135301.
[82] FORBES M. M., GANDOLFI S. and GEZERLIS A., *Phys. Rev. Lett.*, **106** (2011) 235303.
[83] ARNOLD P., DRUT, JOAQUIN E. and SON D. T., *Phys. Rev. A*, **75** (2007) 043605.
[84] CARLSON J., CHANG S.-Y., PANDHARIPANDE V. R. and SCHMIDT K. E., *Phys. Rev. Lett.*, **91** (2003) 050401.
[85] ASTRAKHARCHIK G. E., BORONAT J., CASULLERAS J. and GIORGINI S., *Phys. Rev. Lett.*, **93** (2004) 200404.
[86] WERNER F. and CASTIN Y., *Phys. Rev. A*, **86** (2012) 013626.
[87] LIEB E. H. and LINIGER W., *Phys. Rev.*, **130** (1963) 1605.
[88] OLSHANII M. and DUNJKO V., *Phys. Rev. Lett.*, **91** (2003) 090401.
[89] HOLZMANN M. and CASTIN Y., *The European Physical Journal D - Atomic, Molecular, Optical and Plasma Physics*, **7** (1999) 425.
[90] NARASCHEWSKI M. and GLAUBER R. J., *Phys. Rev. A*, **59** (1999) 4595.
[91] ZWIERLEIN M. W., HADZIBABIC Z., GUPTA S. and KETTERLE W., *Phys. Rev. Lett.*, **91** (2003) 250404.
[92] BAYM G., PETHICK C. J., YU Z. and ZWIERLEIN M. W., *Phys. Rev. Lett.*, **99** (2007) 190407.
[93] DALFOVO F., GIORGINI S., PITAEVSKII L. and STRINGARI S., *Rev. Mod. Phys.*, **71** (1999) 463.
[94] LEE T. and YANG C., *Phys. Rev.*, **105** (1957) 1119.
[95] LEE T., HUANG K. and YANG C., *Phys. Rev.*, **106** (1957) 1135.
[96] PETROV D., SALOMON C. and SHLYAPNIKOV G., *Phys. Rev. Lett.*, **93** (2004) 090404.
[97] HAUSSMANN R. and ZWERGER W., *Phys. Rev. A*, **78** (2008) 063602.
[98] HAUSSMANN R., PUNK M. and ZWERGER W., *Phys. Rev. A*, **80** (2009) 063612.
[99] PUNK M. and ZWERGER W., *Phys. Rev. Lett.*, **99** (2007) 170404.
[100] CHANG S. Y., PANDHARIPANDE V. R., CARLSON J. and SCHMIDT K. E., *Phys. Rev. A*, **70** (2004) 043602.
[101] LOBO C., CARUSOTTO I., GIORGINI S., RECATI A. and STRINGARI S., *Phys. Rev. Lett.*, **97** (2006) 100405.
[102] STEWART J. T., GAEBLER J. P., DRAKE T. E. and JIN D. S., *Phys. Rev. Lett.*, **104** (2010) 235301.
[103] ZHANG S. and LEGGETT A. J., *Phys. Rev. A*, **77** (2008) 033614.
[104] SAGI Y., DRAKE T. E., PAUDEL R. and JIN D. S., *Phys. Rev. Lett.*, **109** (2012) 220402.
[105] VEERAVALLI G., KUHNLE E., DYKE P. and VALE C. J., *Phys. Rev. Lett.*, **101** (2008) 250403.

[106] Regal C., Greiner M., Giorgini S., Holland M. and Jin D., *Phys. Rev. Lett.*, **95** (2005) 250404.
[107] Son D. T. and Thompson E. G., *Phys. Rev. A*, **81** (2010) 063634.
[108] Kuhnle E. D., Hu H., Liu X. J., Dyke P., Mark M., Drummond P. D., Hannaford P. and Vale C. J., *Phys. Rev. Lett.*, **105** (2010) 070402.
[109] Hoinka S., Lingham M., Fenech K., Hu H., Vale C. J., Drut J. E. and Gandolfi S., *Phys. Rev. Lett.*, **110** (2013) 055305.
[110] Enss T., Haussmann R. and Zwerger W., *Annals of Physics*, **326** (2011) 770.
[111] Regal C. A., Ticknor C., Bohn J. L. and Jin D. S., *Nature*, **424** (2003) 47.
[112] Schunck C., Shin Y.-I., Schirotzek A., Zwierlein M. and Ketterle W., *Science*, **316** (2007) 867.
[113] Schunck C. H., Shin Y., Schirotzek A. and Ketterle W., *Nature*, **454** (2008) 739.
[114] Harber D. M., Lewandowski H. J., McGuirk J. M. and Cornell E. A., *Phys. Rev. A*, **66** (2002) 053616.
[115] Campbell G. K., Boyd M. M., Thomsen J. W., Martin M. J., Blatt S., Swallows M. D., Nicholson T. L., Fortier T., Oates C. W., Diddams S. A., Lemke N. D., Naidon P., Julienne P., Ye J. and Ludlow A. D., *Science*, **324** (2009) 360.
[116] Bishof M., Martin M. J., Swallows M. D., Benko C., Lin Y., Quemener G., Rey A. M. and Ye J., *Phys. Rev. A*, **84** (2011) 052716.
[117] Martin M. J., Bishof M., Swallows M. D., Zhang X., Benko C., von Stecher J., Gorshkov A. V., Rey A. M. and Ye J., *preprint arXiv:1212.6291*, (2012) .
[118] Perali A., Pieri P. and Strinati G. C., *Phys. Rev. Lett.*, **100** (2008) 010402.
[119] Pieri P., Perali A. and Strinati G. C., *Nat Phys*, **5** (2009) 736.
[120] Chin C. and Julienne P. S., *Phys. Rev. A*, **71** (2005) 012713.
[121] Pieri P., Perali A., Strinati G. C., Riedl S., Wright M. J., Altmeyer A., Kohstall C., Sanchez Guajardo E. R., Hecker Denschlag J. and Grimm R., *Phys. Rev. A*, **84** (2011) 011608.
[122] Schneider W., Shenoy V. B. and Randeria M., *preprint arXiv:0903.3006*, (2009) .
[123] Schneider W. and Randeria M., *Phys. Rev. A*, **81** (2010) 021601.
[124] Chen Q., Regal C. A., Jin D. S. and Levin K., *Phys. Rev. A*, **74** (2006) 011601.
[125] Combescot R., Giorgini S. and Stringari S., *EPL (Europhysics Letters)*, **75** (2006) 695.
[126] Stenger J., Inouye S., Chikkatur A. P., Stamper-Kurn D. M., Pritchard D. E. and Ketterle W., *Phys. Rev. Lett.*, **82** (1999) 4569.
[127] Stamper-Kurn D., Chikkatur A., Görlitz A., Inouye S., Gupta S., Pritchard D. and Ketterle W., *Phys. Rev. Lett.*, **83** (1999) 2876.
[128] Zambelli F., Pitaevskii L., Stamper-Kurn D. M. and Stringari S., *Phys. Rev. A*, **61** (2000) 063608.
[129] Steinhauer J., Ozeri R., Katz N. and Davidson N., *Phys. Rev. Lett.*, **88** (2002) 120407.
[130] Kuhnle E. D., Hoinka S., Dyke P., Hu H., Hannaford P. and Vale C. J., *Phys. Rev. Lett.*, **106** (2011) 170402.
[131] Houcke K. V., Werner F., Kozik E., Prokof'ev N. and Svistunov B., *preprint arXiv:1303.6245*, (2013) .
[132] Drut J. E., Lähde T. A. and Ten T., *Phys. Rev. Lett.*, **106** (2011) 205302.
[133] Palestini F., Perali A., Pieri P. and Strinati G. C., *Phys. Rev. A*, **82** (2010) 021605.
[134] Hui H., Xia-Ji L. and Peter D. D., *New Journal of Physics*, **13** (2011) 035007.
[135] Stringari S., *Europhys. Lett.*, **65** (2004) 749.
[136] Altmeyer A., Riedl S., Kohstall C., Wright M. J., Geursen R., Bartenstein M., Chin C., Hecker-Denschlag J. and Grimm R., *Phys. Rev. Lett.*, **98** (2007) 040401.

[137] ASTRAKHARCHIK G. E., COMBESCOT R., LEYRONAS X. and STRINGARI S., *Phys. Rev. Lett.*, **95** (2005) 030404.
[138] HOU Y.-H., PITAEVSKII L. P. and STRINGARI S., *Phys. Rev. A*, **87** (2013) 033620.
[139] ZWIERLEIN M. W., SCHUNCK C. H., SCHIROTZEK A. and KETTERLE W., *Nature*, **442** (2006) 54.
[140] NAVON N., NASCIMBÈNE S., LEYRONAS X., CHEVY F. and SALOMON C., *preprint arXiv:1304.1661*, (2013) .
[141] CHEN Q., STAJIC J., TAN S. and LEVIN K., *Phys. Rep.*, **412** (2005) 1.
[142] GAEBLER J. P., STEWART J. T., DRAKE T. E., JIN D. S., PERALI A., PIERI P. and STRINATI G. C., *Nat Phys*, **6** (2010) 569.
[143] NASCIMBÈNE S., NAVON N., PILATI S., CHEVY F., GIORGINI S., GEORGES A. and SALOMON C., *Phys. Rev. Lett.*, **106** (2011) 215303.
[144] WANG Y., LI L. and ONG N. P., *Phys. Rev. B*, **73** (2006) 024510.
[145] LEE P. A., NAGAOSA N. and WEN X.-G., *Rev. Mod. Phys.*, **78** (2006) 17.
[146] ALLAN A., LINCOLN D. C., THOMAS S., PETER S. and JOHN E. T., *New Journal of Physics*, **14** (2012) 115009.
[147] PARISH M. M. and HUSE D. A., *Preprint arXiv:0903.5324*, (2009) .
[148] ENSS T., *Phys. Rev. A*, **88** (2013) 033630.
[149] FELD M., FROHLICH B., VOGT E., KOSCHORRECK M. and KOHL M., *Nature*, **480** (2011) 75.
[150] SOMMER A. T., CHEUK L. W., KU M. J. H., BAKR W. S. and ZWIERLEIN M. W., *Phys. Rev. Lett.*, **108** (2012) 045302.
[151] NGAMPRUETIKORN V., LEVINSEN J. and PARISH M. M., *preprint arXiv:1309.0272*, (2013) .
[152] PERALI A., PALESTINI F., PIERI P., STRINATI G. C., STEWART J. T., GAEBLER J. P., DRAKE T. E. and JIN D. S., *Phys. Rev. Lett.*, **106** (2011) 060402.
[153] PROKOF'EV N. and SVISTUNOV B., *Phys. Rev. B*, **77** (2008) 020408.
[154] LOBO C., RECATI A., GIORGINI S. and STRINGARI S., *Phys. Rev. Lett.*, **97** (2006) 200403.
[155] COMBESCOT R., RECATI A., LOBO C. and CHEVY F., *Phys. Rev. Lett.*, **98** (2007) 180402.
[156] COMBESCOT R. and GIRAUD S., *Phys. Rev. Lett.*, **101** (2008) 050404.
[157] RECATI A. and STRINGARI S., *Phys. Rev. Lett.*, **106** (2011) 080402.
[158] MAGIERSKI P., WLAZLOWSKI G. and BULGAC A., *Phys. Rev. Lett.*, **107** (2011) 145304.
[159] WLAZLOWSKI G., MAGIERSKI P., DRUT J. E., BULGAC A. and ROCHE K. J., *Phys. Rev. Lett.*, **110** (2013) 090401.
[160] SANNER C., SU E. J., KESHET A., HUANG W., GILLEN J., GOMMERS R. and KETTERLE W., *Phys. Rev. Lett.*, **106** (2011) 010402.
[161] ALFORD M., BERGES J. and RAJAGOPAL K., *Phys. Rev. Lett.*, **84** (2000) 598.
[162] PARTRIDGE G. B., LI W., LIAO Y., HULET R. G., HAQUE M. and STOOF H. T. C., *Phys. Rev. Lett.*, **97** (2006) 190407.
[163] PARISH M. M., MARCHETTI F. M., LAMACRAFT A. and SIMONS B. D., *Nature Physics*, **3** (2007) 124.
[164] CHEVY F., *Physics*, **2** (2009) 48.
[165] CHEVY F., *Phys. Rev. Lett.*, **96** (2006) 130401.
[166] CHEVY F., *Phys. Rev. A*, **74** (2006) 063628.
[167] PROKOF'EV N. and SVISTUNOV B., *Phys. Rev. Lett.*, **99** (2007) 250201.
[168] PROKOF'EV N. V. and SVISTUNOV B. V., *Phys. Rev. B*, **77** (2008) 125101.
[169] CHANDRASEKHAR B., *Appl. Phys. Lett.*, **1** (1962) 7.
[170] CLOGSTON A., *Phys. Rev. Lett.*, **9** (1962) 266.
[171] SARMA G., *J. Phys. Chem. Solids*, **24** (1963) 1029.
[172] FULDE P. and FERRELL R., *Phys. Rev.*, **135** (1964) A550.

[173] LARKIN A. and OVCHINNIKOV Y., *Sov. Phys. JETP, 19, 1228 (1964)*, **47** (1964) 1136.
[174] CASALBUONI R. and NARDULLI G., *Rev. Mod. Phys.*, **76** (2004) 263.
[175] RADOVAN H. A., FORTUNE N. A., MURPHY T. P., HANNAHS S. T., PALM E. C., TOZER S. W. and HALL D., *Nature*, **425** (2003) 51.
[176] BIANCHI A., MOVSHOVICH R., CAPAN C., PAGLIUSO P. and SARRAO J. L., *Phys. Rev. Lett.*, **91** (2003) 187004.
[177] PFLEIDERER C., *Rev. Mod. Phys.*, **81** (2009) 1551.
[178] GOR'KOV L. and MELIK-BARKHUDAROV T., *Zh. Eskp. Theor. Fiz.*, **40** (1961) 1452.
[179] LIAO Y. A., REVELLE M., PAPROTTA T., RITTNER A. S. C., LI W., PARTRIDGE G. B. and HULET R. G., *Phys. Rev. Lett.*, **107** (2011) 145305.
[180] SOMMER A., KU M. and ZWIERLEIN M. W., *New J. Phys.*, **13** (2011) 055009.
[181] SHIN Y.-I., SCHIROTZEK A., SCHUNCK C. H. and KETTERLE W., *Phys. Rev. Lett.*, **101** (2008) 070404.
[182] PUNK M., DUMITRESCU P. T. and ZWERGER W., *Phys. Rev. A*, **80** (2009) 053605.
[183] LANDAU L., *Phys. Z. Sowjetunion*, **3** (1933) 644.
[184] BULGAC A. and FORBES M. M., *Phys. Rev. A*, **75** (2007) 031605.
[185] VEILLETTE M., MOON E. G., LAMACRAFT A., RADZIHOVSKY L., SACHDEV S. and SHEEHY D. E., *Phys. Rev. A*, **78** (2008) 033614.
[186] PILATI S. and GIORGINI S., *Phys. Rev. Lett.*, **100** (2008) 030401.
[187] MASSIGNAN P., BRUUN G. M. and STOOF H. T. C., *Phys. Rev. A*, **78** (2008) 031602.
[188] SCHMIDT R. and ENSS T., *Phys. Rev. A*, **83** (2011) 063620.
[189] MORA C. and CHEVY F., *Phys. Rev. A*, **80** (2009) 033607.
[190] COMBESCOT R., GIRAUD S. and LEYRONAS X., *EPL (Europhysics Letters)*, **88** (2009) 60007.
[191] MORA C. and CHEVY F., *Phys. Rev. Lett.*, **104** (2010) 230402.
[192] YU Z., ZÖLLNER S. and PETHICK C. J., *Phys. Rev. Lett.*, **105** (2010) 188901.
[193] LUTCHYN R. M., DZERO M. and YAKOVENKO V. M., *Phys. Rev. A*, **84** (2011) 033609.
[194] MACHIDA K. and NAKANISHI H., *Phys. Rev. B*, **30** (1984) 122.
[195] YOSHIDA N. and YIP S. K., *Phys. Rev. A*, **75** (2007) 063601.
[196] RADZIHOVSKY L., *Phys. Rev. A*, **84** (2011) 023611.
[197] JACKIW R. and REBBI C., *Phys. Rev. D*, **13** (1976) 3398.
[198] HEEGER A. J., KIVELSON S., SCHRIEFFER J. R. and SU W. P., *Rev. Mod. Phys.*, **60** (1988) 781.
[199] MATSUO S., HIGASHITANI S., NAGATO Y. and NAGAI K., *J. Phys. Soc. Jap.*, **67** (1998) 280.
[200] GAUNT A. L., SCHMIDUTZ T. F., GOTLIBOVYCH I., SMITH R. P. and HADZIBABIC Z., *Phys. Rev. Lett.*, **110** (2013) 200406.
[201] YEFSAH T., SOMMER A. T., KU M. J. H., CHEUK L. W., JI W., BAKR W. S. and ZWIERLEIN M. W., *Nature*, **499** (2013) 426.
[202] SON D. T., *Phys. Rev. D*, **78** (2008) 046003.
[203] BALASUBRAMANIAN K. and MCGREEVY J., *Phys. Rev. Lett.*, **101** (2008) 061601.
[204] HERZOG C. P., KOVTUN P. K. and SON D. T., *Phys. Rev. D*, **79** (2009) 066002.
[205] SCOTT R. G., DALFOVO F., PITAEVSKII L. P. and STRINGARI S., *Phys. Rev. Lett.*, **106** (2011) 185301.
[206] SCOTT R. G., DALFOVO F., PITAEVSKII L. P., STRINGARI S., FIALKO O., LIAO R. and BRAND J., *New Journal of Physics*, **14** (2012) 023044.
[207] OTTENSTEIN T. B., LOMPE T., KOHNEN M., WENZ A. N. and JOCHIM S., *Phys. Rev. Lett.*, **101** (2008) 203202.
[208] KRAUSER J. S., HEINZE J., FLASCHNER N., GOTZE S., JURGENSEN O., LUHMANN D.-S., BECKER C. and SENGSTOCK K., *Nat Phys*, **8** (2012) 813.

[209] RAPP A., ZARAND G., HONERKAMP C. and HOFSTETTER W., *Phys. Rev. Lett.*, **98** (2007) 160405.
[210] TAGLIEBER M., VOIGT A.-C., AOKI T., HÄNSCH T. W. and DIECKMANN K., *Phys. Rev. Lett.*, **100** (2008) 010401.
[211] WILLE E., SPIEGELHALDER F., KERNER G., NAIK D., TRENKWALDER A., HENDL G., SCHRECK F., GRIMM R., TIECKE T., WALRAVEN J., KOKKELMANS S., TIESINGA E. and JULIENNE P., *Phys. Rev. Lett.*, **100** (2008) 053201.
[212] TRENKWALDER A., KOHSTALL C., ZACCANTI M., NAIK D., SIDOROV A. I., SCHRECK F. and GRIMM R., *Phys. Rev. Lett.*, **106** (2011) 115304.
[213] OSPELKAUS S., OSPELKAUS C., WILLE O., SUCCO M., ERNST P., SENGSTOCK K. and BONGS K., *Phys. Rev. Lett.*, **96** (2006) 180403.
[214] GÜNTER K., STÖFERLE T., MORITZ H., KÖHL M. and ESSLINGER T., *Phys. Rev. Lett.*, **96** (2006) 180402.
[215] HEISELBERG H., PETHICK C. J., SMITH H. and VIVERIT L., *Phys. Rev. Lett.*, **85** (2000) 2418.
[216] BIJLSMA M. J., HERINGA B. A. and STOOF H. T. C., *Phys. Rev. A*, **61** (2000) 053601.
[217] STAN C. A., ZWIERLEIN M. W., SCHUNCK C. H., RAUPACH S. M. F. and KETTERLE W., *Phys. Rev. Lett.*, **93** (2004) 143001.
[218] INOUYE S., GOLDWIN J., OLSEN M. L., TICKNOR C., BOHN J. L. and JIN D. S., *Phys. Rev. Lett.*, **93** (2004) 183201.
[219] PARK J. W., WU C.-H., SANTIAGO I., TIECKE T. G., WILL S., AHMADI P. and ZWIERLEIN M. W., *Phys. Rev. A*, **85** (2012) 051602.
[220] OSPELKAUS C., OSPELKAUS S., HUMBERT L., ERNST P., SENGSTOCK K. and BONGS K., *Phys. Rev. Lett.*, **97** (2006) 120402.
[221] ZIRBEL J. J., NI K. K., OSPELKAUS S., D'INCAO J. P., WIEMAN C. E., YE J. and JIN D. S., *Phys. Rev. Lett.*, **100** (2008) 143201.
[222] WU C.-H., PARK J. W., AHMADI P., WILL S. and ZWIERLEIN M. W., *Phys. Rev. Lett.*, **109** (2012) 085301.
[223] HEO M.-S., WANG T. T., CHRISTENSEN C. A., RVACHOV T. M., COTTA D. A., CHOI J.-H., LEE Y.-R. and KETTERLE W., *Phys. Rev. A*, **86** (2012) 021602.
[224] MORITZ H., STÖFERLE T., GÜNTER K., KÖHL M. and ESSLINGER T., *Phys. Rev. Lett.*, **94** (2005) 210401.
[225] LIAO Y.-A., RITTNER A. S. C., PAPROTTA T., LI W., PARTRIDGE G. B., HULET R. G., BAUR S. K. and MUELLER E. J., *Preprint arXiv:0912.0092*, (2010) .
[226] SERWANE F., ZÜRN G., LOMPE T., OTTENSTEIN T. B., WENZ A. N. and JOCHIM S., *Science*, **332** (2011) 336.
[227] ZÜRN G., WENZ A. N., MURMANN S., LOMPE T. and JOCHIM S., *preprint arXiv:1307.5153*, (2013) .
[228] WENZ A. N., ZÜRN G., MURMANN S., BROUZOS I., LOMPE T. and JOCHIM S., *preprint arXiv:1307.3443*, (2013) .
[229] FRÖHLICH B., FELD M., VOGT E., KOSCHORRECK M., ZWERGER W. and KÖHL M., *Phys. Rev. Lett.*, **106** (2011) 105301.
[230] ZHANG Y., ONG W., ARAKELYAN I. and THOMAS J. E., *Phys. Rev. Lett.*, **108** (2012) 235302.
[231] KÖHL M., MORITZ H., STÖFERLE T., GÜNTER K. and ESSLINGER T., *Phys. Rev. Lett.*, **94** (2005) 080403.
[232] ROM T., BEST T., OOSTEN D. V., SCHNEIDER U., FÖLLING S., PAREDES B. and BLOCH I., *Nature*, **444** (2006) 733.
[233] CHIN J., MILLER D., LIU Y., STAN C., SETIAWAN W., SANNER C., XU K. and KETTERLE W., *Nature*, **443** (2006) 961.

[234] Jordens R., Strohmaier N., Gunter K., Moritz H. and Esslinger T., *Nature*, **455** (2008) 204.
[235] Schneider U., Hackermuller L., Will S., Best T., Bloch I., Costi T. A., Helmes R. W., Rasch D. and Rosch A., *Science*, **322** (2008) 1520.
[236] Imrika J., Iazzi M., Wang L., Gull E., Greif D., Uehlinger T., Jotzu G., Tarruell L., Esslinger T. and Troyer M., *preprint arXiv:1309.7362*, (2013) .
[237] Bakr W. S., Gillen J. I., Peng A., Folling S. and Greiner M., *Nature*, **462** (2009) 74.
[238] Bakr W. S., Peng A., Tai M. E., Ma R., Simon J., Gillen J. I., Foelling S., Pollet L. and Greiner M., *Science*, **329** (2010) 547.
[239] Sherson J. F., Weitenberg C., Endres M., Cheneau M., Bloch I. and Kuhr S., *Nature*, **467** (2010) 68.
[240] Vernier E., Pekker D., Zwierlein M. W. and Demler E., *Phys. Rev. A*, **83** (2011) 033619.
[241] Bauer J., Salomon C. and Demler E., *preprint arXiv:1308.0603*, (2013) .
[242] Regal C. A., Ticknor C., Bohn J. L. and Jin D. S., *Phys. Rev. Lett.*, **90** (2003) 053201.
[243] Schunck C. H., Zwierlein M. W., Stan C. A., Raupach S. M. F., Ketterle W., Simoni A., Tiesinga E., Williams C. and Julienne P. S., *Phys. Rev. A*, **71** (2004) 045601.
[244] Zhang J., Kempen E. V., Bourdel T., Khaykovich L., Cubizolles J., Chevy F., Teichmann M., Tarruell L., Kokkelmans S. and Salomon C., *Phys. Rev. A*, **70** (2004) 030702.
[245] Günter K., Stöferle T., Moritz H., Köhl M. and Esslinger T., *Phys. Rev. Lett.*, **95** (2005) 230401.
[246] Gaebler J. P., Stewart J. T., Bohn J. L. and Jin D. S., *Phys. Rev. Lett.*, **98** (2007) 200403.
[247] Lin Y. J., Jimenez-Garcia K. and Spielman I. B., *Nature*, **471** (2011) 83.
[248] Hasan M. Z. and Kane C. L., *Rev. Mod. Phys.*, **82** (2010) 3045.
[249] Qi X.-L. and Zhang S.-C., *Rev. Mod. Phys.*, **83** (2011) 1057.
[250] Wang P., Yu Z.-Q., Fu Z., Miao J., Huang L., Chai S., Zhai H. and Zhang J., *Phys. Rev. Lett.*, **109** (2012) 095301.
[251] Cheuk L. W., Sommer A. T., Hadzibabic Z., Yefsah T., Bakr W. S. and Zwierlein M. W., *Phys. Rev. Lett.*, **109** (2012) 095302.
[252] Williams R. A., Beeler M. C., LeBlanc L. J., Jiménez-Garca K. and Spielman I. B., *Phys. Rev. Lett.*, **111** (2013) 095301.
[253] Zhang C., Tewari S., Lutchyn R. M. and Das Sarma S., *Phys. Rev. Lett.*, **101** (2008) 160401.
[254] Sau J. D., Tewari S., Lutchyn R. M., Stanescu T. D. and Das Sarma S., *Phys. Rev. B*, **82** (2010) 214509.
[255] Fu Z., Huang L., Meng Z., Wang P., Liu X.-J., Pu H., Hu H. and Zhang J., *Phys. Rev. A*, **87** (2013) 053619.
[256] Aidelsburger M., Atala M., Nascimbène S., Trotzky S., Chen Y. A. and Bloch I., *Phys. Rev. Lett.*, **107** (2011) 255301.
[257] Aidelsburger M., Atala M., Lohse M., Barreiro J. T., Paredes B. and Bloch I., *preprint arXiv:1308.0321*, (2013) .
[258] Miyake H., Siviloglou G. A., Kennedy C. J., Burton W. C. and Ketterle W., *preprint arXiv:1308.1431*, (2013) .
[259] Lu M., Burdick N. Q. and Lev B. L., *Phys. Rev. Lett.*, **108** (2012) 215301.

[260] AIKAWA K., FRISCH A., MARK M., BAIER S., GRIMM R. and FERLAINO F., *preprint arXiv:1310.5676*, (2013) .
[261] NI K. K., OSPELKAUS S., DE MIRANDA M. H. G., PE'ER A., NEYENHUIS B., ZIRBEL J. J., KOTOCHIGOVA S., JULIENNE P. S., JIN D. S. and YE J., *Science*, **322** (2008) 231.
[262] DANZL J. G., HALLER E., GUSTAVSSON M., MARK M. J., HART R., BOULOUFA N., DULIEU O., RITSCH H. and NAGERL H.-C., *Science*, **321** (2008) 1062.
[263] OSPELKAUS S., NI K. K., WANG D., DE MIRANDA M. H. G., NEYENHUIS B., QUÉMÉNER G., JULIENNE P. S., BOHN J. L., JIN D. S. and YE J., *Science*, **327** (2010) 853.
[264] CHOTIA A., NEYENHUIS B., MOSES S. A., YAN B., COVEY J. P., FOSS-FEIG M., REY A. M., JIN D. S. and YE J., *Phys. Rev. Lett.*, **108** (2012) 080405.
[265] NI K. K., OSPELKAUS S., WANG D., QUEMENER G., NEYENHUIS B., DE MIRANDA M. H. G., BOHN J. L., YE J. and JIN D. S., *Nature*, **464** (2010) 1324.
[266] YAN B., MOSES S. A., GADWAY B., COVEY J. P., HAZZARD K. R. A., REY A. M., JIN D. S. and YE J., *Nature*, **501** (2013) 521.